Effects of tyrosine kinase inhibitors on cardiopulmonary remodeling and hemodynamics in animal models of pulmonary arterial hypertension

（肺高血圧症モデル動物における
心臓と肺血管リモデリングおよび循環動態に対する
チロシンキナーゼ阻害薬の効果）

**The United Graduate School of Veterinary Science,
Yamaguchi University**

LEONG ZI PING

March 2019

Content

General Introduction

Pulmonary hypertension (PH) is a complex disease characterized by an elevated mean pulmonary arterial pressure above 25 mmHg at rest or 30 mmHg with exercise. The Word Health Organization (WHO) classifies PH into five groups: Group 1 PH, also known as pulmonary arterial hypertension (PAH) entails narrowing of the pulmonary arteries and it may be idiopathic, familial or acquired; Group 2 PH is caused by the left-sided heart disease due to valvular disorders or myocardial dysfunction; Group 3 is associated with chronic obstructive lung disease; Group 4 refers to PH that is caused by chronic thromboembolism, and Group 5 PH includes miscellaneous diseases with unclear multifactorial mechanisms [1]. In the canine populations, the left-sided heart failure due to chronic degenerative mitral valve disease (CDMVD) represents the most common cause of PH [2].

Unfortunately, the prognosis for PAH remains poor. In humans, the REVEAL Registry showed the 5-year survival rates of 65.4% and 61.2% for previously and newly diagnosed PAH patients [3], respectively, whereas another study reported the 1-, 2- and 3-year survival rate of 87%, 67%, and 54%, respectively [4]. In the canine patients, Bach JF et al. [5] reported the median survival time of 91 days in 13 dogs, while Atkinson KJ et al. [6] reported a longer median survival time of 352 days in 10 dogs with CDMVD-associated PH.

For the past 20 years, the treatment for PAH relies mainly on the various agents which dilate the constricted pulmonary vessels. These include phosphodiesterase-5 inhibitors (sildenafil and tadalafil), endothelin receptor antagonists (ambrisentan,

bosentan, and macitentan), and prostaglandins (iloprost, epoprostenol, and treprostinil). Besides, soluble guanylate cyclase stimulator (riociguat) and selective prostacyclin receptor agonist (selexipag) also represent the relatively new therapeutic agents. Despite so, a large proportion of PAH patients failed to respond satisfactorily after receiving the monotherapy, yielding a mortality rate as high as 15% per year [7]. In the continuous effort to improve survival outcome in the PAH patients, the combination therapy has emerged as an alternative to the conventional monotherapy for PAH, by reducing the risk of clinical worsening by 35% compared with monotherapy [7]. In veterinary medicine, the treatment options that are available remain limited.

All forms of pulmonary hypertension is characterized by pulmonary vascular remodeling [8]. During the vascular remodeling, there is an abnormal increase in proliferation and resistance to apoptosis of fibroblasts, smooth muscle cells and endothelial cells in the pulmonary arteries [9]. In year 2005, Schermuly RT et al. [10] demonstrated an abnormal signaling from the platelet-derived growth factor (PDGF) pathway in the PAH rat lungs, and imatinib, a tyrosine kinase inhibitor (TKI) reversed the PAH, right ventricular hypertrophy and pulmonary vascular remodeling via the PDGF inhibition. The results had then spurred a great interest among researchers and clinicians, and gave rise to many experimental and clinical studies which evaluated the potential use of various tyrosine kinase inhibitors including nilotinib [11], gefitinib, erlotinib, and lapatinib [12], sorafenib [13] for treating the PAH. However, the long-term imatinib therapy was associated with serious adverse events such as cardiotoxicity and subdural hematoma which hampered the use for the treatment of PAH [14].

Indeed, the many experimental and clinical studies did not examine the potential

use of a low-dose TKI therapy which may potentially offset the side effects of a neoplastic dose. Since the vasodilators which constitute the current treatment algorithm do not directly or potently target the cardiopulmonary remodeling, this had compellingly driven us to investigate the reversal effect and potential use of the low-dose TKIs for the treatment of PAH. Using an animal model, the rats were induced with PAH by the injection of monocrotaline (MCT), a pyrrolizidine alkaloid derived from *Crotolaria spectabili*s [15].

As the high-dose imatinib had had been well studied, we examined the anti-remodeling effects of a low-dose imatinib, and compared the treatment outcomes with sunitinib, a multi-kinase inhibitor in chapter 1. In this study, a high dose was defined as an anti-cancer dose, whereas a 1/3 reduction of the preceding dose gave rise to lower doses. Next, in chapter 2, a special interest was given to elucidate the reversal properties as well as the hemodynamic effects of toceranib, a veterinary TKI in comparison with sorafenib. In chapter 3, masitinib, another veterinary TKI was also investigated. Because the cardiopulmonary reversal effects of tadalafil, a FDA-approved phosphodiesterase inhibitor for the treatment of PAH are unclear, we also sought to compare the treatment effects and survival benefits of masitinib with tadalafil. Lastly, the long-term effects of the low-dose imatinib therapy in the dogs was studied in chapter 4.

Chapter 1

Reversal effects of low-dose imatinib compared with sunitinib on monocrotaline-induced pulmonary and right ventricular remodeling in rats

Introduction

Pulmonary arterial hypertension (PAH) entails small pulmonary artery proliferation and remodeling, resulting in a rise in mean pulmonary pressure > 25 mmHg at rest [16] and eventually right-sided heart failure [17, 18]. With a poor prognosis of reported survival rates of 58%, 41% and 24% in patients receiving a single therapy after 1, 2 and 3 years, respectively [19], dual or triple combination therapy targeting any of the three main mechanistic pathways (endothelin, nitric oxide, and prostacyclin) for PAH treatment improved the survival outcome [4, 16, 20, 21, 22, 23, 24]. However, long-term prognosis of PAH treatment remains poor [3, 25].Role of mitogen-activated protein kinase (MAPK) pathway in pathogenesis of PAH has been documented [10, 26], which involves upstream signaling from various receptor tyrosine kinases (TK) such as platelet-derived growth factor receptor beta (PDGFR-β) [10, 27, 28], fibroblast growth factor receptor (FGFR)-1 [29, 30, 31], endothelial growth factor receptor (EGFR) [12], and C-Kit receptor [32, 33]. Imatinib, a TK inhibitor, reverses pulmonary and myocardial remodeling in the rodent models [10, 11, 34] and significantly improves right ventricular (RV) functions in the PAH patients [35, 36, 37] and the Phase III Imatinib in Pulmonary Arterial Hypertension, A Randomized, Efficacy Study (IMPRES) [38]. However, an extension of the IMPRES revealed disappointing outcomes and adverse effects in imatinib-treated PAH patients [14]. In 2013, Novartis withdrew imatinib for PAH treatment.

To develop new therapies for PAH, sparing of the receptor TK pathways from the current treatment algorithm is our concern. Many experimental and clinical PAH studies did not investigate whether low-dose TK inhibitors are effective without producing associated deleterious effects. Our study on PAH dogs showed that a low-dose

imatinib therapy for 30 days reduced pulmonary arterial pressure and improved cardiac function and hemodynamics [39]. Similarly, a clinical study using low-dose imatinib in PAH patients showed improved diffusion capacity of the lung for carbon monoxide (DLCO) and varying hemodynamic responses [40]. However, these clinical studies did not investigate anti-remodeling effects of the low-dose therapy on cardiopulmonary remodeling assessed at tissue and molecular levels. Thus, we revised the study to investigate several imatinib and sunitinib doses, emphasizing on the lowest anti-remodeling dose possible. We also aimed to compare the effects of imatinib with sunitinib on pulmonary and RV remodeling to determine whether imatinib yields a greater anti-remodeling effect than sunitinib.

Materials and methods

Monocrotaline-induced pulmonary arterial remodeling

Eight-week-old, male, Wistar-Imamichi rats were purchased from the Institute for Animal Reproduction, Ibaraki, Japan, and randomized into control, placebo, and treatment groups. Under isoflurane anesthesia, monocrotaline (MCT, Sigma-Aldrich, China) was subcutaneously injected at 60 mg/kg body weight to the placebo and treatment rats to induce pulmonary arterial remodeling. Physiological saline solution was injected to the control rats. Fourteen days after the injection, oral gavage was started once daily, such that the treatment rats received imatinib mesylate [Glivec, Novartis: 5 (Ima-5), 15 (Ima-15), or 50 (Ima-50) mg/kg per day] or sunitinib malate [SUTENT®, Pfizer: 0.1 (Suni-0.1), 1 (Suni-1), 3 (Suni-3), or 10 (Suni-10) mg/kg per day], whereas the control and placebo rats received water. The oral gavage was continued for 14 days after which the rats were euthanized for tissue sampling. All protocols were approved by the Institutional Animal Care and Use Committee of the Tottori University.

Assessment of RV hypertrophy

The right ventricular (RV) tissue was separated from the left ventricle and septum (LV + S). RV and (LV + S) wet weights were determined to obtain the RV hypertrophy (RVH) index given by the formula: RV / (LV + S).

Pulmonary artery histology and pulmonary arterial muscularization assessment

The left lung lobe caudal to the bronchus was excised and fixed in 10% formalin neutral buffer solution. Lung tissues were outsourced to Sapporo General Pathology Laboratory Co. Ltd., Japan, for histology and slide preparation, as well as staining with elastic van Gieson (EVG) and double staining of EVG and alpha-smooth muscle actin (α-

SMA) antibody. Under light microscopy (400 × magnification), pulmonary artery (PA) images were captured by an Olympus Digital Camera DP21. Approximately 300 PAs (20–50 μm in diameter) were identified and counted as fully muscularized (FMPA), partially muscular (PMPA), and non-muscular (NMPA) to obtain the proportion of each artery type and calculate muscularization percentage (Fig. 1A). For FMPAs between 20–50 μm and 51–100 μm in diameter, external diameter (d) and medial wall thickness (MWT) were measured using Image J software. In addition, medial MWT ratio given by MWT normalized to diameter ($2 \times MWT / d$), lumen diameter ($d - 2 \times MWT$), and lumen area [$3.142 \times (d / 2)^2$] of the FMPAs were also determined.

ELISA measurement of serum N-terminal pro-brain natriuretic peptide (NT-proBNP) levels

Blood was sampled via cardiac puncture into plain blood tubes. Serum was obtained after centrifuging the clotted blood at 3500 rpm for 5 min (Kubota 4000, Japan). Enzyme-linked immunosorbent assay (ELISA) for rat serum NT-proBNP was performed using a commercial kit (Cloud-Clone Corp., Wuhan, China), in accordance to the manufacturer's protocol. Absorbance was read at 450 nm by an iMark^{TM} microplate reader (BIORAD, Japan). A standard curve was constructed to give readings of serum NT-proBNP levels (ng/mL).

RNA extraction, reverse transcription, and semi-quantitative fast real-time polymerase chain reaction

The RV tissue and the right caudal lung lobe were stored in RNA*later*® solution (Ambion™, Austin, TX, USA). Total RNA was isolated from tissue homogenates using TRIzol® Reagent (Ambion™, USA), in accordance to the manufacturer's specifications.

First-strand cDNA was synthesized from 2 μg of the total RNA using the Superscript®

III First-Strand Synthesis System (Invitrogen, USA). Primers were designed and ordered

from the Japan Food Assessment and Management Center (FASMAC) (Fig. 1B). Relative

quantifications of the target mRNAs of PDGFR-β, FGFR-1, VGFR-2, VEGF-A, nestin,

Raf-1, b-type natriuretic peptide (BNP), and the house-keeping gene glyceraldehyde 3-

phosphate dehydrogenase (GAPDH) were determined by Applied Biosystems 7500 Fast

Real-Time PCR System using SYBR® Fast qPCR Mix (Takara Bio Inc., Shiga, Japan)

containing 400 nM of each forward and reverse primers for rats.

Western blotting assay

Lung tissues were homogenized in T-PER® Tissue Protein Extraction Reagent

(Thermo Fisher Scientific, USA) containing 1% protease and phosphatase inhibitors

(Thermo Fisher Scientific, USA). Total protein concentrations were determined by

Bradford assay (Quick Start™ Bradford Protein Assay Kit, Bio-Rad, USA). Lysates

containing 50 μg total soluble protein were resolved on 4 − 15 % SDS-polyacrylamide

gels (Mini-PROTEAN® TGX™ Precast Protein Gels, Bio-Rad, USA) and transferred to

polyvinylidene difluoride membranes. The membranes were blocked in Tris-buffered

saline (EzTBS, Atto, Tokyo, Japan) containing 1% bovine serum albumin and then probed

with a specific primary antibody of either anti-phospho-ERK 1/2 (Cell Signaling

Technology, Inc., USA), anti-ERK 1/2 (C9) (Santa Cruz Biotechnology Inc., Santa Cruz,

CA, USA), anti-VEGF-A (Abcam, Cambridge, UK) or anti-β-actin (Santa Cruz

Biotechnology Inc., Santa Cruz, CA, USA), followed by a secondary antibody conjugated

to horseradish peroxidase. Chemiluminescence was visualized using Bio-Rad Universal

Hood II and quantified by Image Lab Software 6.0 (Bio-Rad Laboratories).

Statistical analyses

All data are expressed as mean ± standard error of mean (SEM). Data were analyzed for statistical differences using the StatMate3 analysis software (ATMS, Tokyo, Japan). Inter-group differences for normally distributed data were analyzed using one-way analysis of variance, followed by a least significant difference post-hoc test for multiple comparisons. Differences between two independent groups were analyzed using student T-test for normally distributed data or Mann–Whitney U test for non-normally distributed data. The relationship between treatment effects and dosages was analyzed using simple linear regression and Pearson correlation test. $P < 0.05$ was considered to be significant.

Results

Effect of imatinib and sunitinib on RVH and cardiac remodeling biomarkers

The placebo developed a severe RVH with a significant increase in the RV / [LV + S] ratio (0.54 ± 0.03) compared with the control (0.22 ± 0.01) (Fig. 2A). Treatment with ima-15 and ima-50 significantly reversed the RVH, yielding a stronger dose-dependency (R^2: 0.16; $P < 0.05$) than sunitinib (R^2: 0.09; $P < 0.05$) (Fig. 2B). None of the sunitinib-treated groups significantly reduced the RVH, although a weak reversal tendency was observed.

BNP mRNA was markedly increased in the placebo (0.54 ± 0.03) and lowest in the control group (0.07 ± 0.01) (Fig. 2C). All imatinib treatment groups showed reduced BNP mRNA expression compared with the placebo, of which significant reductions were observed in ima-15 (0.36 ± 0.08) and ima-50 (0.31 ± 0.05) groups. Sunitinib-treated rats also showed a slight reduction in BNP mRNA expression. Only the suni-10 group had a significant reduction (0.38 ± 0.06) compared with the placebo.

In tandem with the mRNA results, serum NT-proBNP levels were the highest in the placebo (0.68 ± 0.22 ng/mL) (Fig. 2D). Compared with the placebo, treatment with imatinib or sunitinib reduced serum NT-proBNP levels in rats, although none reached statistical significance.

Effect of imatinib and sunitinib on pulmonary remodeling

Muscularization of 20 – 50 μm PAs

Control rats had the highest NMPA percentage (39.08 ± 1.91 %). The MCT injection induced remodeling in the rat pulmonary vasculature indicated by the lowest NMPA percentage in the placebo (8.33 ± 1.14 %) (Fig. 3A). Compared with the placebo,

imatinib-treated groups showed an approximately two-fold increase in the NMPA percentage (16.67 ± 1.93 % for ima-5; 17.22 ± 2.22 % for ima-15; 21.50 ± 2.18 % for ima-50) and these increases achieved a statistical significance. Except the suni-3 group (12.53 ± 0.87 %), the other sunitinib-treated groups significantly increased the NMPA percentage (12.69 ± 1.48 % for suni-0.3; 15.86 ± 1.94 % for suni-1; 17.15 ± 1.34 % for suni-10). Imatinib exhibited a stronger dose-dependency than sunitinib (R^2: 0.29; $P < 0.05$ and R^2: 0.14, respectively).

Conversely, the FMPA percentage was the lowest in the control rats (15.14 ± 1.73 %) and the highest in the placebo rats (42.39 ± 2.06 %) due to proliferation of the arterial smooth muscle cells. Treatment with imatinib significantly and dose-dependently reversed muscularization degree in the pulmonary vasculature (R^2: 0.17; $P < 0.05$) (Fig. 3B). However, muscularization reduction was not statistically significant in sunitinib-treated rats (R^2: 0.01; $P < 0.05$).

Medial hypertrophy and lumen area of 20 − 50 µm FMPAs

We investigated degree of smooth muscle proliferation of the FMPAs by examining the MWT ratio and the lumen area of the PAs. The MWT ratio was the highest in the placebo (49.37 ± 1.26 %) and the lowest in the control (34.95 ± 1.23 %) (Fig. 3C). Although all imatinib and sunitinib groups showed decreased MWT ratios, the reduction was only significant in the groups of ima-15 (45.79 ± 1.17 %), ima-50 (45.38 ± 1.08 %), and suni-1 (46.00 ± 0.87 %).

The placebo had the smallest lumen area (229.10 ± 8.69 µm²), which differed significantly from that of the control (392.87 ± 15.60 µm²) (Fig. 3D). Ima-15 (296.70 ± 10.77 µm²), ima-50 (298.51 ± 26.94 µm²) and suni-1 (281.92 ± 14.55 µm²) groups had

significantly larger lumen areas than the placebo. Only imatinib dose-dependently normalized the lumen area of the PAs (R^2: 0.22; $P < 0.05$ for imatinib and R^2: 0.002 for sunitinib).

Medial hypertrophy and lumen area of 51 – 100 μm FMPAs

The MCT injection also significantly induced medial wall thickening of the 51 – 100 μm PAs in the placebo (53.58 ± 1.86 %) compared with that of the control (38.89 ± 1.86 %) (Fig. 4A). Imatinib and sunitinib treatments significantly reduced the MWT but only the imatinib groups produced a noticeable dose-dependency (R^2: 0.22; $P < 0.05$ for imatinib; R^2: 0.01 for sunitinib).

The lumen area of the 51–100 μm FMPAs was the smallest in the placebo (899.50 ± 68.10 μm²), which differed significantly compared to that of the control group (1514.44 ± 87.05 μm²) and all the treatment groups (Fig. 4B). Increases in lumen area in the imatinib groups were dose-dependently compared to those in the sunitinib groups (R^2: 0.15; $P < 0.05$ for imatinib; R^2: 0.02 for sunitinib).

Effect of imatinib and sunitinib on relative expression of PDGFR-β and FGFR-1 mRNA in the lungs

The MCT injection significantly upregulated the PDGFR-β mRNA expression in the placebo (0.088 ± 0.013) compared with that in the control (0.032 ± 0.005) (Fig. 5A), suggesting a role of PDGFR-β in the vascular remodeling process. Imatinib and sunitinib treatments reduced PDGFR-β mRNA expression, with significant reductions observed in ima-15 (0.048 ± 0.007), ima-50 (0.051 ± 0.008), suni-1 (0.023 ± 0.008), suni-3 (0.016 ± 0.005), and suni-10 (0.023 ± 0.002) groups.

The marked upregulation of FGFR-1 mRNA in the placebo group (0.056 ±

16

0.008) also confirmed the role of FGFR-1 in vascular remodeling (Fig. 5B). None of the imatinib groups showed significant downregulation of FGFR-1 mRNA expression. Conversely, suni-1 (0.024 ± 0.006), suni-3 (0.022 ± 0.003), and suni-10 (0.024 ± 0.002) groups showed significant downregulation of FGFR-1 mRNA expression compared with that in the placebo. Suni-3 and suni-10 groups had significantly lower mRNA expression than the control (0.037 ± 0.003).

Effect of imatinib and sunitinib on VEGF signaling pathway in the lungs

VEGFR-2 mRNA expression

VEGFR-2 mRNA expression was comparable between control (0.292 ± 0.035), placebo (0.287 ± 0.021), and all imatinib groups (Fig. 6A). However, VEGFR-2 mRNA expression was significantly downregulated in suni-1 (0.176 ± 0.023), suni-3 (0.173 ± 0.022), and suni-10 (0.136 ± 0.014) groups compared with those of control and placebo. VEGFR-2 was also dose-dependently inhibited by sunitinib (R^2: 0.28; $P < 0.05$).

VEGF-A mRNA and protein expression

Since VEGF-A supplies the VEGF signaling pathway, we further investigated the mRNA (Fig. 6B) and protein (Fig. 6C) expression. Surprisingly, the control had insignificantly higher levels of mRNA (0.074 ± 0.016) and protein (0.519 ± 0.063) than the placebo (0.052 ± 0.005 for mRNA; 0.489 ± 0.010 for protein). Compared with the above groups, the mRNA and protein levels were significantly lower in suni-3 (0.026 ± 0.004 for mRNA; 0.286 ± 0.022 for protein) and suni-10 (0.025 ± 0.003 for mRNA; 0.281 ± 0.010 for protein) groups. Suni-1 also significantly inhibited the protein expression (0.317 ± 0.008). In the ima-15 group, a significant reduction of the mRNA (0.036 ± 0.005) but not the protein (0.469 ± 0.056) was seen compared with that of the placebo. Further,

17

we observed a stronger dose-dependent VEGF-A inhibition in sunitinib (R^2: 0.24, $P <$ 0.05 for mRNA; R^2: 0.36, $P < 0.05$ for protein) than imatinib (R^2: 0.09 for mRNA; R^2: 0.02 for protein).

Effect of imatinib and sunitinib on relative VEGFR-2 mRNA expression in the RV

VEGFR-2 mRNA expression of RV tissues did not significantly differ among the groups (Fig. 6D). The placebo showed a lower VEGFR-2 mRNA expression level than the control, whereas suni-1, suni-3 and suni-10 groups had a lower mRNA level than the placebo.

Effect of imatinib and sunitinib on MAPK signaling pathway in the lungs

Raf-1 mRNA expression

The placebo exhibited significant upregulation of Raf-1 mRNA expression (0.15 ± 0.02) compared with control (0.07 ± 0.01) (Fig. 7A). Ima-15 (0.10 ± 0.01) and ima-50 (0.08 ± 0.01) significantly inhibited the Raf-1 mRNA expression. The inhibition was not significant in all sunitinib groups except for suni-10 (0.06 ± 0.01).

**Phosphorylated ERK-1/2 protein expression**

Phosphorylated ERK-1/2 protein expression was noticeably increased in the placebo (3.26 ± 0.38), suni-3 (2.12 ± 0.43) and suni-1 (2.37 ± 0.16) groups, compared with that in the control group (0.39 ± 0.12) (Fig. 7B). Ima-15 (0.48 ± 0.09), ima-50 (0.19 ± 0.10), and suni-10 groups (0.06 ± 0.02) significantly suppressed the protein phosphorylation to a level comparable with that of the control group.

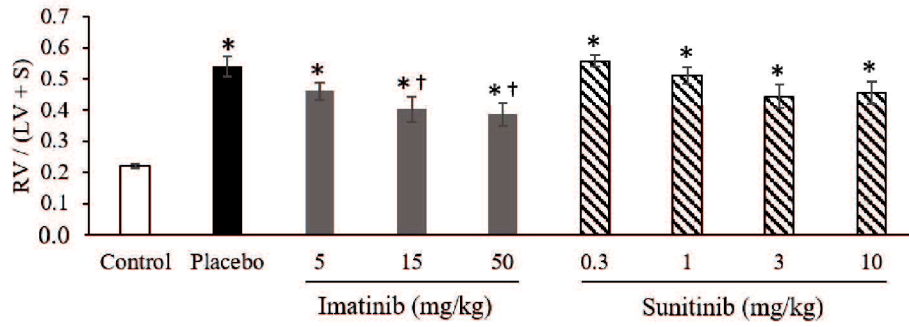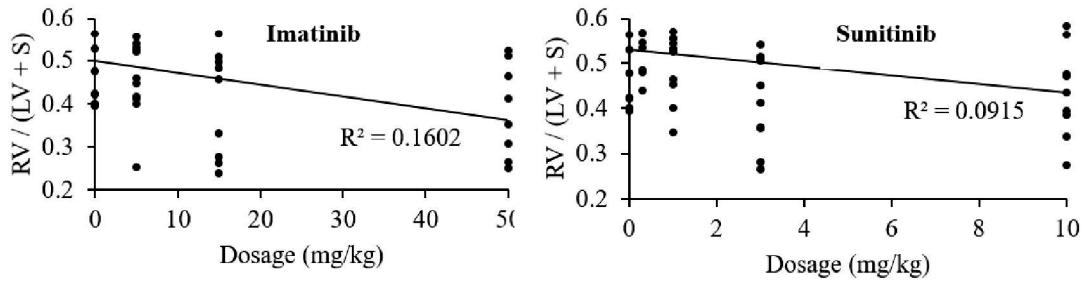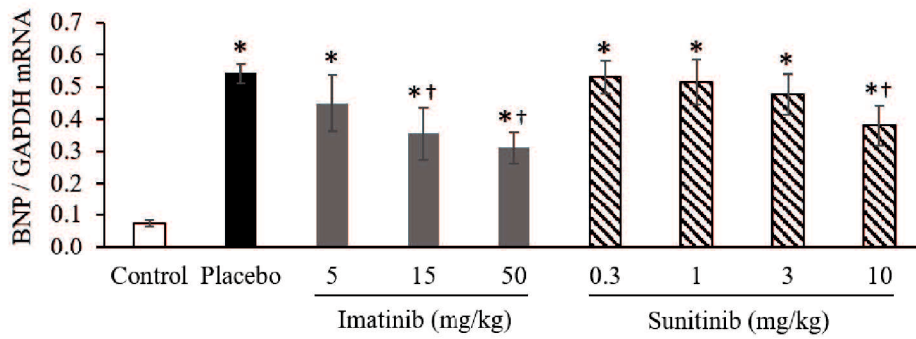**Effect of imatinib and sunitinib on relative nestin mRNA expression in the lungs**

To explain reversal differences between imatinib and sunitinib on pulmonary remodeling, we examined nestin mRNA expression in all groups (Fig. 8A). The placebo

had nestin mRNA levels statistically comparable with the control 28 days after the MCT injection (0.047 ± 0.013 for placebo versus 0.034 ± 0.006 for control). However, ima-5 (0.068 ± 0.012), suni-0.3 (0.062 ± 0.011), suni-1 (0.062 ± 0.011), and suni-3 (0.068 ± 0.013) groups had significantly upregulated nestin mRNA levels. There were no significant changes in expression levels between control and placebo groups even 42 days after the injection (0.025 ± 0.006 for placebo versus 0.055 ± 0.015 for control) (Fig. 8B).

A
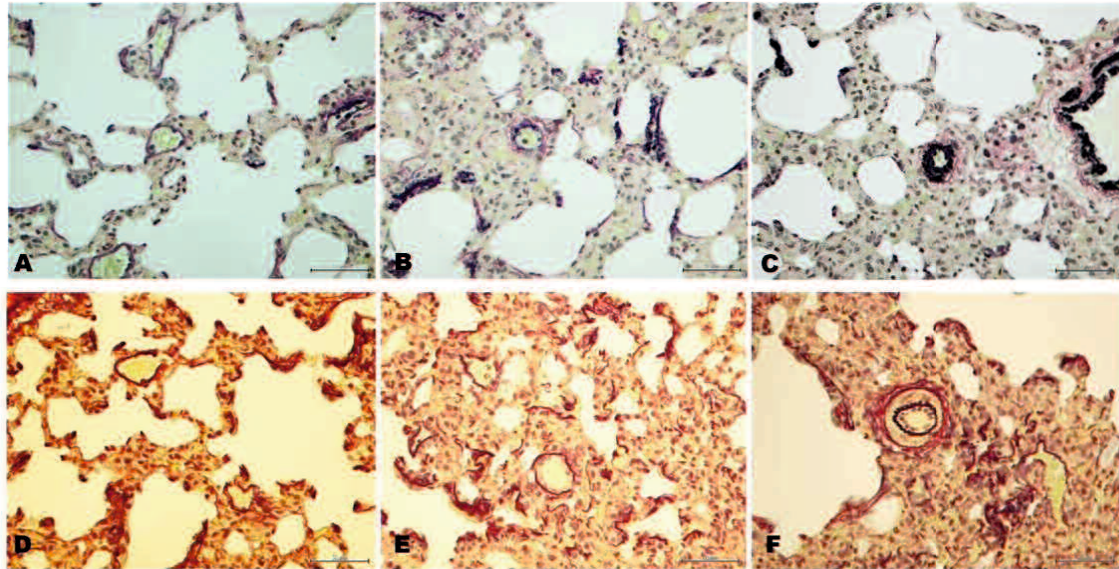
B

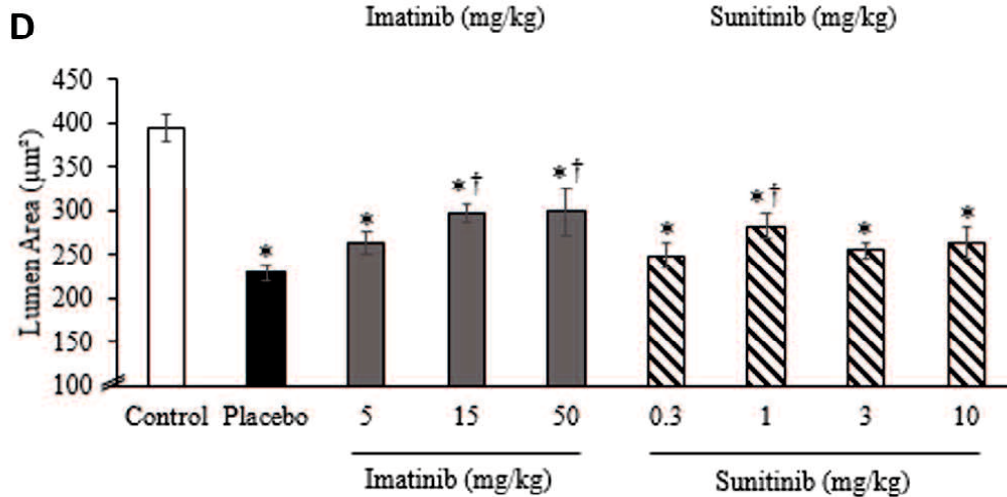| Gene	Accession Number	Symbol	Forward Primer	Reverse Primer
B-type natriuretic peptide	NM_031545.1	BNP	CAGAAGCTGCTGGAGCTGATA	GGCGCTGTCTTGAGACCTAA
Fibroblast growth factor receptor type 1	NM_024146.1	FGFR-1	GCAGCGATACCACCTACTTCT	CCTACGGTTTGGTTTGGTGTT
Vascular endothelial growth factor receptor 2	NM_013062.1	VEGFR-2	AGAAGGAACGAGAATGCGGG	CTCTGAAAACGCGGGTCTCT
Vascular endothelial growth factor A	NM_031836.3	VEGF-A	GGAGTCTGTGCTCTGGGATTT	GTGAAGGAGCAACCTCTCCA
Platelet-derived growth factor receptor-β	NM_031525.1	PDGFR-β	GCCCTCATGTCGGAGTTGAA	GTTTCGGTGCAGGTAGTCCA
Raf-1 proto-oncogene, serine/threonine kinase	NM_012639.2	Raf-1	CAACGTCCACTCCCAATGTC	CTTCGAATTGCATCCTCAATCA
Nestin	NM_001308239.1	Nestin	CCCTTAGTCTGGAGGTGGCT	GGGTCCAGAAAGCCAAGAGA
Glyceraldehyde 3-phosphate dehydrogenase	NM_017008.4	GAPDH	TCTCTGCTCCTCCCTGTTCT	GGTAACCAGGCGTCCGATAC

Fig. 1. (A) Representative histological images of non-muscularized, partially muscularized, and fully muscularized intra-acinar arteries of 20 – 50 μm in diameter, respectively. NM, Non-muscular; PM, Partially muscular; FM, Fully muscular; EVG, elastic van Gieson; α-SMA, Alpha-smooth muscle actin. (B) Primer sequences for real-time polymerase chain reaction analysis of rat b-type brain natriuretic peptide (BNP), fibroblast growth factor receptor (FGFR)-1, vascular endothelial growth factor receptor (VEGFR)-2, vascular endothelial growth factor (VEGF)-A, platelet-derived growth factor receptor (PDGFR)-β, Raf-1 proto-oncogene serine/threonine kinase (Raf-1), nestin, and glyceraldehyde 3-phosphate dehydrogenase (GAPDH).

A

B

C

D

22
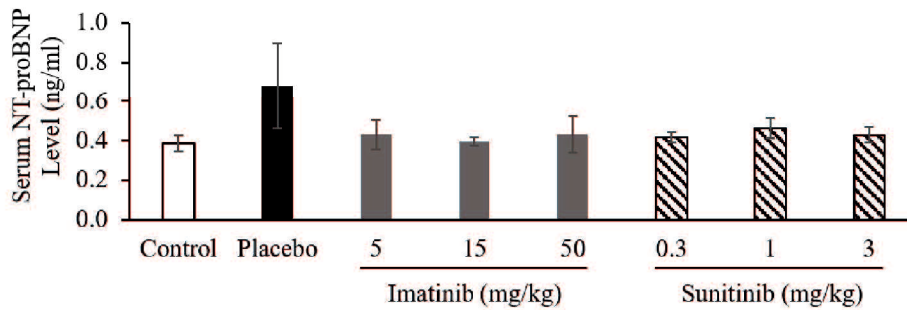
Fig. 2. Effects of imatinib and sunitinib on monocrotaline-induced right ventricular hypertrophy (RVH) and hypertrophy markers. (A) RVH of different groups (n = 8 – 14). (B) RVH reversal dose-dependency of imatinib and sunitinib (n = 8 – 14). (C) Relative brain natriuretic peptide (BNP) mRNA expression in the RV tissue (n = 8 – 14). (D) Serum level of N-terminal pro-brain natriuretic peptide (NT-proBNP) (n = 5 – 6). Data are means ± SEM. *$P < 0.05$ vs. control; $^{†}P < 0.05$ vs. placebo.

A

FMIA PMIA NMIA

Vascular Muscularization (%)

Control Placebo

Imatinib (mg/kg): 5, 15, 50

Sunitinib (mg/kg): 0.3, 1, 3, 10

B

Imatinib — Muscularized Intra-Acinar Arteries (%) vs Dosage (mg/kg), $R^2 = 0.173$

Sunitinib — Muscularized Intra-Acinar Arteries (%) vs Dosage (mg/kg), $R^2 = 0.0036$

C

Medial Wall Thickness Ratio (%)

Control Placebo

Imatinib (mg/kg): 5, 15, 50

Sunitinib (mg/kg): 0.3, 1, 3, 10

D

Lumen Area (μm^2)

Control Placebo

Imatinib (mg/kg): 5, 15, 50

Sunitinib (mg/kg): 0.3, 1, 3, 10

Fig. 3. Effects of imatinib and sunitinib on vascular muscularization in intra-acinar arteries of 20–50 μm in diameter. (A) Non-muscularized (NMIA), partially muscularized (PMIA), and fully muscularized (FMIA) intra-acinar artery percentage related to the total number of pulmonary arteries quantified. (B) Dose-dependency of imatinib and sunitinib on pulmonary muscularization reversal. (C) Medial wall thickness normalized to the external diameter of the fully muscularized intra-acinar arteries. (D) Lumen area of the fully muscularized intra-acinar arteries. Data are means ± SEM (n = 8 − 14). *$P < 0.05$ vs. control; †$P < 0.05$ vs. placebo.
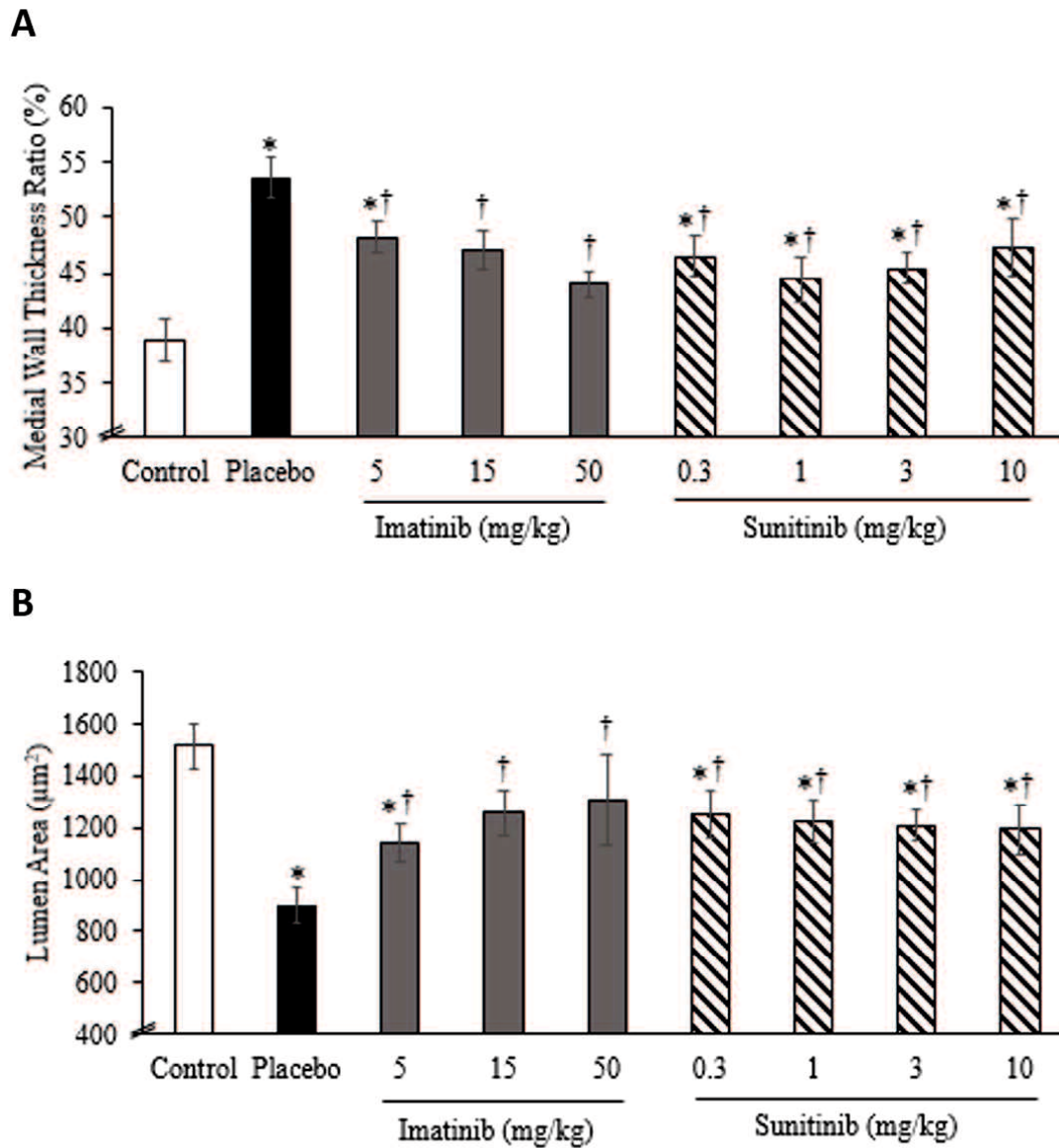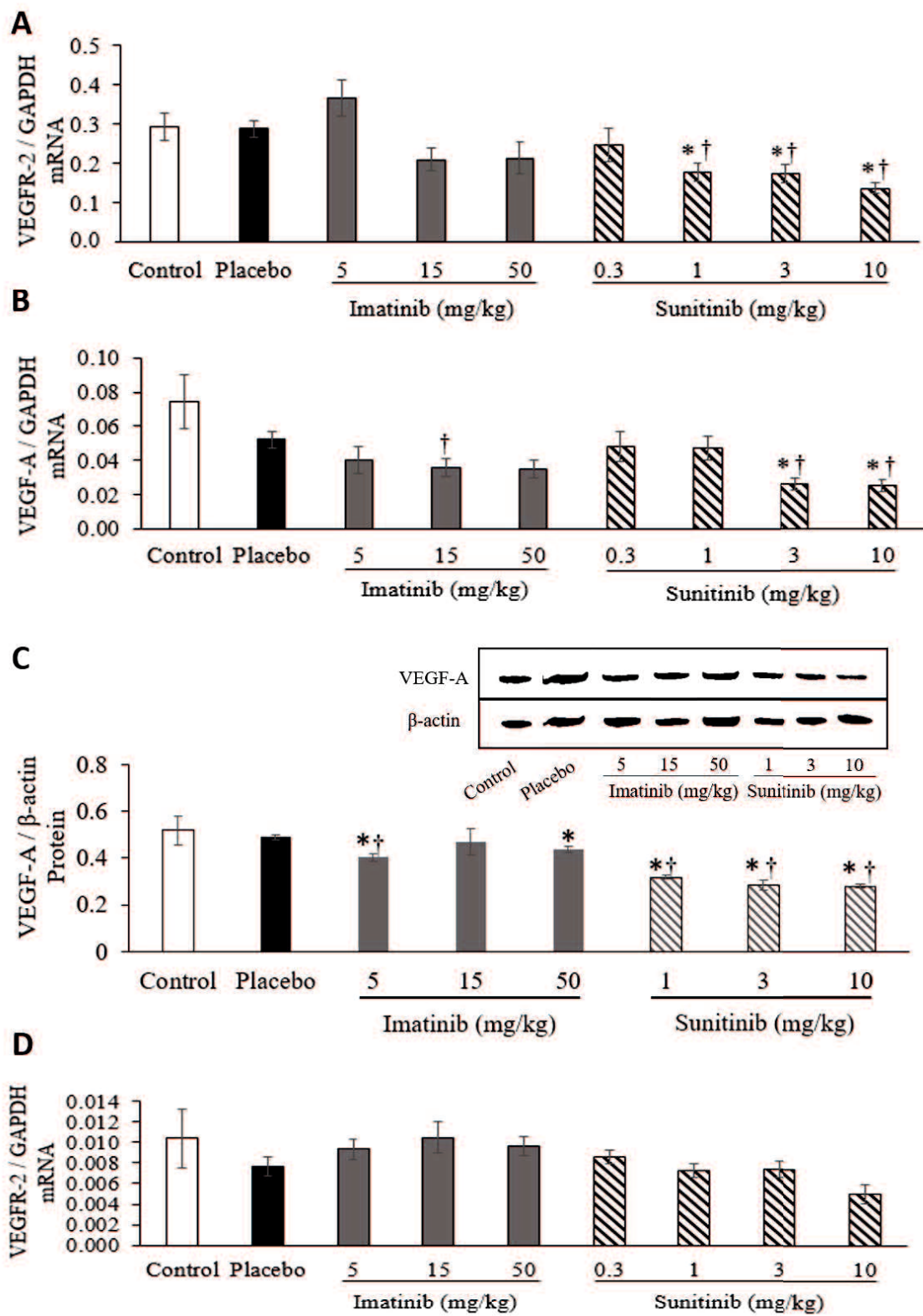
Fig. 4. Effects of imatinib and sunitinib on vascular muscularization in the intra-acinar arteries of 51–100 μm in diameter. (A) Medial wall thickness normalized to the external diameter of the fully muscularized intra-acinar arteries. (B) Lumen area of the fully muscularized intra-acinar arteries. Data are means ± SEM (n = 8 − 14). *$P < 0.05$ vs. control; †$P < 0.05$ vs. placebo.
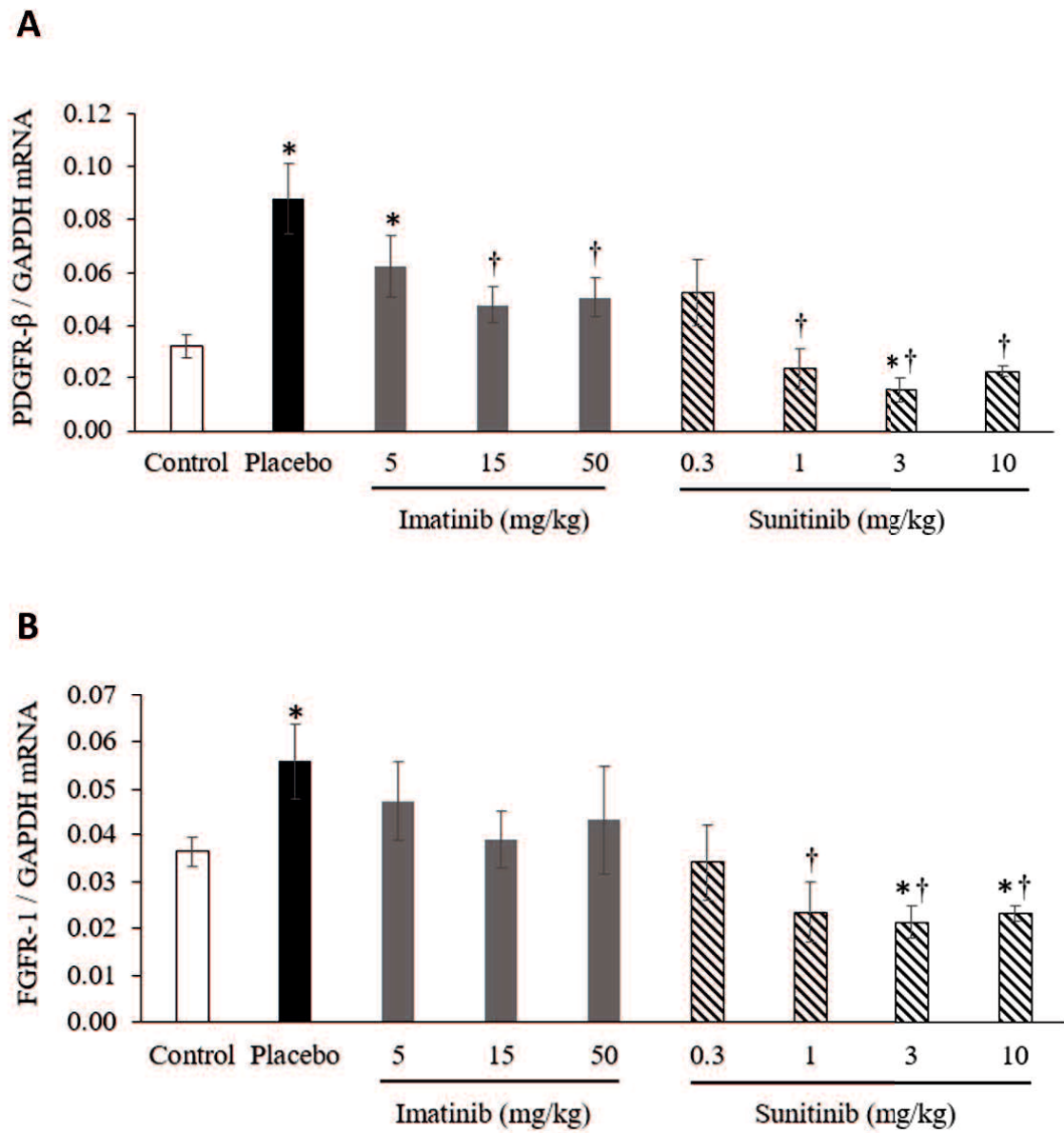
Fig. 5. Effects of imatinib and sunitinib on monocrotaline-induced receptor tyrosine kinase mRNA expression in the rat lungs. (A) Platelet-derived growth factor receptor (PDGFR)-β (n = 6 – 12). (B) Fibroblast growth factor receptor (FGFR)-1 (n = 7 – 10). Data are means ± SEM. *$P < 0.05$ vs. control; †$P < 0.05$ vs. placebo.

27

A

VEGFR-2 / GAPDH mRNA

Control, Placebo, Imatinib (mg/kg): 5, 15, 50, Sunitinib (mg/kg): 0.3, 1 *†, 3 *†, 10 *†

B

VEGF-A / GAPDH mRNA

Control, Placebo, Imatinib (mg/kg): 5, 15 †, 50, Sunitinib (mg/kg): 0.3, 1, 3 *†, 10 *†

C

VEGF-A
β-actin

Control   Placebo   5 15 50   1 3 10
                    Imatinib (mg/kg) Sunitinib (mg/kg)

VEGF-A / β-actin Protein

Control, Placebo, Imatinib (mg/kg): 5 *†, 15, 50 *, Sunitinib (mg/kg): 1 *†, 3 *†, 10 *†

D

VEGFR-2 / GAPDH mRNA

Control, Placebo, Imatinib (mg/kg): 5, 15, 50, Sunitinib (mg/kg): 0.3, 1, 3, 10

28

Fig. 6. Effects of imatinib and sunitinib on monocrotaline-induced vascular endothelial growth factor receptor (VEGFR)-2 mRNA expression in the rat RV and lungs, and vascular endothelial growth factor (VEGF)-A mRNA and protein expression in the rat lungs. (A) VEGFR-2 mRNA in the lungs (n = 7 − 11). (B) VEGF-A mRNA in the lungs (n = 7 − 9). (C) VEGF-A proteins in the lungs. Western blots are representative of one individual from each group (n = 3). (D) VEGFR-2 in the RV (n = 6 − 13). Data are means ± SEM. *$P < 0.05$ vs. control; $^{\dagger}P < 0.05$ vs. placebo.

A
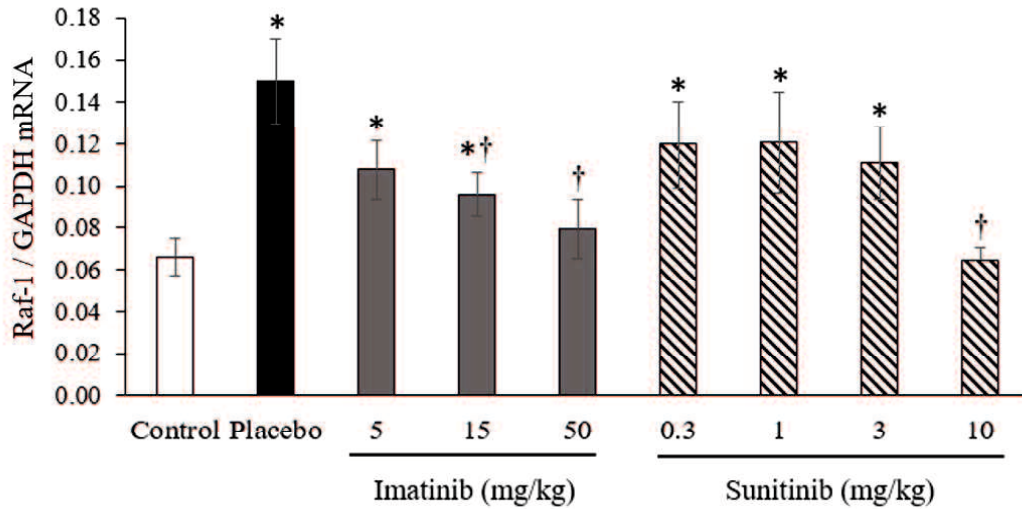
B
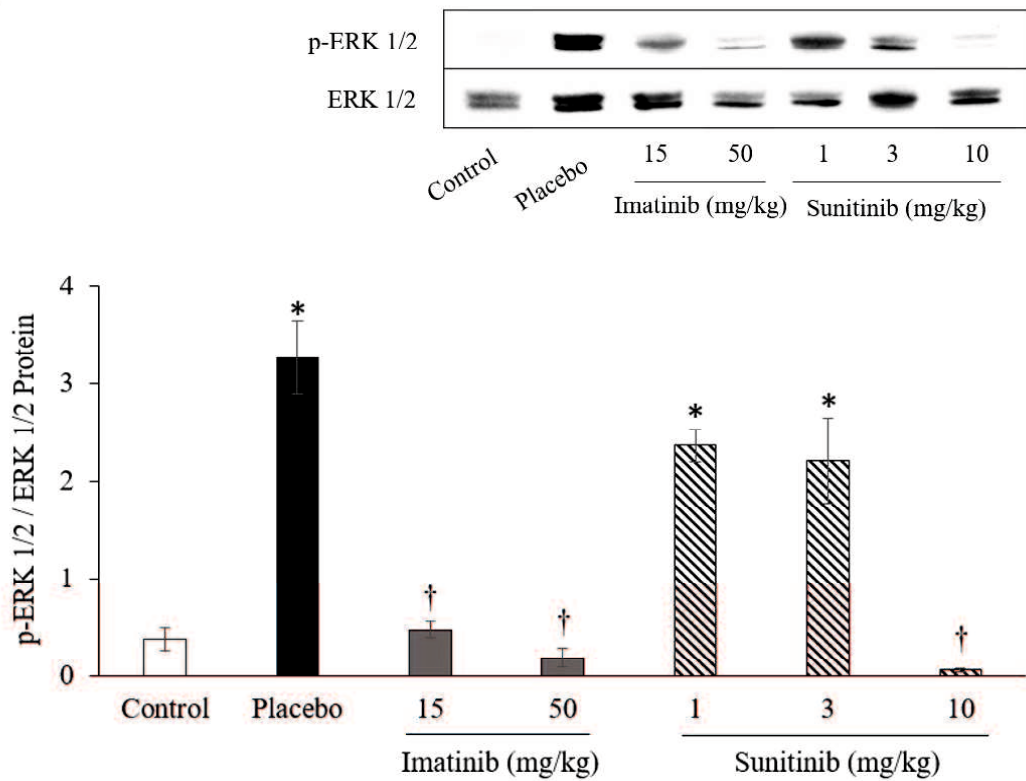
Fig. 7. Effects of imatinib and sunitinib on mitogen-activated protein kinase (MAPK) signaling pathway. (A) Raf-1 proto-oncogene serine/threonine kinase (Raf-1) mRNA expression in the lungs (n = 8 − 14). (B) Phosphorylation of extra-cellular-signal-related kinase (ERK)-1/2 protein expression in the lungs. Western blots are representative of one individual from each group (n = 3). Data are means ± SEM. $*P < 0.05$ vs. control; $^{\dagger}P < 0.05$ vs. placebo.
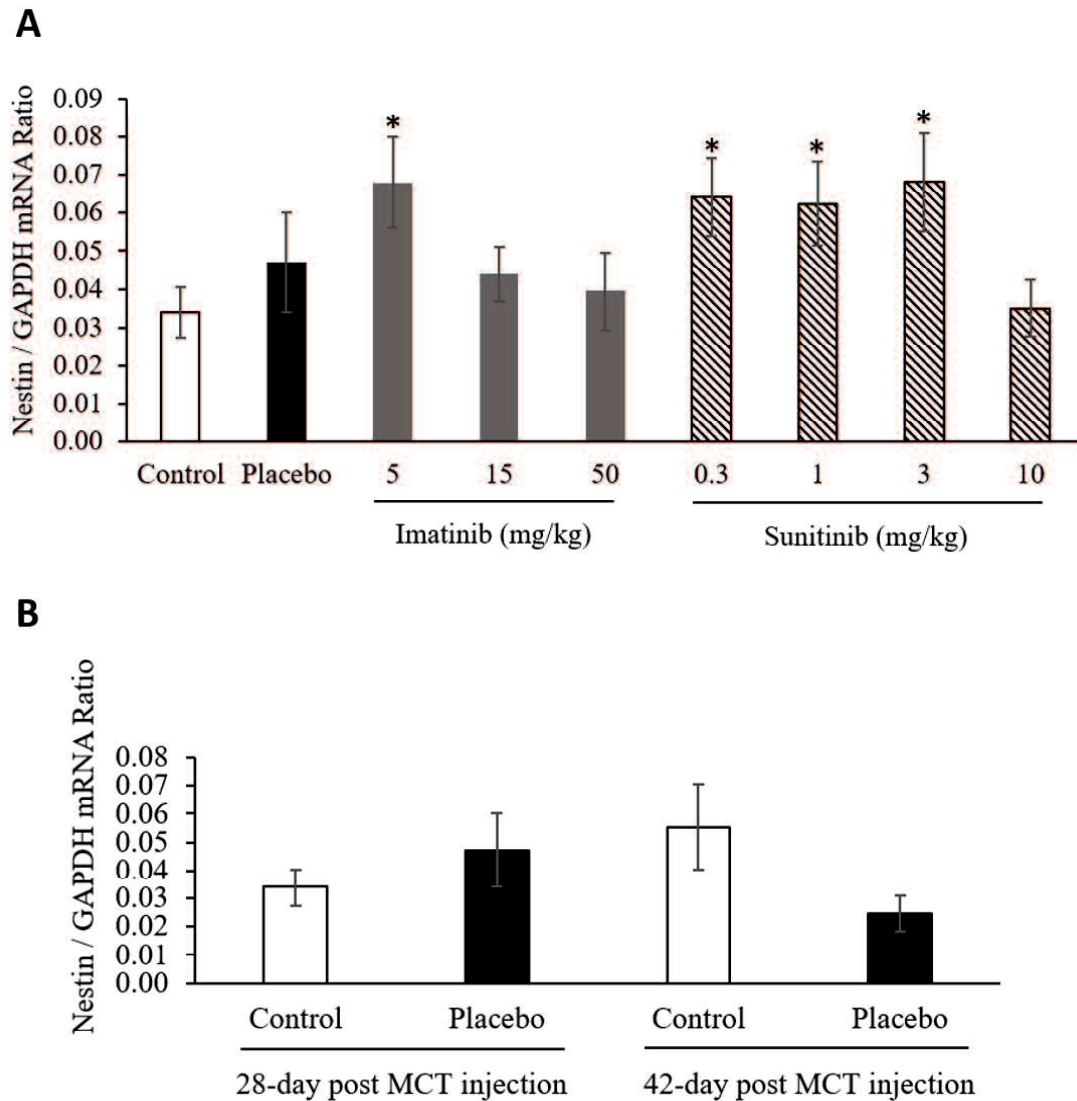
Fig. 8. Effects of imatinib and sunitinib on monocrotaline-induced angiogenesis marker nestin mRNA expression in the rat lungs. (A) Nestin mRNA expression in the different groups (n = 7 – 9). (B) The comparison of nestin mRNA expression between the control and the placebo 28 and 42 days after the MCT injection (n = 6 – 13). Data are means ± SEM. *$P < 0.05$ vs control; [†]$P < 0.05$ vs. placebo.

Discussion

This study provides a new perspective on the effects of imatinib by investigating its dose-dependency to show that a lower dose (15 mg/kg) is equally effective compared with a high dose (50 mg/kg) in the reversal of monocrotaline-induced pulmonary and cardiac remodeling in rats. We also show that imatinib exerts stronger anti-remodeling actions than sunitinib perhaps attributable to on-going proliferation of pulmonary arteries due to VEGF signaling disruption by sunitinib.

Twenty-eight days post-MCT injection, the muscularized small intra-acinar arteries markedly increased at the expense of the non-muscularized arteries in rat lungs. This is accompanied by a severe medial hypertrophy, leading to narrowing of the lumen area of the arteries as highlighted by EVG and/or α-SMA staining, indicating the occurrence of a vascular remodeling process. We also observed significant RVH, indicative of myocardial remodeling after the MCT injection. The above results are consistent with those of previous studies that used MCT as a toxic model of PAH [10, 26, 41, 42].

We confirmed the previously reported data of elevated PDGFR-β [10, 27, 42] and FGFR-1 transcript levels [29, 30, 31], and decreased VEGFR-2 and the VEGF-A levels [43, 44, 45, 46, 47] thus affirming the pathogenic role of PDGFR-β and FGFR-1 in MCT-induced pulmonary remodeling. In terms of kinase selectivity, imatinib targets 9 kinases whereas sunitinib possesses a greater spectrum of activity which targets 30 receptor tyrosine kinases [48]. In our study, sunitinib potently blocked PDGFR-β, FGFR-1, VEGFR-2, and VEGF-A mRNAs, while imatinib only significantly inhibited PDGFR-β mRNA in rat lungs. Given that these receptor tyrosine kinases and their respective

growth factors activate the MAPK signaling pathway [49], and Raf-1 kinase is the entry point to this downstream signaling pathway [50], we expected a greater downregulation of the MAPK signaling pathway in the sunitinib-treated groups. However, significant down-regulation of Raf-1 mRNA and phosphorylated ERK-1/2 protein expressions was only seen in the highest dose of sunitinib treatment group. As for the imatinib treatment groups, ima-15 and ima-50 significantly blocked the MAPK pathway. This suggests that sunitinib's multiple kinase inhibition did not translate into a greater inhibition of the MAPK downstream signaling pathway in MCT-induced cardiopulmonary remodeling compared with imatinib of a narrower kinase target.

For myocardial remodeling, imatinib reversed RVH at 15 and 50 mg/kg and elicited a higher dose-dependency than sunitinib. However, despite the weak reversal observed, none of the sunitinib groups produced a significant RVH reversal, which disagrees with the findings of Kojonazarov et al [19]. Our data agree with those of Hung et al [18] and Vitalia et al [51], that mice subjected to hypoxia developed a more severe form of RVH after receiving Sugen (SU5416), an anti-VEGF therapy than those subjected to hypoxia alone. As for the cardiac biomarker, the 15 and 50 mg/kg imatinib groups significantly down-regulated the BNP mRNAs, but only rats on a 10 mg/kg dose in the sunitinib groups produced a significant decrease in the BNP mRNA expression. Because VEGFR-2 mRNA levels of RV did not differ significantly among all groups, the lack of a significant reversal by sunitinib might be related to the remodeling process in the pulmonary vasculature.

Imatinib was reported to reverse pulmonary remodeling at a dose of 50 and 100 mg/kg/day [10]. However, the anti-remodeling effect of lower doses remains uncertain,

although studies which evaluated clinical effectiveness of low-dose imatinib on PAH have been conducted on a small sample of human patients [40] and dogs [39], respectively. Our present study shows that imatinib at 5, 15 and 15 mg/kg significantly reduced the FMPAs and increased the NMPAs of 20–50 μm in diameter, consistent with the clinical observations in the above studies. Conversely, sunitinib did not significantly normalize medial hypertrophy nor lumen area of the FMPAs in rats. These findings support the earlier statement of an equivocal RVH improvement in sunitinib groups, which may be attributable to a lack of pulmonary remodeling reversal.

Further, we examined nestin mRNA expression in lungs of the MCT-injected rats. Nestin, an intermediate filament protein recently discovered as a more specific angiogenesis marker for small arteries than CD31, CD34, and von Willebrand factor [52, 53], is highly expressed during angiogenesis following a vascular insult and in various forms of neoplasm [53, 54, 55, 56] as well as in pulmonary remodeling [57]. Saboor et al recently showed that nestin plays a role in the proliferation of vascular smooth muscle cells and provides a diagnostic tool for pulmonary hypertension [58]. However, to the best of our knowledge, no studies have reported on nestin expression in rat lungs after treatment with imatinib or sunitinib. We demonstrated that the sunitinib treatment groups (0.3, 1 and 3 mg/kg) significantly upregulated nestin mRNA expression compared with that in imatinib, control, and placebo groups. Twenty-eight days after the MCT injection, the placebo group did not show increased nestin mRNA expression, which agrees well with findings of Saboor et al [58], which stated that nestin expression is upregulated only during the initial phase of pulmonary remodeling. To further clarify this finding, we showed that the placebo rat lungs did not upregulate nestin mRNA expression even after

42 days after the MCT injection, indicating that the pulmonary vasculature had established a quiescent state. Therefore, upregulated nestin mRNA expression and increased pulmonary muscularization, further evident by the lack of significant MAPK pathway inhibition in the sunitinib groups compared with that in the imatinib groups, led us to believe that sunitinib but not imatinib treatment induced on-going proliferation of the smooth muscle cells in the small intra-acinar arteries, in a phenomenon known as "escape angiogenesis" [59, 60] and/or non-canonical angiogenesis [61].

Since VEGF overexpression protects against hypoxic and MCT-induced PAH [62], one possible reason to explain continued proliferation of smooth muscle cells induced by sunitinib is inhibition of the VEGF signaling pathway. Despite the severe pulmonary remodeling in the placebo group, an apparent overexpression of VEGFR-2 and VEGF-A mRNAs as well as VEGF-A protein was not observed, consistent with the results by Arcot et al [43], Nadeau et al [45], and Farkas et al [44], which also reported decreased VEGF and/or VEGFR mRNA expression levels in PAH rats induced with monocrotaline and/or chronic hypoxia. While imatinib did not affect the VEGF signaling pathway, sunitinib significantly and dose-dependently downregulated VEGFR-2 and VEGF-A levels. Since Sugen (SU5416) was used for its VEGFR inhibiting actions to further enhance the angioproliferative PAH in mice subjected to hypoxia [18, 51] or mice were treated with a repeated immunization of ovalbumin [63], we believe that the lack of effectiveness in reversing the vascular remodeling in sunitinib groups is attributable to its potent inhibition of the VEGF signaling pathway.

In a study which evaluated the long-term safety and efficacy of imatinib in human PAH [14], the authors concluded that imatinib resulted in severe adverse effects,

significant side effects, and a high discontinuation rate that limited imatinib use in PAH treatment. The study utilized a starting dose of 200 mg once daily and up-titrated to 400 mg once daily (which is equivalent to a rat dose of 50 mg/kg in our study and the neoplastic dose indicated for gastrointestinal stromal carcinoma and chronic myeloid leukemia treatment in humans) [64]. In a study by Hatano et al [40], five PAH patients who received a low-dose imatinib at 100 mg/day (equivalent to a rat dose of 12.5 mg/kg) for 12 weeks, showed improved DLCO and hemodynamic parameters as indicated by either a decreased mean pulmonary arterial pressure, a decreased pulmonary venous resistance, or an increased cardiac index. When the treatment was extended to 24 weeks, only three patients showed sustained favorable effects. Further, our previous PAH study in dogs also showed that treatment with 3 mg/kg of imatinib, a dose equivalent to a 1/3 dose of the 10 mg/kg used to treat canine malignancies [65], improved clinical scores and echocardiographic outcomes in dogs [39]. Taken together, the above clinical observations could be explained by the potent anti-remodeling of low-dose imatinib (15 mg/kg). Therefore, we believe that low-dose of imatinib has the advantage of reducing side effects, yet is effective to reverse pulmonary vascular remodeling and right ventricular hypertrophy that characterize PAH.

In conclusion, imatinib elicited dose-dependent anti-remodeling actions, and a dose as low as 15 mg/kg, significantly inhibited the MAPK signaling pathway responsible for pulmonary vascular remodeling and RVH in MCT-injected rats. Imatinib is more effective than sunitinib in reversing MCT-induced cardiopulmonary remodeling in rats, through inhibition of PDGFR-β while sparing VEGF inhibition in the lungs. Therefore, low-dose imatinib therapy may provide an option for treatment of PAH and RVH.

Chapter 2

Effects of toceranib compared with sorafenib on monocrotaline-induced pulmonary arterial hypertension and cardiopulmonary remodeling in rats

Introduction

Pulmonary arterial hypertension (PAH) is characterized by proliferation of pulmonary arterial smooth muscle cells and right ventricular hypertrophy (RVH), and remains an incurable disease with a poor long-term prognosis [3, 25]. After the discovery of an increased downstream mitogen-activated protein kinase (MAPK) signaling from the receptor TKs in the PAH pathogenesis, many studies have investigated the reversal effects of tyrosine kinase (TK) inhibitors, such as imatinib [10, 35, 38], sunitinib [19], and sorafenib [26, 66] on experimental and clinical PAH. However, most of the studies evaluated the effects of high doses of the TK inhibitors, and only a few examined those of low doses [39, 40, 67]. Nonetheless, we recently showed that low-dose imatinib significantly reversed monocrotaline (MCT)-induced RVH and pulmonary remodeling in rats [67] and improved hemodynamics in dogs with PAH [39].

In the continuous search for a TK inhibitor which possesses potent properties against cardiopulmonary remodeling (CPR) to allow administration at a lower, non-neoplastic dose and avoid adverse effects, we investigated toceranib (SU11654), a veterinary TK inhibitor approved for the therapy of canine mast cell tumors. Several studies of canine malignancies have shown that toceranib acts via the inhibition of mutated C-KIT receptors and angiogenesis [68, 69, 70]. However, no single study has reported its efficacy in reversing the PAH nor CPR. The structural and functional similarities of toceranib and sunitinib [70] provide a compelling rationale for investigating whether toceranib reverses PAH and CPR or otherwise aggravates angioproliferation via vascular endothelial growth factor (VEGF) signaling inhibition [60] as reported in our recent study [67].

Sorafenib, a multi-kinase inhibitor, shows favorable hemodynamic effects in patients with refractory PAH [13], and potent anti-remodeling effects against RVH and pulmonary muscularization in rats treated with MCT or hypoxia [26, 66]. Therefore, we compared the reversal effects of toceranib with sorafenib on MCT-induced PAH and CPR in rats. The present study also improved the shortcoming of our previous study by scrutinizing effects of both agents on the right ventricular hemodynamics, and determined the optimal dose of each agent for the treatment of severe PAH. Besides, sorafenib has also been reported to induce apoptosis and affects autophagy in myeloid dendritic cells [71], human macrophages [72], and hepatic carcinoma cells [73], thus raising the possibility that it may also confer a beneficial effect by improving the impaired autophagy in the PAH lungs [74, 75, 76]. Because both sorafenib and toceranib act on the PDGF and C-KIT receptors, in which their expression and accumulation are in turn influenced by the C-X-C motif chemokine ligand 12/ C-X-C motif chemokine receptor 4 (CXCL12/CXCR4) pathway [77], we also investigated the unclear role of the CXCL12/CXCR4 axis in the MCT-induced PAH.

Materials and methods

Monocrotaline-induced pulmonary arterial hypertension and treatments

All experimental procedures were approved by the Institutional Animal Care and Use Committee of the Tottori University and carried out as described in the previous chapter with some modifications. Male Wistar-Imamichi rats were randomized into three groups: the placebo and treatment groups received a single subcutaneous injection of 60 mg/kg of MCT (Sigma-Aldrich, China), whereas the control group received physiological saline. On day 14 after the injection, the treatment rats were medicated with either sorafenib [Nexavar 200 mg, Bayer: 10 (sora-10), 30 (sora-30), or 100 (sora-100) mg/kg per day] or toceranib phosphate [Palladia 50 mg, Pfizer: 1 (toce-1), 3 (toce-3), or 10 (toce-10) mg/kg per day]. The control and placebo rats were given water. All the treatments were administered orally, once daily for 14 days.

Measurement of RV hemodynamic parameters

The rats were anesthetized with 2% isoflurane via a face mask. A polyethene catheter (PE-50 Intramedic PE tubing, Becton Dickinson) was advanced into the RV via the right jugular vein to measure RV systolic pressure (RVSP), mean RV pressure (RVP) and heart rate (HR). The position of the catheter was confirmed by the pressure waveforms. The data were recorded and analyzed with the PowerLab System connected a pressure transducer (ADInstruments), after which the rats were euthanized for tissue sampling.

Assessment of RVH

The RV tissue was dissected from the left ventricle and septum (LV+S). Wet weights of the RV and LV+S were determined to derive the RVH index: [RV/(LV+S)].

Histology of pulmonary arterial muscularization

Left lung lobes were subjected for histological preparation and elastic van Gieson (EVG) staining. The proportions of pulmonary arteries of 20–50 μm in diameter that were fully muscularized (FMPA), partially muscularized (PMPA), and non-muscularized (NMPA) were determined as described previously. In addition, we also measured the external diameter (d), medial wall thickness (MWT), MWT ratio ($2 \times \text{MWT} / d \times 100\%$), lumen diameter ($d - 2 \times \text{MWT}$), and lumen area [$3.142 \times (d/2)^2$] of FMPAs that were 20–50 μm and 51–100 μm in diameter using Image J software.

Semi-quantitative fast real-time polymerase chain reaction

First-strand complementary DNA was synthesized from 2 μg RNA, which was isolated from the RV tissue and the right caudal lung lobes, respectively, using the Superscript® III First-Strand Synthesis System (Invitrogen, USA). In addition to the previously described target messenger RNAs (mRNAs), p-62 (forward: CCTGAAGAATGTGGGGGAGAG; reverse: TGTGCCTGTGCTGGAACTTT), KIT proto-oncogene receptor TK (C-KIT) (forward: GGCAAATACACGTGCGTCAG; reverse: AAACAAGGGAAGGCCAACCA), C-X-C motif chemokine (CXC) receptor 4 (CXCR4) (forward: CCGTCTATGTGGGTGTCTGG; reverse: CACAGATGTACCTGCCGTCC), and CXC ligand 12 (CXCL12) (forward: CACTCCAAACTGTGCCCTTC; reverse: CGGGTCAATGCACACTTGTCT) expression levels were also determined with Applied Biosystems 7500 Fast Real-Time PCR System using SYBR® Fast qPCR Mix (Takara Bio Inc., Shiga, Japan).

Western blotting assay

Lysates of lung tissues were separated on 4–15% sodium dodecyl sulfate-polyacrylamide gels (Mini-PROTEAN® TGX™ Precast Protein Gels, Bio-Rad, USA) and transferred to polyvinylidene difluoride membranes. The membranes were blocked with Tris-buffered saline (EzTBS, Atto, Japan) containing 1% bovine serum albumin for 1 hour at room temperature, and incubated with one of the following primary antibodies: anti-phospho-extracellular-signal-related kinase (ERK) 1/2 (Cell Signaling Technology, Inc., USA), anti-ERK 1/2 (Santa Cruz Biotechnology Inc., Santa Cruz, CA, USA), anti-VEGF-A, anti-VEGF receptor (VEGFR) 2, anti-microtubule-associated protein 1 light chain (LC) 3B (Abcam, Cambridge, UK), or anti-β-actin (Santa Cruz Biotechnology Inc., Santa Cruz, CA, USA). Then, we performed a subsequent incubation using a specific secondary antibody conjugated to horseradish peroxidase. Bio-Rad Universal Hood II and Image Lab Software 6.0 (Bio-Rad Laboratories) were used to visualize and quantify the chemiluminescence, respectively.

Statistical analyses

All data are expressed as means±standard error of the mean (SEM) and tested for significance using one-way analysis of variance and Tukey's post-hoc test for inter-group differences. Non-normally distributed data were analyzed using the Mann–Whitney U test to determine the differences between two independent groups. The relationship between treatment effects and dosages was analyzed using simple linear regression and the Pearson correlation test. Significance was set at $P<0.05$.

Results

RV hemodynamic parameters and HR

The control rats had RVSP of 24.05 ± 1.00 mmHg and mean RVP of 5.88 ± 0.77 mmHg, whereas rats in the placebo group had higher RVSP and mean RVP of 70.46±2.00 mmHg and 25.03 ± 1.47 mmHg, respectively (Fig. 9A). Compared with placebo, the rats in sora-10 group had significantly lower RVSP (52.07 ± 6.67 mmHg), mean RVP (17.48 ± 1.84 mmHg), and HR (246.06 ± 15.39 bpm). By contrast, toce-10 did not significantly decrease the RVSP (69.65 ± 8.44 mmHg) nor mean RVP (22.20 ± 3.29 mmHg).

RV remodeling

Compared with the placebo (0.55 ± 0.03), sora-10 (0.38 ± 0.03), sora-30 (0.37 ± 0.04), and sora-100 (0.29 ± 0.03) significantly and dose-dependently ($R^2 = 0.35$, $P < 0.05$) reversed RVH (Fig. 9B). In the toceranib groups, a significant RVH reversal was observed only in the toce-10 (0.34 ± 0.04) group. Further, BNP mRNA expression as a RVH marker also exhibited a similar trend (Fig. 9C). Compared with the placebo with the highest BNP mRNA expression (0.53 ± 0.03), all doses of sorafenib, and toce-10 (0.26 ± 0.06) significantly and dose-dependently ($_{sorafenib}R^2:0.38$, $_{toceranib}R^2:0.27$, $P < 0.05$) downregulated the BNP mRNA expression.

Muscularization of 20–50 μm pulmonary arteries

Representative photomicrographs of NMPAs, PMPAs, and FMPAs are shown in Fig. 10A. The proportion of FMPAs in the placebo (43.13 ± 2.41%) was significantly increased after the MCT injection (Fig. 10B) to indicate an occurrence of pulmonary remodeling. Compared with the placebo, only the sora-100 group showed significant FMPA reduction (29.71 ± 2.14%), although treatments with sora-10 (39.88 ± 2.70%) and

sora-30 (38.07 ± 1.88%) insignificantly reduced the proportion of FMPAs. In the toceranib groups, neither dose significantly decreased the proportion of FMPAs. Furthermore, dose-dependent FMPA reduction was stronger in sorafenib (R^2 = 0.33, $P <$ 0.05) than in toceranib (R^2 = 0.01) (Fig. 10C). Besides, the proportion of NMPAs was significantly increased in all sorafenib groups and the toce-10 group (17.18 ± 1.02%). In this aspect, sorafenib and toceranib produced R^2 values of 0.51 and 0.34 ($P <$ 0.05), respectively (Fig. 10D). The proportion of PMPAs was significantly higher in the placebo (50.62 ± 2.75%) but did not differ significantly between the treatment and control groups.

Medial hypertrophy and lumen area of 20–50 μm FMPAs

In the placebo group, proliferation of smooth muscle cells increased the MWT ratio (49.91 ± 1.41%) and reduced the lumen area (224.03 ± 9.35 μm^2) of the 20–50 μm FMPAs (Fig. 11A, B). These values differed significantly from those in the control (MWT ratio = 34.38 ± 1.19%, lumen area = 399.15 ± 15.52 μm^2). In the treatment groups, all doses of sorafenib significantly reversed the medial hypertrophy and increased the lumen area. Although all doses of toceranib produced a significant MWT reduction, the increase in lumen area was significant only in the toce-10 group (293.66 ± 10.97 μm^2).

Medial hypertrophy and lumen area of 51–100 μm FMPAs

The 51–100 μm FMPAs of the placebo group also noticeably increased MWT ratios (54.73 ± 1.95%) and decreased lumen areas (842.64 ± 53.97 μm^2) (Fig. 11C, D). Both sorafenib and toceranib significantly reversed the MWT ratio and increased the lumen area of the FMPAs.

PDGFR-β, C-KIT, CXCR4, CXCL12 and nestin mRNA expression in the lungs

The pathogenic role of PDGFR-β in MCT-induced pulmonary remodeling was

shown by a significant, 3-fold mRNA upregulation in the placebo (0.090 ± 0.019) compared with that in the control (0.029 ± 0.004) (Fig. 12A). Except for the toce-1 group (0.048 ± 0.008), all treatment groups significantly normalized the mRNA expression to a level comparable with that of the control. Besides, the C-KIT mRNA level was higher in the placebo (0.038 ± 0.007) than that in the control (0.028 ± 0.005), although insignificantly (Fig. 12B). In the treatment groups, it was significantly decreased by sora-10 (0.019 ± 0.003), sora-30 ($0.017 \pm 0,005$), toce-3 (0.018 ± 0.005) and toce-10 (0.019 ± 0.003) compared with the placebo, indicating an inhibitory property against C-KIT by both TK inhibitors. The MCT treatment also upregulated the mRNA levels of the stem cell mobilizers: a 2-fold increase in CXCR4 (0.179 ± 0.044; $P = 0.196$) and a 3-fold increase in CXCL12 (0.241 ± 0.043; $P < 0.05$) (Fig. 12C), compared with that in the control (CXCR4: 0.088 ± 0.008; CXCL12: 0.070 ± 0.010). In the treatment groups, only sorafenib (sora-10: 0.075 ± 0.016; sora-30: 0.054 ± 0.007 and sora-100: 0.054 ± 0.005) significantly downregulated the CXCR4 mRNA. However, neither sorafenib nor toceranib significantly suppressed the CXCL12 mRNA levels, although both tended to reduce it. Further, the nestin mRNA levels did not vary significantly among the control (0.023 ± 0.002), placebo (0.023 ± 0.004), and treatment groups (Fig. 13D). However, compared with the placebo group, the toce-1 group insignificantly upregulated the mRNA level (0.031 ± 0.007).

VEGF signaling pathway in the lungs

Since sorafenib and toceranib are VEGFR inhibitors, we studied their inhibitory effects on mRNA and protein levels of VEGFR-2 (Fig. 13A, B) and VEGF-A (Fig. 13B, C) in the lungs. The MCT administration did not increase levels of VEGFR-2 mRNA

(0.272 ± 0.024) and protein (0.41 ± 0.07), nor VEGF-A mRNA (0.052 ± 0.008) and protein (0.138 ± 0.004) levels. The VEGFR-2 protein expression also did not remarkably differ among the treatment groups, although the sora-100 group showed a significant lower mRNA level (0.182 ± 0.026) than the placebo. With respect to the VEGF-A levels, sora-30 (mRNA = 0.024 ± 0.004, protein = 0.121 ± 0.001) and sora-100 (mRNA = 0.029 ± 0.004, protein = 0.117 ± 0.006) significantly suppressed the mRNA and protein levels. Although the mRNA levels were significantly reduced in the toce-3 (0.022 ± 0.004) and toce-10 (0.021 ± 0.022) groups, a significant protein reduction was observed only in the toce-10 group (0.155 ± 0.002) compared with the placebo.

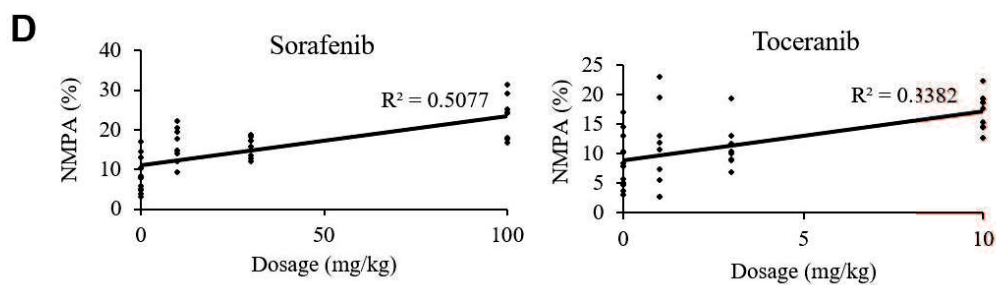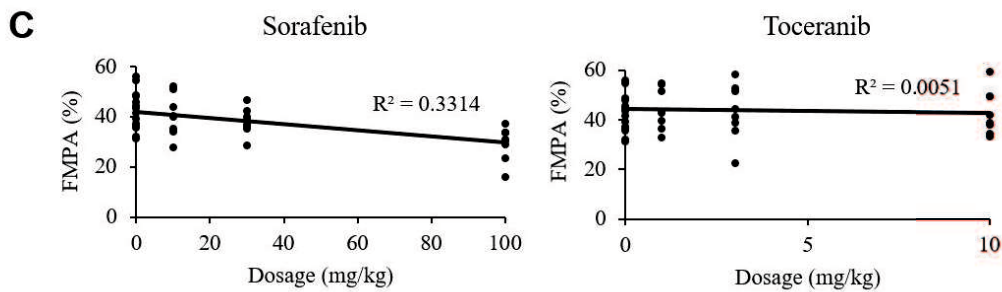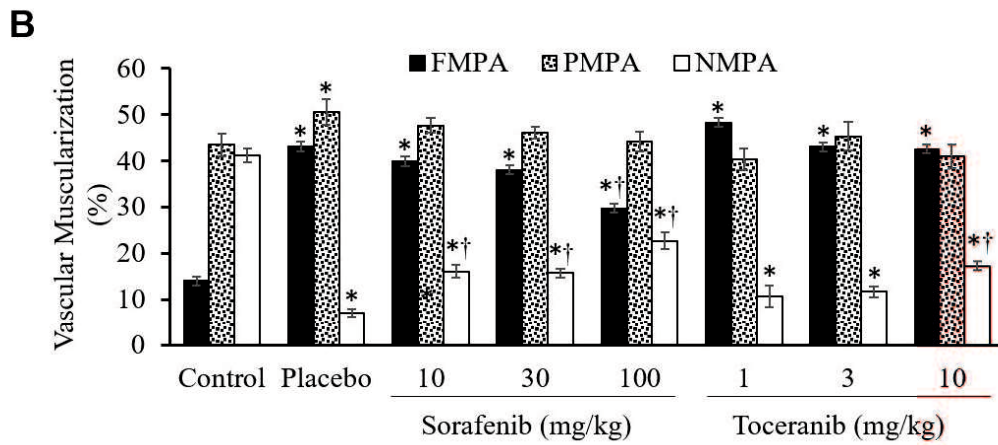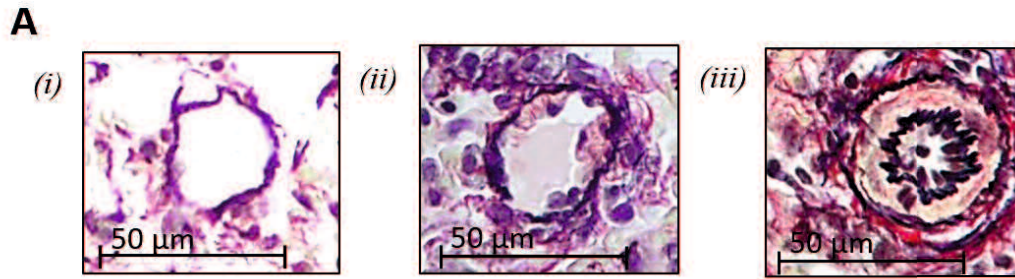**MAPK signaling pathway in the lung**

We investigated Raf-1 mRNA (Fig. 14A) and phosphorylated ERK-1/2 protein (Fig. 14B, C) expression, which constitute the MAPK signaling pathway. Compared with the control (0.066 ± 0.010), the placebo noticeably elevated the Raf-1 mRNA expression (0.150 ± 0.020). Downregulation of the mRNA was significant in the sora-30 (0.082 ± 0.012), sora-100 (0.058 ± 0.008), and toce-10 (0.097 ± 0.011) groups. Further, the dose-dependent Raf-1 inhibition of sorafenib ($R^2 = 0.27$, $P < 0.05$) was stronger than that of toceranib ($R^2 = 0.10$) (Fig. 14A). Phosphorylation of the ERK-1/2 protein was markedly upregulated in the placebo (2.82 ± 0.13) compared with the control (0.44 ± 0.17). In comparison with the placebo, all doses of sorafenib, but only toce-10 (1.42 ± 0.29) for the toceranib groups, significantly inhibited the ERK-1/2 phosphorylation. Notably, rats that received the lowest sorafenib dose (1.43 ± 0.36) had a phosphorylated protein level that is comparable with that received the highest toceranib dose, suggesting an equal inhibitory strength on the MAPK pathway by sorafenib and toceranib at 10 mg/kg.
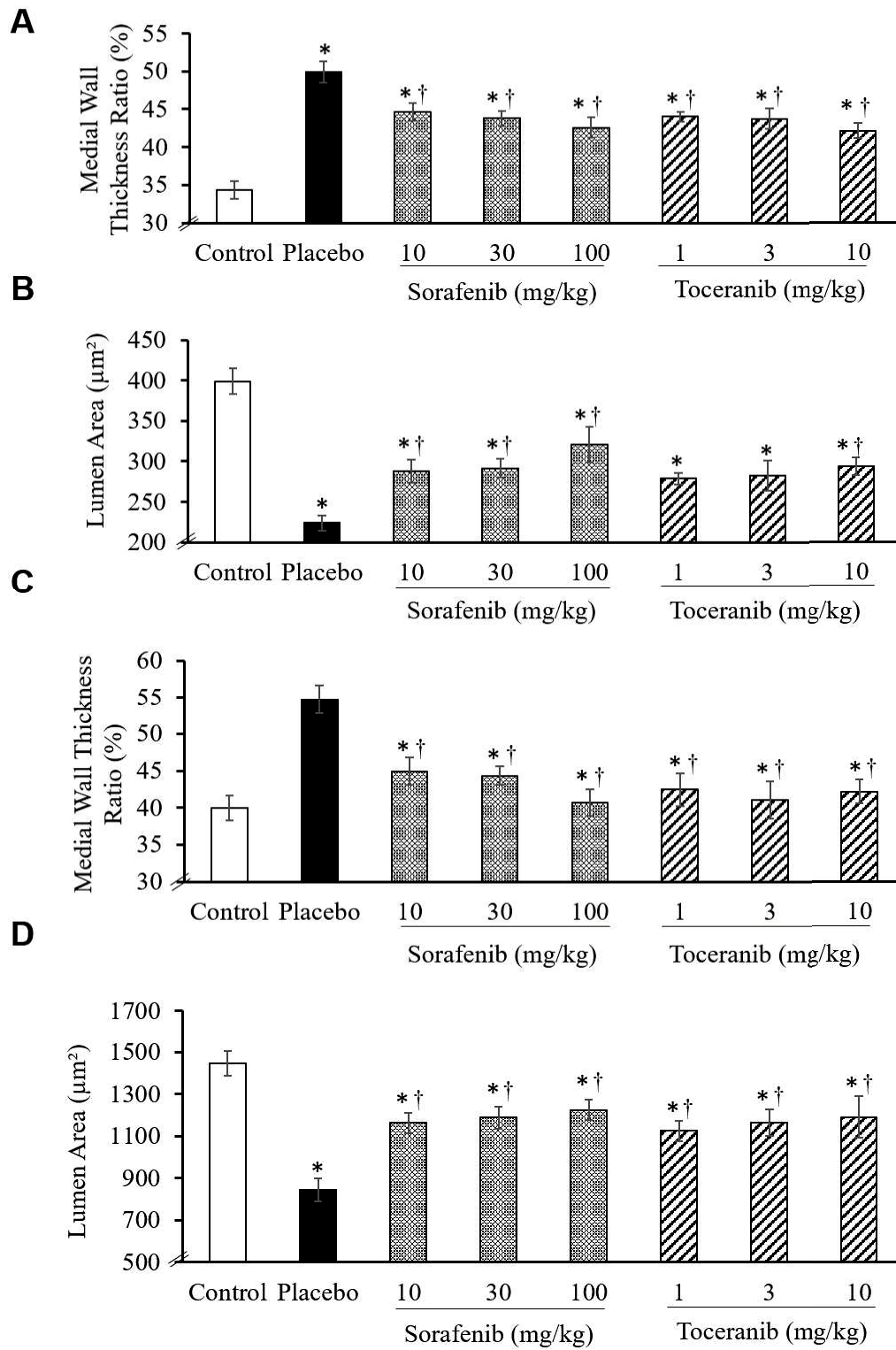
47

Autophagy markers in the lungs

Because LC3-1 detection is affected by many factors and LC3-II/LC3-I ratio is an unreliable indicator for autophagy [78], we compared the amount of LC3-II with β-actin. The LC3-II/β-actin protein level did not differ significantly between the control (0.34 ± 0.06) and placebo (0.37 ± 0.06) groups (Fig. 15A). Compared with the placebo, sora-10 (0.44 ± 0.04) and sora-30 (0.40 ± 0.07) tended to increase the protein level, whereas toce-3 (0.32 ± 0.05) and toce-10 (0.24 ± 0.04) tended to suppress the protein level. As for the p-62 mRNA levels, the control (0.217 ± 0.029), placebo (0.208 ± 0.030), toce-3 (0.254 ± 0.025), and toce-10 (0.249 ± 0.032) groups showed comparable levels (Fig. 15B). By contrast, sora-10 (0.324 ± 0.064; P=0.06) and sora-30 (0.362 ± 0.055; $P <$ 0.05) upregulated the mRNA levels, indicating a higher autophagy level in the rat lungs. Besides, sorafenib also produced a higher dose-dependency ($R^2 = 0.15$, $P < 0.05$) than toceranib ($R^2 = 0.02$).

A

B

C

49
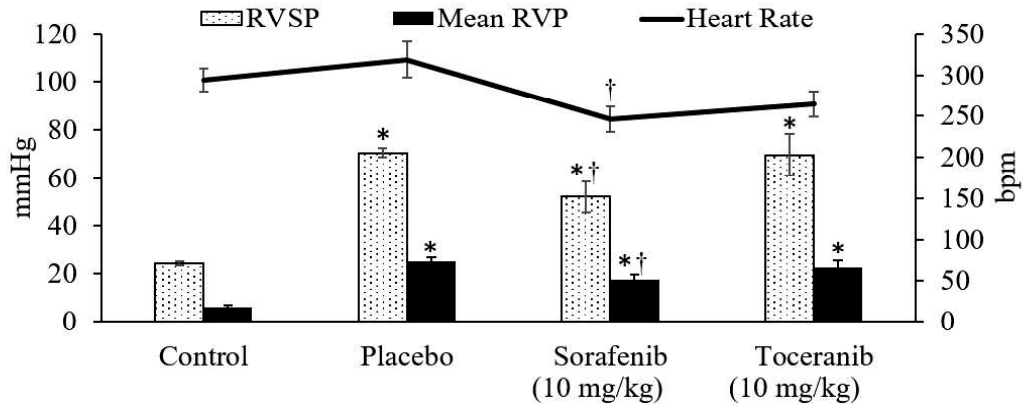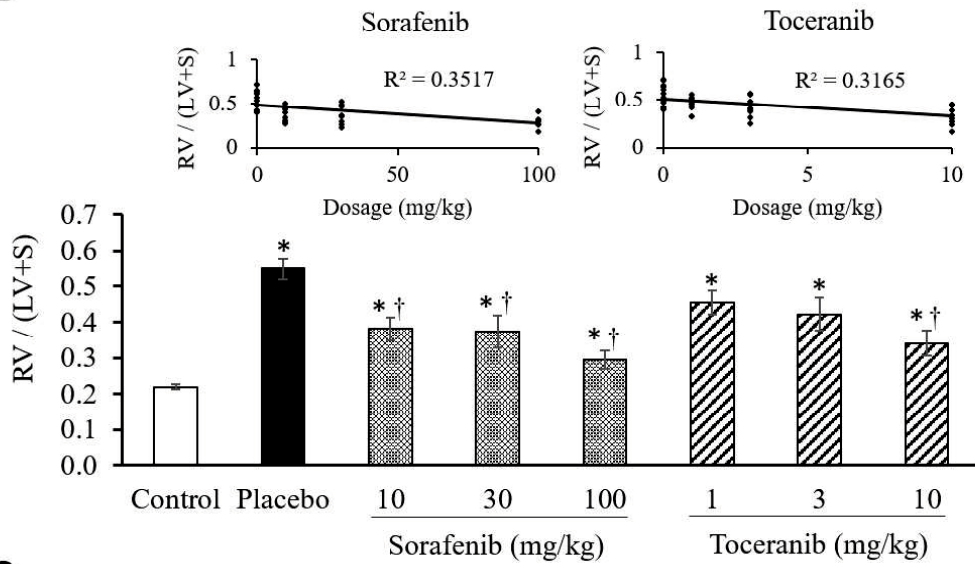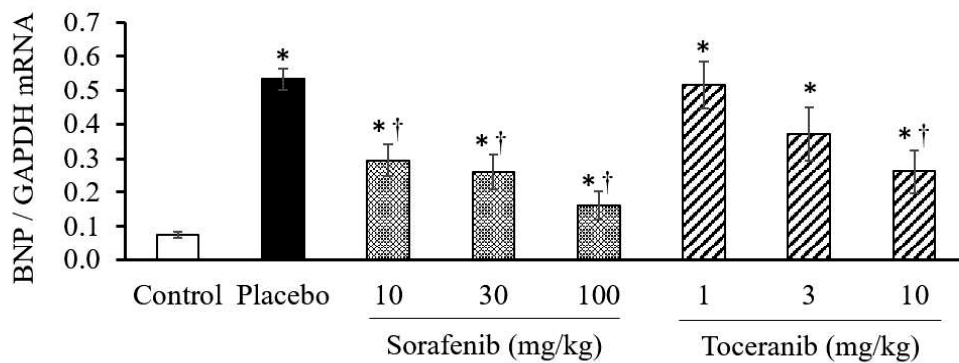
Fig. 9. Effects of sorafenib and toceranib on (A) right ventricular systolic pressure (RVSP), mean right ventricular pressure (RVP) and heart rate (n = 4 – 6), (B) right ventricular hypertrophy (RVH) and dose-dependent reversal (n = 8 – 14), and (C) b-type natriuretic peptide messenger RNA (mRNA) expression normalized to glyceraldehyde-3-phosphate dehydrogenase (GAPDH) of the right ventricle tissue (n = 8 – 14). Data are means $\pm$ standard error of mean (SEM). $*P < 0.05$ versus control, $\dagger P < 0.05$ versus placebo.

A

(i)   50 µm   *(ii)*   50 µm   *(iii)*   50 µm

B

Vascular Muscularization (%)

■ FMPA   ▥ PMPA   □ NMPA

Control   Placebo   10   30   100   1   3   10

Sorafenib (mg/kg)   Toceranib (mg/kg)

C

Sorafenib   Toceranib

FMPA (%) $R^2 = 0.3314$ FMPA (%) $R^2 = 0.0051$

Dosage (mg/kg)   Dosage (mg/kg)

D

Sorafenib   Toceranib

NMPA (%) $R^2 = 0.5077$ NMPA (%) $R^2 = 0.3382$

Dosage (mg/kg)   Dosage (mg/kg)

51

Fig. 10. Effects of sorafenib and toceranib on vascular muscularization in 20–50 μm intra-acinar arteries. (A) Photomicrographs represent intra-acinar pulmonary arteries that are (i) non-muscularized (NMPA), (ii) partially muscularized (PMPA), and (iii) fully muscularized (FMPA). (B) Proportion of each artery type related to the total number of pulmonary arteries. Dose-dependent reversal of sorafenib and toceranib on (C) FMPAs and (D) NMPAs are shown. Data are means ± SEM (n = 8 – 12). *$P < 0.05$ versus control, †$P < 0.05$ versus placebo.

A

Medial Wall Thickness Ratio (%)

Control Placebo | 10 30 100 | 1 3 10
Sorafenib (mg/kg) | Toceranib (mg/kg)

B

Lumen Area (μm²)

Control Placebo | 10 30 100 | 1 3 10
Sorafenib (mg/kg) | Toceranib (mg/kg)

C

Medial Wall Thickness Ratio (%)

Control Placebo | 10 30 100 | 1 3 10
Sorafenib (mg/kg) | Toceranib (mg/kg)

D

Lumen Area (μm²)

Control Placebo | 10 30 100 | 1 3 10
Sorafenib (mg/kg) | Toceranib (mg/kg)

Fig. 11. Effects of sorafenib and toceranib on (A, C) medial wall thickness normalized to the external diameter and (B, D) lumen area of the (A, B) 20–50 μm and (C, D) 51–100 μm FMPAs, respectively. Data are means ± SEM (n = 8 − 12). *$P < 0.05$ versus control, †$P < 0.05$ versus placebo.

A
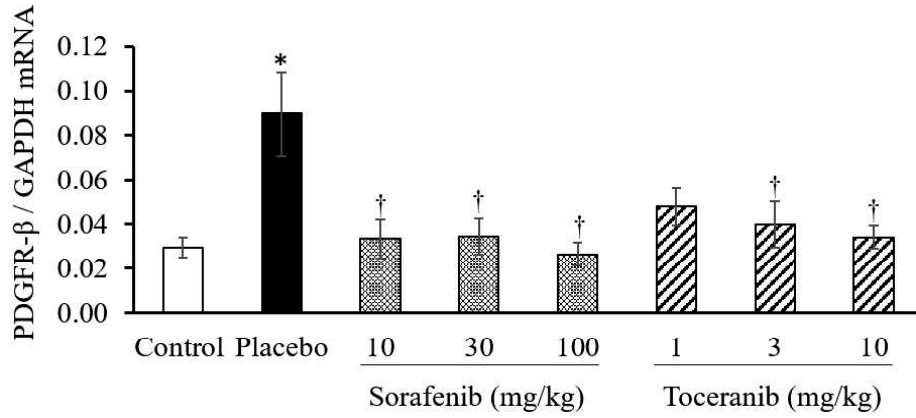
B
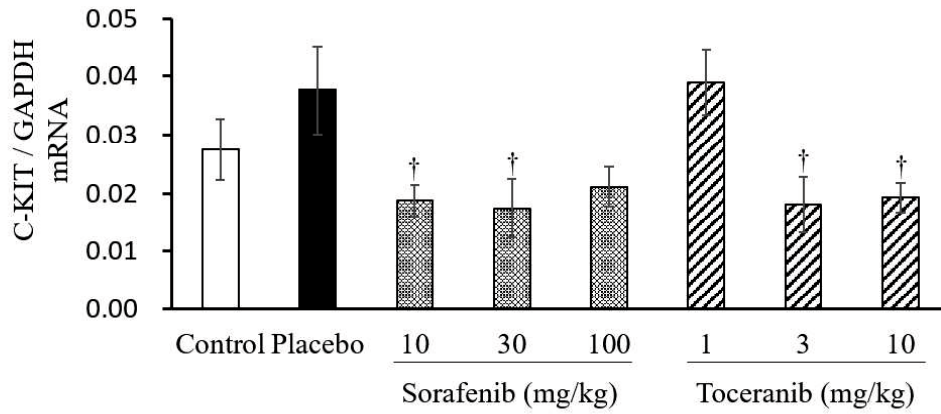
C
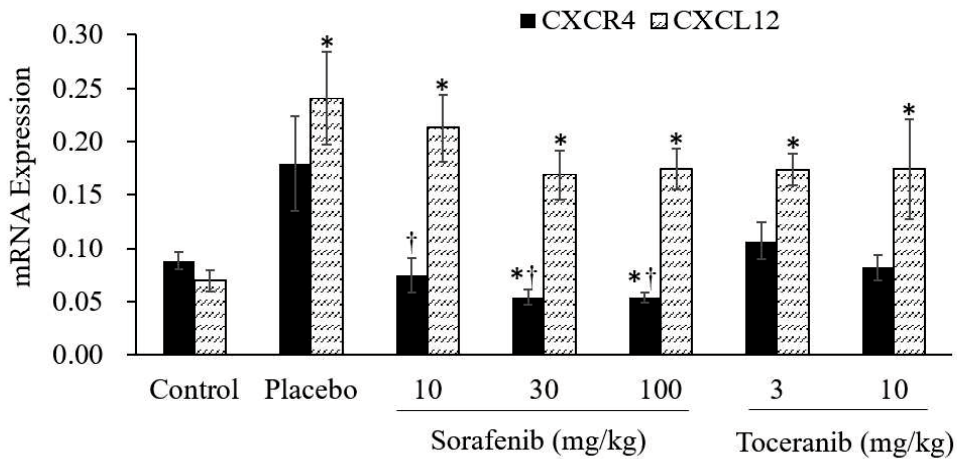
Fig. 12. Effects of sorafenib and toceranib on monocrotaline-induced mRNA expression of (A) platelet-derived growth factor receptor-β (PDGFR-β) (n = 8 − 14), (B) KIT proto-oncogene receptor tyrosine kinase (C-KIT) (n = 8 − 10), (C) C-X-C chemokine receptor type 4 (CXCR4) (n = 8 − 11) and ligand 12 (CXCL12) (n = 8 − 12) in rat lungs. Data are means ± SEM. *$P < 0.05$ vs control, †$P < 0.05$ vs placebo.

A

B

C

D
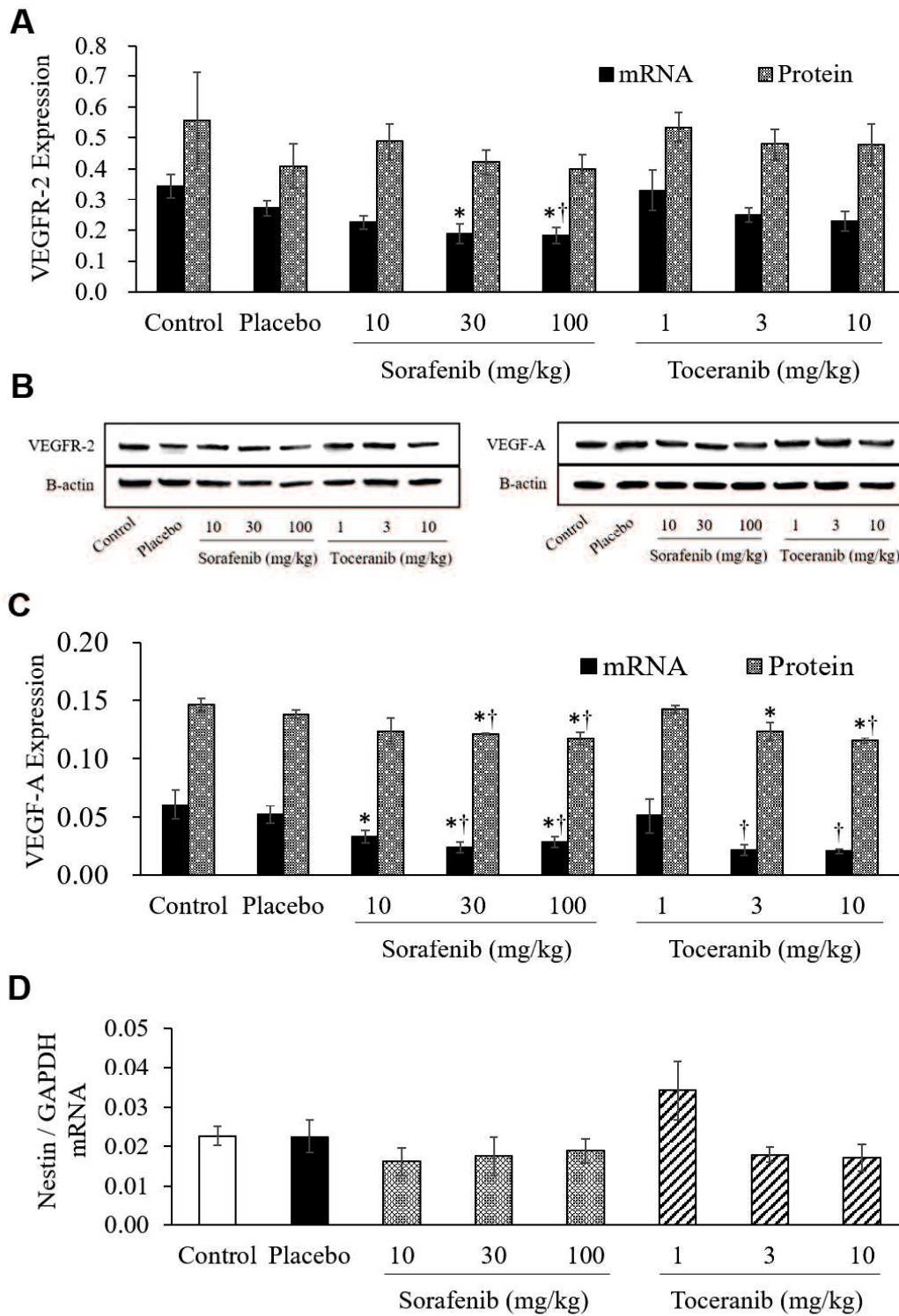
Fig. 13. Effects of sorafenib and toceranib on monocrotaline-induced vascular endothelial growth factor (VEGF) signaling pathway (A, B, C) and nestin mRNA expression (n = 8 −14) (D) in rat lungs. The VEGF signaling pathway is represented by (A) VEGF receptor-2 (VEGFR-2) mRNA (n = 8 − 12) and protein expression (n = 4 − 5), and (C) VEGF-A mRNA (n = 7 − 9) and protein expression (n = 3 − 4). (B) Western blots represent VEGFR-2 and VEGFR-A protein expression of one individual from each group. Data are means ± SEM. *$P < 0.05$ versus control, $^{†}P < 0.05$ versus placebo.

A

B

C

59
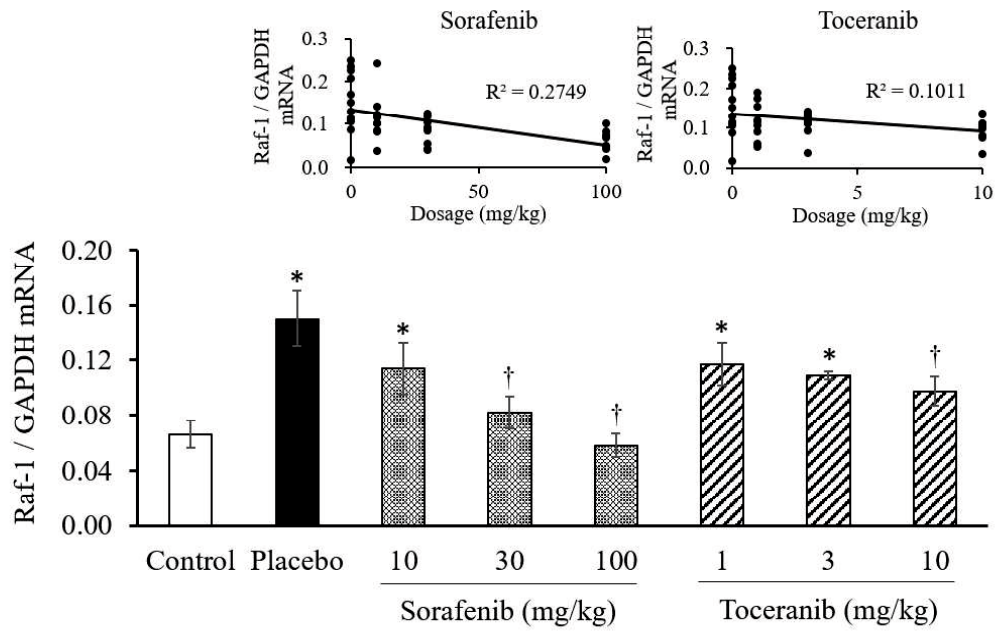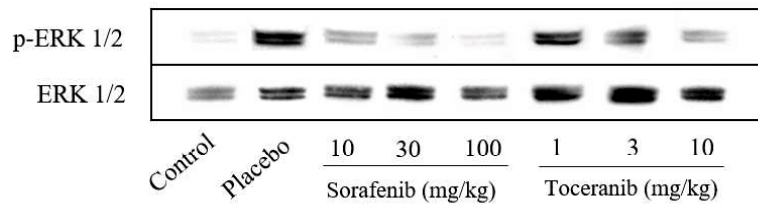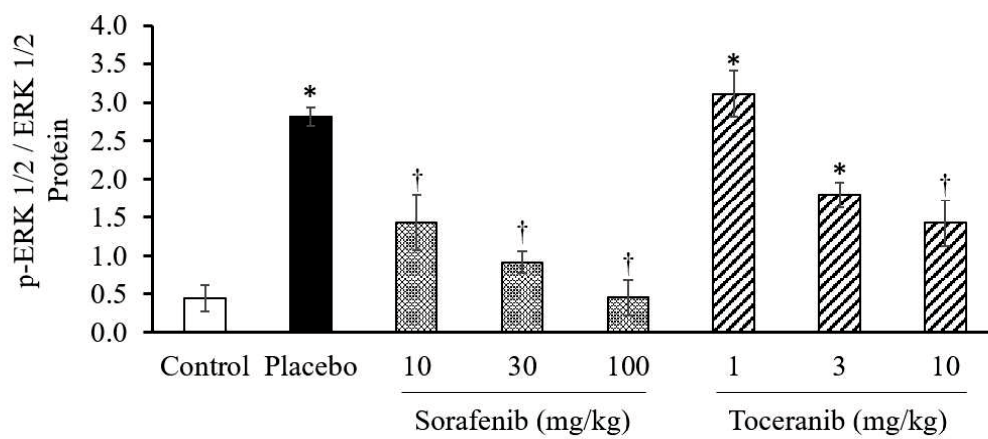
Fig. 14. Effects of sorafenib and toceranib on mitogen-activated protein kinase signaling in rat lungs, indicated by (A) Raf-1 proto-oncogene serine/threonine kinase (Raf-1) mRNA expression (n = 8 − 14) and (C) extracellular-signal-related kinase (ERK)-1/2 protein phosphorylation. (B) Western blots represent phosphorylated versus total ERK protein of one individual from each group (n = 3 − 4). Data are means ± SEM. *$P < 0.05$ versus control, $^{\dagger}P < 0.05$ versus placebo.

A
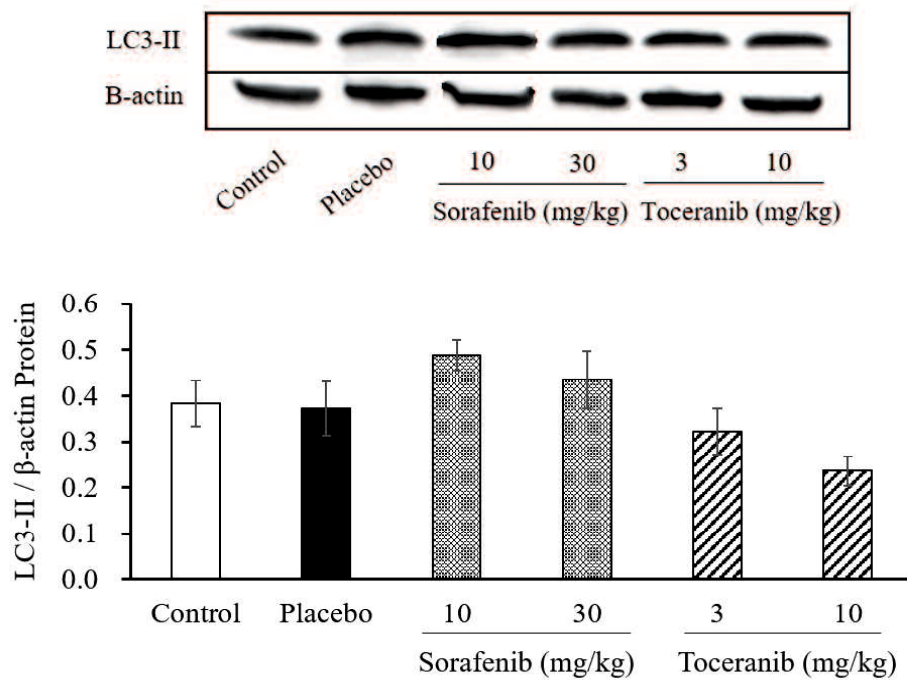
B
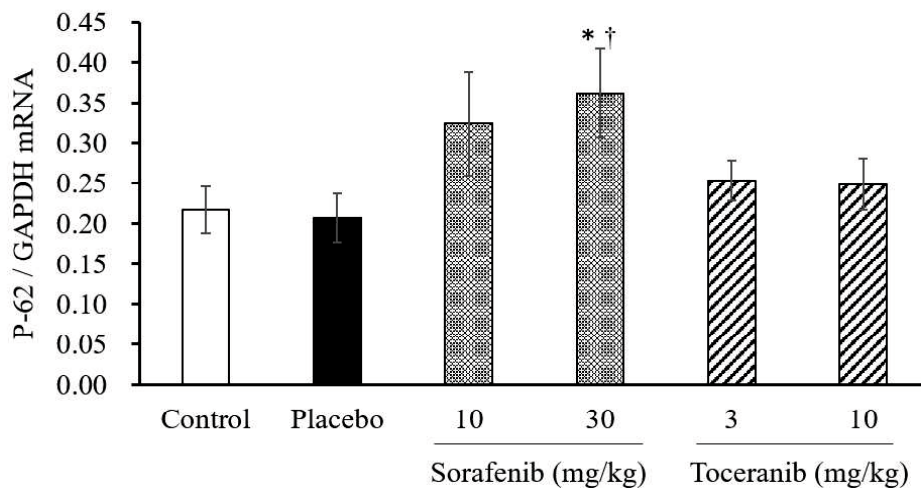
Fig. 15. Effects of sorafenib and toceranib on expression of (A) microtubule-associated protein 1 light chain (LC) 3-II protein normalized to β-actin (n = 5 − 6), and (B) p-62 mRNA (n = 8 − 17). (A) Western blots represent LC3-II protein expression of one individual from each group. Data are means ± SEM. *$P < 0.05$ versus control, †$P < 0.05$ versus placebo.

Discussion

This study is the first to demonstrate the reversal effects of toceranib on MCT-induced pulmonary arterial hypertension and cardiopulmonary remodeling in rats. Our results show that treatment with a high dose of toceranib (10 mg/kg) led to only a partial inhibition of pulmonary muscularization without improving the RV hemodynamic outcomes, whereas treatment with low doses (1 and 3 mg/kg) yielded insignificant anti-remodeling effects on RV and pulmonary muscularization. Besides, we also confirm the potent cardiopulmonary reversal effects of sorafenib. A low-dose sorafenib therapy (10 mg/kg) significantly improved PAH not only via a potent inhibition on the MAPK but also the CXCL12/CXCR4 signaling pathways, as well as an autophagy induction in the lungs.

Toceranib phosphate is a veterinary TK inhibitor licensed for the treatment of canine mast cell tumors. In terms of kinase selectivity, toceranib targets PDGFR-β, VEGFR-2, and C-KIT receptors and has cellular half-maximal inhibitory concentrations of 0.01–0.1, 0.005–0.05, and 0.01–0.1 μM, respectively [79]. Sorafenib has a wider activity spectrum that inhibits not only C-KIT, VEGFR-2, and PDGFR-β but also serine/threonine kinase Raf-1 [48]. Consistently, rats that received any dose of sorafenib, and 3 or 10 mg/kg of toceranib had lower PDGFR-β and C-KIT mRNA levels. Notably, the PDGFR-β mRNA downregulation by toceranib was weaker than sorafenib. Expectedly, the Raf-1 inhibiting sorafenib resulted in a greater inhibition on the Raf-1 mRNA than toceranib.

In beagle dogs receiving a 14-day course of an anti-neoplastic toceranib dose (3.25 mg/kg, orally, every other day), it achieved elimination half-life ($T_{1/2}$) of 17.2 ± 3.9

62

hours, time to maximum plasma concentration (Tmax) of 6.2 ± 2.6 hours, and area under the plasma concentration time-curve (AUC_{0-48}) of 2640 ± 940 ng·h/ml [80]. By contrast, the 14-day therapy with a low-dose sorafenib (100 mg, orally, twice daily) in the Japanese patients yielded mean $T_{1/2}$ of 27.1 hours, Tmax of 4 hours, and AUC_{0-12} of 9400 ng·h/ml [81]. The pharmacokinetic differences imply that a further increment in the toceranib dose may augment the reversal potency by optimizing the drug exposure to a level that is comparable to that of sorafenib. However, the full-blown toxicity and side effects associated with the dose escalation may raise a safety concern.

With respect to pulmonary arterial remodeling, we showed that sorafenib dose-dependently reversed muscularization by increasing the proportion of NMPAs. This reversal achieved a statistical significance even in rats that received the lowest dose (10 mg/kg) and confirmed the results by Klein et al. [26]. However, a high dose (10 mg/kg) of toceranib was required to produce a significant increase in NMPAs. In addition, low, medium, and high doses of sorafenib dose-dependently reduced the proportion of FMPAs by 7.5%, 11.7%, and 31.1%, respectively. Conversely, in the toceranib groups, the high dose normalized the FMPAs by 1.4%, whereas the low dose caused an additional increase of 12%. The above findings may explain the reason of an insignificant reduction in RVSP and mean RVP in the rats at the highest dose of toceranib. Further, the increase in the lumen area of the 20–50 μm FMPAs and the insignificant ERK 1/2 de-phosphorylation in the toce-1 and toce-3 groups also indicate that toceranib has a weak reversal effect on pulmonary remodeling when administered at lower doses.

Moreno-Vinasco et al. [66] showed that sorafenib administered at a dose of 2.5 mg/kg significantly reversed RVH and pulmonary arterial muscularization, and improved

RV systolic pressure in rats subjected to hypoxia alone or combined hypoxia and SU5416 treatments. However, rats in the placebo had a RVH index of approximately 0.4 and a mean RVSP of less than 30 mmHg, which collectively indicated a mild PAH. In the present study, we documented a greater RVSP (70.46 ± 2.00 mmHg) and a higher RVH index (0.55 ± 0.03) in the placebo rats, indicating that a severe PAH occurred 28 days after the MCT administration. This finding also agreed with the results of studies by Schermuly et al. [10] and Klein et al. [26], which reported RVH indexes of 0.71 ± 0.03 (RVSP > 60 mmHg) and 0.51 ± 0.02 (RVSP = 82.9 ± 6.0 mmHg), respectively. Therefore, we believe that the dose of 2.5 mg/kg may be too low for effective cardiopulmonary reversal, at least for the MCT-induced severe PAH model.

We previously showed that potent VEGF signaling inhibition by sunitinib elevated nestin mRNA levels, exacerbated vascular remodeling, and caused an on-going angiogenesis [67]. In the present study, sorafenib exhibited an inhibitory trend on pulmonary VEGFR-2 and VEGF-A transcripts, and caused a significant suppression on VEGF-A protein level, which were consistent with the results by Moreno-Vinasco et al. [66]. However, an escape angiogenesis [59] did not occur in these groups. Instead, all of the sorafenib groups showed significant ERK 1/2 de-phosphorylation and low nestin mRNA levels. This was further evident by the concurrent low level of the CXCR4 mRNA, a vascular marker for vessel sprouting [82, 83] and the main inducer of vasculogenesis [84] in the sorafenib groups. We speculate that sorafenib preserves its potent anti-remodeling property via direct Raf-1 inhibition which cuts the entry signal [50] from the VEGFR-2 to the downstream MAPK pathway [49]. On the contrary, the potent VEGFR-2 inhibitor toceranib surprisingly did not significantly reduce pulmonary VEGFR-2

mRNA nor protein levels, and only the highest dose significantly suppressed VEGF-A protein expression. We also observed no significant nestin nor CXCR4 mRNA upregulation in the toceranib groups to indicate small vessel proliferation [52, 53, 58] or sprouting [82, 83] in the lungs. Taken together, these results suggest that the weak reversal effects of toceranib on pulmonary remodeling may not be due to VEGF signaling inhibition.

Because the lowest sorafenib dose and the highest toceranib dose yielded comparable phosphorylated ERK protein levels, we speculated that the stronger reversal effects by sorafenib compared with toceranib might be also governed by other mechanisms or pathways, in addition to the MAPK pathway. Long et al. [76] showed that rats treated for 3 weeks with MCT had an increased LC3B-II level in the small pulmonary arterial walls and a decreased p-62 staining in the medial layer of FMPAs. However, a recent study of Sugen/hypoxia-induced PAH by Kato et al. [74] revealed that the autophagy in endothelial cells was time-dependent, in which the LC3 level decreased by 3 weeks after an initial increase, and rapamycin as an autophagy activator ameliorated PAH and CPR. Consistent with the above finding, we showed that the MCT-treated rats did not upregulate the LC3-II protein nor p-62 transcript levels, suggesting the presence of apoptosis-resistant cells [74] at 4 weeks after the MCT injection. In the treatment groups, sorafenib but not toceranib increased the LC3-II protein and p-62 mRNA expression, implying an autophagy induction in the lungs by sorafenib, probably via inhibition on the PI3K/AKT/mTOR signaling pathway [71, 73]. Furthermore, while Lin et al. [71, 72] showed that sorafenib influenced interleukin secretion and function of dendritic cells and macrophages, several studies reported that the CXCL12/CXCR4

65

inhibition improved hypoxia-induced PAH [77, 85, 86]. The present study is the first to document that the MCT treatment upregulated the CXCL12/CXCR4 transcript levels, suggesting a pathogenic role of this pathway in the MCT-induced PAH. With respect to this, since the CXCR4 mRNA downregulation was greater in sorafenib than in toceranib, we speculate that sorafenib may also ameliorate PAH by blocking the CXCR4/SDF-1 signaling which further suppressed recruitment of PDGF and C-KIT receptors in the lungs [87].

The present study has some limitations as we did not evaluate the PI3K/AKT/mTOR and adenosine monophosphate-activated protein kinase (AMPK) signaling pathways which may further elucidate the reversal differences between sorafenib and toceranib. However, the above results led us to believe that sorafenib strongly reversed PAH and CPR by not only mainly blocking the MAPK, but also the CXCL12/CXCR4 signaling, and inducing autophagy in the apoptosis-resistant pulmonary tissues.

In conclusion, toceranib showed weaker reversal effects on cardiopulmonary remodeling and RV hemodynamic improvement compared with sorafenib. A high dose (10 mg/kg) of toceranib partially ameliorated pulmonary arterial muscularization but did not improve PAH, precluding the use of toceranib in the treatment of PAH. On the contrary, despite the stronger VEGF inhibitory activity in the lungs, sorafenib did not exaggerate but significantly and dose-dependently reversed cardiopulmonary remodeling and PAH at even a low dose (10 mg/kg). This may be due to the concurrent potent inhibition on Raf-1 kinase and CXCR4, and possibly the autophagy-inducing property of sorafenib, which made a low dose suitable for the treatment of PAH.

Chapter 3

Effects of masitinib compared with tadalafil

for the treatment of monocrotaline-induced pulmonary

arterial hypertension in rats

Introduction

Pulmonary arterial hypertension (PAH) is a complex disease, which comprises remodeling [25] and imbalance of constriction-dilation tonus [88] of the pulmonary vasculature. In an effort to improve response rates and to prolong survival times in patients with PAH, combination therapy has emerged as an alternative to the conventional vasodilator monotherapy [7] which is no longer recommended for patients newly diagnosed with classic forms of PAH [8]. Nevertheless, the lack of a potent anti-remodeling ability of endothelin receptor antagonists, phosphodiesterase-5 inhibitors, guanylate cyclase stimulators, and prostacyclin derivatives which constitute the current treatment algorithm [8] remains an inconvenient truth.

Vascular remodeling, an important aspect of the PAH pathobiology, is driven by a dysregulated signaling from various pathways [8], particularly the mitogen-activated protein kinase (MAPK) pathway [89]. While searching for the MAPK-targeting tyrosine kinase inhibitors which potently reverse the cardiopulmonary remodeling, we demonstrated that lower doses of imatinib [67] and sorafenib [90] ameliorated pulmonary vascular remodeling and right ventricular (RV) hypertrophy in rats with monocrotaline (MCT)-induced PAH. Hemodynamically, the low-dose sorafenib also decreased the RV systolic pressure (RVSP) in the rats [90], whereas the low-dose imatinib improved the RV hemodynamics in humans [40] and dogs [39, 91].

Masitinib, a C-KIT and platelet-derived growth factor receptor (PDGFR) inhibitor, is approved for the treatment of canine mast cell tumors [92]. In one study, masitinib improved RV contractility and reversed pulmonary medial hypertrophy in rats with PAH at a dose of 50 mg/day/head [93]. However, the reversal and safety profiles of masitinib

at lower therapeutic doses were unaddressed. Because masitinib is safer and more potent than imatinib [94], we hypothesized that low-dose masitinib therapy may be an effective treatment for PAH, while avoiding the side effects of a neoplastic therapeutic dose.

Tadalafil, a phosphodiesterase (PDE)-5 inhibitor, prevents hydrolysis of cyclic guanosine monophosphate (cGMP) to 5'-GMP and causes pulmonary artery vasodilation [95]. As the FDA-approved drug for the PAH treatment [95], the beneficial effects of tadalafil on PAH hemodynamics have been extensively reported [96, 97, 98, 99]. There was a recent report on the reversal abilities of sildenafil, another PDE-5 inhibitor against pulmonary remodeling that acts by antagonizing KIT proto-oncogene receptor tyrosine kinase (C-KIT) and CXC chemokine receptor (CXCR) 4 [100]. However, the cardiopulmonary reversal properties of tadalafil remain unclear, and were therefore given focus in the present study. We also compared the long-term survival benefit in rats treated with masitinib versus tadalafil to determine if the low-dose masitinib was non-inferior than tadalafil for the treatment of PAH.

Methods and materials

Monocrotaline-induced PAH and treatments

The use of Wistar-Imamichi rats in the study was in accordance to the Institutional Animal Care and Use Committee of the Tottori University, as described in the previous chapters. To induce PAH, the placebo and treatment rats were injected with monocrotaline (MCT, 60 mg/kg, Sigma-Aldrich, China), subcutaneously. Rats in the normal group received physiologic saline. Fourteen days after injection, the treatment rats were medicated with masitinib [Masivet 50 mg, AB Science, France: 5 (masi-5), 15 (masi-15), or 50 (masi-50) mg/kg per day] or tadalafil [Tadacip 20 mg, Cipla Ltd, India: 5 (tada-5) or 10 (tada-10) mg/kg per day]. In the control and placebo groups, the rats were given water. The treatments were administered orally, once daily, for 14 days. To compare the long-term survival rate between the masi-15 and tada-10 groups, the treatments were extended for an additional 14 days to reach the end point.

Hemodynamic measurements

To measure the right ventricular systolic (RVSP), mean pressure (mRVP) and heart rate (HR), a polyethene catheter (PE-50 Intramedic PE tubing, Becton Dickinson) was inserted into the right jugular vein and advanced to the RV of the isoflurane-anesthetized rats. The data were recorded and analyzed with the PowerLab System connected to a pressure transducer (ADInstruments).

Assessment of RVH

The RV tissue was separated from the left ventricle and septum (LV+S). Wet weights of the RV and LV+S were used to obtain the RVH index, calculated by [RV/(LV+S)].

Assessment of pulmonary arterial remodeling

Pulmonary arterial vascularization was assessed from the left lung lobes stained with elastic van Gieson (EVG). The number of small pulmonary arteries (20–50 μm) that were fully (FMPA), partially (PMPA), and non-muscularized (NMPA) were counted as described previously. Using Image J software, the FMPA of 20–50 μm and 51–100 μm in diameter were examined further to measure the external diameter (d), medial wall thickness (MWT), MWT ratio ($2 \times$ MWT $/ d \times 100\%$), lumen diameter ($d - 2 \times$ MWT), and lumen area [$3.142 \times (d/2)^2$].

Fast real-time polymerase chain reaction

The expression levels of the target messenger RNAs (mRNAs) in the RV tissues and the right caudal lung lobes were determined by Applied Biosystems 7500 Fast Real-Time PCR System using TB Green Fast qPCR Mix (Takara Bio Inc., Shiga, Japan). In addition to the previously described mRNAs, phosphodiesterase (PDE) 5 (forward: TCCCCGGTTCAATGCAGAAG; reverse: GATGGCCTGAGCTACACCAA) expression levels were also determined.

Western blotting assay

The procedures were carried out as described previously.[6-7] Lysates containing 50 μg total protein from the right caudal lung lobes were electrophoresed on 4–15% sodium dodecyl sulfate-polyacrylamide gels (Mini-PROTEAN® TGX™ Precast Protein Gels, Bio-Rad, USA) and transferred to polyvinylidene difluoride membranes. The membranes were blocked with Tris-buffered saline (EzTBS, Atto, Japan) containing 1% bovine serum albumin for 1 hour at room temperature, and then incubated with anti-phospho-extracellular-signal-related kinase (ERK) 1/2 (Cell Signaling Technology, Inc.,

USA) or anti-ERK 1/2 (Santa Cruz Biotechnology Inc., Santa Cruz, CA, USA) for 5 hours at room temperature, followed by a specific secondary antibody. The antibody-antigen complexes were visualized using Bio-Rad Universal Hood II whereas the protein expression was quantified using Image Lab Software 6.0 (Bio-Rad Laboratories).

ELISA measurement of pulmonary cyclic guanosine monophosphate (cGMP)

The frozen right lung tissues were homogenized in 0.1M hydrochloric acid. The supernatant was collected for the enzyme-linked immunosorbent assay (ELISA) using cGMP Direct Immunoassay Kit (abcam, United Kingdom), in accordance to the manufacturer's instructions. Absorbance was read at 450 nm by an IMark^{TM} microplate reader (Bio-Rad Laboratories, Japan) and a standard curve was constructed to give readings of the cGMP (ρmol/g).

Statistical analyses

For inter-group comparisons, we conducted one-way analysis of variance followed by Fisher's Least Significant Difference post-hoc tests. Non-normally distributed data were analyzed using the Mann–Whitney U test. The dose-effect relationship was determined by simple linear regression and the Pearson correlation test. Data are presented as means ± standard error of the mean (SEM) and considered statistically significant at $P < 0.05$.

Results

Masitinib versus tadalafil treatments on the RV hemodynamics and heart rate (HR)

The placebo rats showed significantly increased RVSP (69.20 ± 2.07 mmHg) and mRVP (25.57 ± 1.31 mmHg) (Fig. 16A), compared with the normal rats (RVSP: 22.96 ± 1.12 mmHg; mRVP: 7.24 ± 1.20 mmHg). Although the reduction in mRVP was insignificant in the treatment groups, the masi-15 (51.97 ± 5.33 mmHg), masi 50 (40.26 ± 7.01 mmHg), tada-5 (51.08 ± 5.30 mmHg), and tada-10 (52.38 ± 3.17 mmHg) rats exhibited significantly reduced RVSP, compared with the placebo group. Further, all groups had comparable HRs (Fig. 16B).

Masitinib versus tadalafil treatments on the RVH and RV BNP mRNA expression

As expected, the rats in the placebo group had the highest RVH indices (0.55 ± 0.02), indicating severe enlargement of the RV (Fig. 16C). In the treatment groups, the masi-15 (0.44 ± 0.03), masi-50 (0.42 ± 0.04), and tada-10 (0.49 ± 0.01) groups significantly reversed RVH, compared with the placebo group. Further, masitinib (R^2: 0.24; $P < 0.05$) elicited a stronger dose-dependency than tadalafil (R^2: 0.17; $P < 0.05$).

The above findings were further supported by the BNP mRNA expression as a cardiac remodeling biomarker (Fig. 16D). The mRNA expression remained low in the normal group (0.05 ± 0.01) but was significantly upregulated in the placebo group (0.58 ± 0.04). In the treatment groups, the masi-15 (0.45 ± 0.03), masi-50 (0.31 ± 0.05), and tada-10 (0.53 ± 0.04) significantly downregulated mRNA expression compared with placebo. In addition, masitinib (R^2: 0.31; $P < 0.05$) also exhibited a stronger dose-dependency than tadalafil (R^2: 0.02).

Masitinib versus tadalafil treatments on remodeling in 20-50 μm pulmonary arteries

(a) Degree of muscularization

The normal rats had the highest percentage NMPA (41.14 ± 2.99%) whereas the placebo group had significantly fewer thin-walled PAs (10.72 ± 1.90%) (Fig. 17A). Compared with the placebo, the masitinib therapy significantly increased the NMPA percentage in a dose-dependent (R^2: 0.46; $P < 0.05$) manner (masi-5: 15.81 ± 1.07%; masi-15: 20.61 ± 0.84%; masi-50: 25.13 ± 2.33%). By contrast, the tadalafil treatment had a weaker dose-dependency (R^2: 0.16; $P < 0.05$), and neither the tada-5 (12.65 ± 0.97%) nor the tada-10 (15.74 ± 1.12%) significantly increased the NMPA percentage.

The MCT-injection also significantly increased the FMPA percentage in the placebo (53.29 ± 2.07%) compared with the normal group (17.23 ± 1.53%), implying a marked appearance of remodeled PAs in the placebo. While the FMPA percentage was markedly decreased in all treatment groups, the masitinib-treated rats (masi-5: 42.84 ± 2.78%; masi-15: 36.64 ± 2.41%; masi-50: 33.70 ± 3.46%) showed a lower FMPA percentage and a higher dose-dependency (R^2: 0.31; $P < 0.05$) than the tadalafil-treated rats (tada-5: 44.53 ± 2.02%; tada-10: 46.02 ± 0.65%; R^2: 0.22; $P < 0.05$).

(b) Medial wall thickness (MWT) ratio, lumen diameter, and lumen area.

The detailed analysis of the FMPA (Fig. 17B) showed noticeable medial hypertrophy in the placebo group, indicated by an increased MWT ratio (45.38 ± 1.02%) compared with the normal group (31.73 ± 1.22%). In the treatment groups, a significant reversal was observed in the masi-15 (40.90 ± 0.68%), masi-50 (39.50 ± 1.49%), tada-5 (41.45 ± 0.78%), and tada-10 (40.13 ± 0.56%) groups.

The lumen diameter (18.32 ± 0.33 μm) and area (280.68 ± 8.14 μm²) of the FMPA in the placebo group (Fig. 17C) were also significantly decreased, compared with those of the normal group (diameter: 22.94 ± 0.59 μm; area: 444.89 ± 22.75 μm²). Except the masi-5, all treatment groups increased the lumen diameter and area. With this respect, the tada-5 (diameter: 19.88 ± 0.27 μm; area: 326.36 ± 8.51 μm²) and tada-10 (diameter: 20.73 ± 0.37 μm; area: 356.82 ± 13.40 μm²) treatments possessed a weaker reversal effect than the masi-15 (diameter: 21.03 ± 0.38 μm; area: 368.24 ± 12.50 μm²) and masi-50 (diameter: 21.06 ± 0.56 μm; area: 368.41 ± 19.32 μm²) treatments.

Masitinib versus tadalafil treatments on remodeling in 51-100 μm pulmonary arteries

In the placebo group, the 51-100 μm pulmonary arteries developed pathological changes, as indicated by a significantly increased MWT ratio (40.80 ± 1.04%), lumen diameter (38.34 ± 0.86 μm), and lumen area (1254.89 ± 57.54 μm²), compared with those of the normal rats (MWT ratio: 33.14 ± 1.90%; lumen diameter: 46.73 ± 1.42 μm; lumen area: 1868.95 ± 114.00 μm²) (Fig. 18A, B, C). Although neither the masitinib nor tadalafil treatments significantly reversed the MWT ratio, a significant reduction in lumen area was observed in the masi-15 (42.51 ± 0.69 μm), masi-50 (43.74 ± 0.72 μm), tada-5 (41.25 ± 0.93 μm), and tada-10 (42.50 ± 1.45 μm) groups. In addition, the masi-15 (1513.68 ± 62.36 μm²), masi-50 (1596.33 ± 61.64 μm²), and tada-10 (1518.36 ± 96.80 μm²) groups also showed significantly increased lumen area of the larger PAs.

Masitinib versus tadalafil treatments on the mRNA expression of receptors PDGFR-β and C-KIT in the lungs

The lungs of the rats in the placebo group exhibited significantly increased PDGFR-β (0.057 ± 0.013) and C-KIT (0.023 ± 0.002) mRNA levels, compared with the normal (PDGFR-β: 0.026 ± 0.003; C-KIT: 0.014 ± 0.002) group (Fig. 19A, B). Compared with the placebo, masitinib significantly normalized both the PDGFR-β and C-KIT mRNA levels. While the significant PDGFR-β mRNA suppression was only seen in the tada-10 group (0.032 ± 0.010), both the tada-5 (0.015 ± 0.003) and tada-10 (0.014 ± 0.003) treatments significantly downregulated C-KIT mRNA expression.

Masitinib versus tadalafil treatments on the pulmonary CXCR4 and CXCL12 mRNA expression

The CXCR4 mRNA expression in the lung tissues of the rats in the placebo group (0.296 ± 0.066) was significantly upregulated, compared with the normal group (0.117 ± 0.010) (Fig. 19C). In the treatment groups, only the masi-15 (0.082 ± 0.017) and masi-50 (0.065 ± 0.014) treatments significantly suppressed CXCR4 mRNA expression. There was no significant inhibition by the masi-5 (0.180 ± 0.037), tada-5 (0.177 ± 0.054), and tada-10 (0.208 ± 0.057) treatments.

In line with the above, the placebo (0.129 ± 0.029), masi-15 (0.113 ± 0.031), tada-5 (0.107 ± 0.021), and tada-10 (0.124 ± 0.016) groups had significantly higher CXCL12 mRNA levels than the normal (0.012 ± 0.002) group (Fig. 19D). However, the mRNA levels in the masi-15 (0.113 ± 0.031) and masi-50 (0.043 ± 0.013) groups were statistically comparable to that of the normal group.

Masitinib versus tadalafil treatments on the MAPK signaling pathway.

The Raf-1 mRNA expression remained low in the normal group (0.030 ± 0.004) but was significantly upregulated in the placebo group (0.085 ± 0.006) (Fig. 20A). Among the treatment groups, only the masi-15 (0.050 ± 0.011) and masi-50 (0.043 ± 0.009) treatment groups significantly normalized mRNA expression compared with the placebo group.

Similarly, the ERK protein phosphorylation was significantly induced in the placebo (2.20 ± 0.21), compared with the normal group (0.40 ± 0.14) (Fig. 20B, C). While the tadalafil treatment (tada-5: 1.45 ± 0.50; tada-10: 1.72 ± 0.49) did not significantly alter protein phosphorylation, the masi-15 (0.50 ± 0.08) and masi-50 (0.36 ± 0.11) groups exhibited significant dephosphorylation of the ERK protein.

**Masitinib versus tadalafil treatments on the pulmonary PDE-5 mRNA expression and cGMP level**

PDE-5 mRNA was significantly expressed in the placebo group (0.112 ± 0.035), approximately 3 times higher than that of the normal group (0.038 ± 0.004) (Fig. 21A). The treatment rats had comparable mRNA levels to that of the normal rats. However, rats in the masi-50 (0.034 ± 0.006) and tada-5 (0.039 ± 0.003) groups showed significantly lower mRNA levels compared with rats in the placebo group.

Given the significant suppression of PDE-5 mRNA in the masi-50 group, we compared tissue cGMP levels between the masi-50 and tada-10 rats (Fig. 21B). The lung tissues of the masi-50 rats had cGMP levels of 220.24 ± 76.61 ρmol/g; the tada-10 rats had cGMP levels of 203.50 ± 53.95 ρmol/g.

Masitinib 15 mg/kg versus tadalafil 10 mg/kg treatments on the long-term survival rate in the rats

In the placebo group, death occurred as early as 22 days after the MCT-injection (Fig. 22A), and eight of 10 (80%) rats were alive at the end point on day 40. In the masi-15 group, seven of 9 (78%) rats survived whereas in the tada-10 group, seven of 10 (70%) rats reached the end point.

The RV hemodynamic evaluation on day 42 post MCT-injection revealed a further rise in the RVSP (81.18 ± 4.56 mmHg) in the placebo rats, with a HR of 275.85 ± 10.49 bpm (Fig. 22B, C). Compared with that of the placebo, the aggravated RVSP was significantly normalized by the masi-15 (62.47 ± 6.60 mmHg) but not the tada-10 (65.94 ± 5.06 mmHg) treatments. Besides, the rats in both treatment groups also showed a significant higher HR (masi-15: 343.93 ± 11.87 bpm; tada-10: 323.39 ± 10.5 bpm) than the placebo rats.
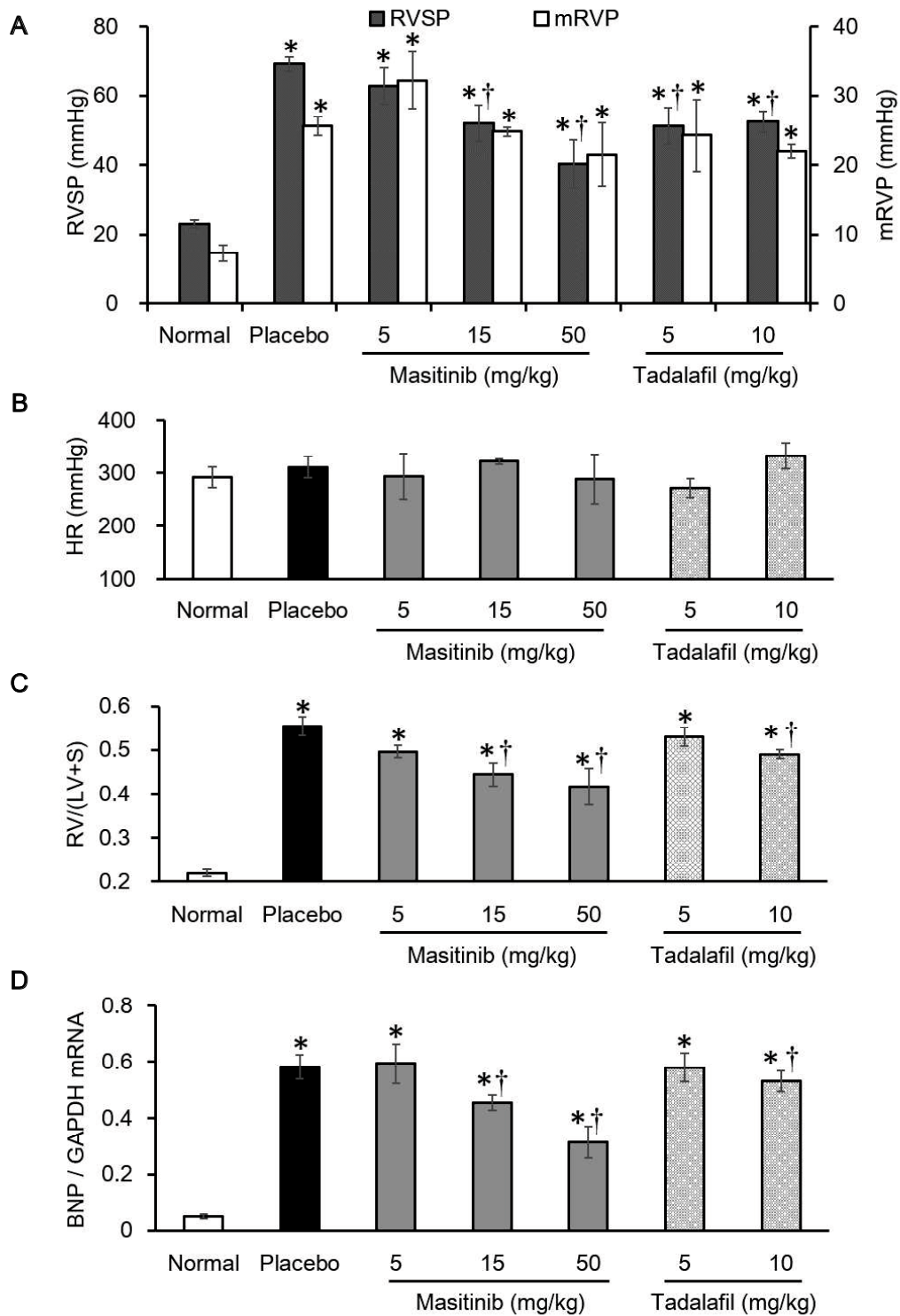
Fig. 16. Effects of masitinib and tadalafil on (A) right ventricular systolic pressure (RVSP) and mean right ventricular pressure (mRVP) (n = 3 – 6), (B) heart rate (n = 3 – 6), (C) right ventricular hypertrophy (RVH) (n = 8 – 12), and (D) b-type natriuretic peptide (BNP) mRNA expression normalized to glyceraldehyde-3-phosphate dehydrogenase (GAPDH) of the right ventricle tissue (n = 7 – 14). Data are means ± standard error of mean (SEM). *$P < 0.05$ versus control, †$P < 0.05$ versus placebo.

A

B

C

81
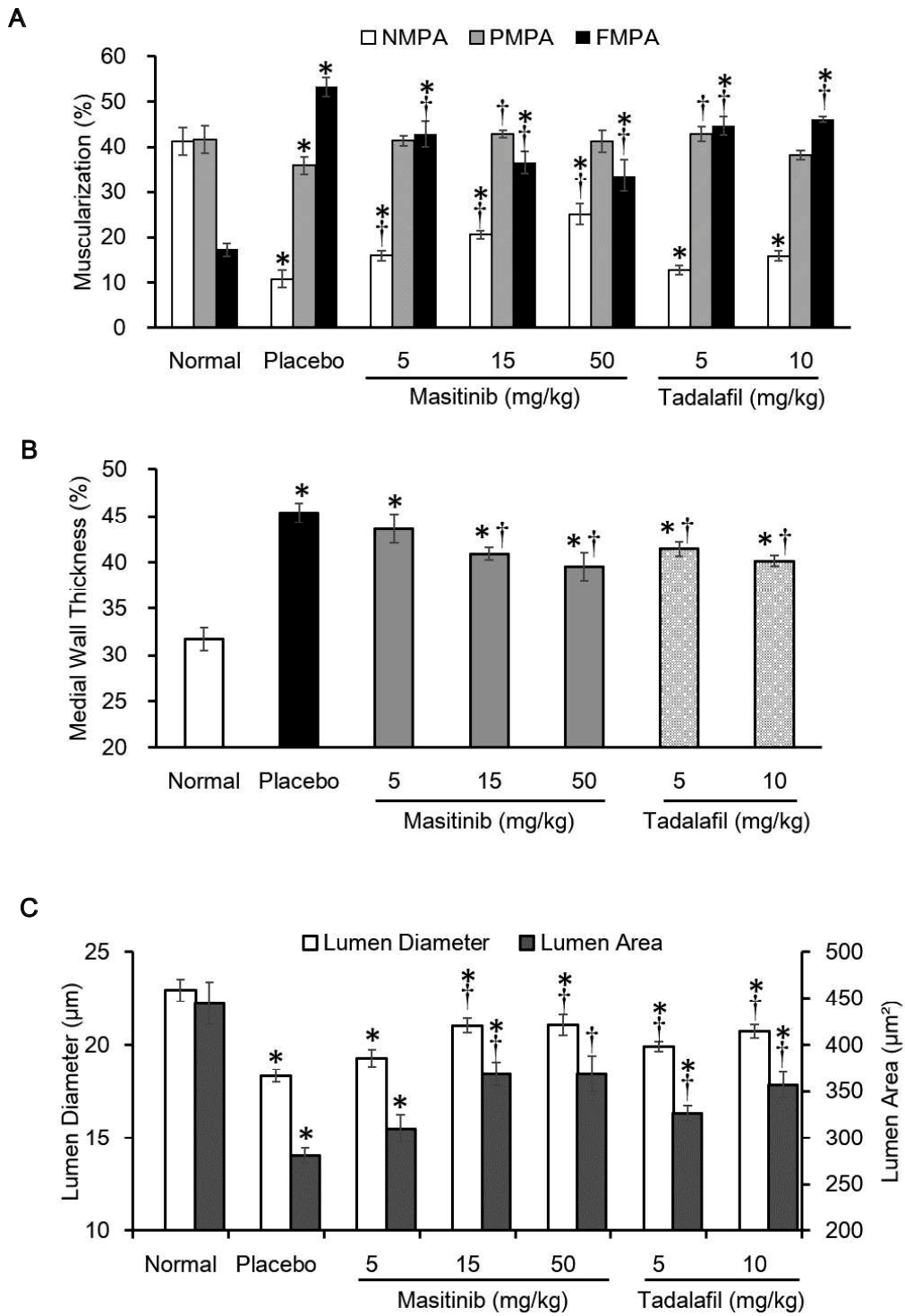
Fig. 17. Effects of masitinib and tadalafil on vascular muscularization in 20–50 μm pulmonary arteries. (A) Percentage is given by the number of fully (FMPA), partially (PMPA), and non-muscularized (NMPA) pulmonary artery normalized to the total number of pulmonary arteries counted, (B) medial wall thickness normalized to the external diameter of FMPAs, and (C) lumen diameter and area of FMPAs. Data are means ± SEM (n = 8 − 11). *$P < 0.05$ versus control, †$P < 0.05$ versus placebo.

A

Medial Wall Thickness (%)

Normal | Placebo | 5 | 15 | 50 | 5 | 10
Masitinib (mg/kg) | Tadalafil (mg/kg)

B

Lumen Diameter (µm)

Normal | Placebo | 5 | 15 | 50 | 5 | 10
Masitinib (mg/kg) | Tadalafil (mg/kg)

C

Lumen Area (µm²)

Normal | Placebo | 5 | 15 | 50 | 5 | 10
Masitinib (mg/kg) | Tadalafil (mg/kg)
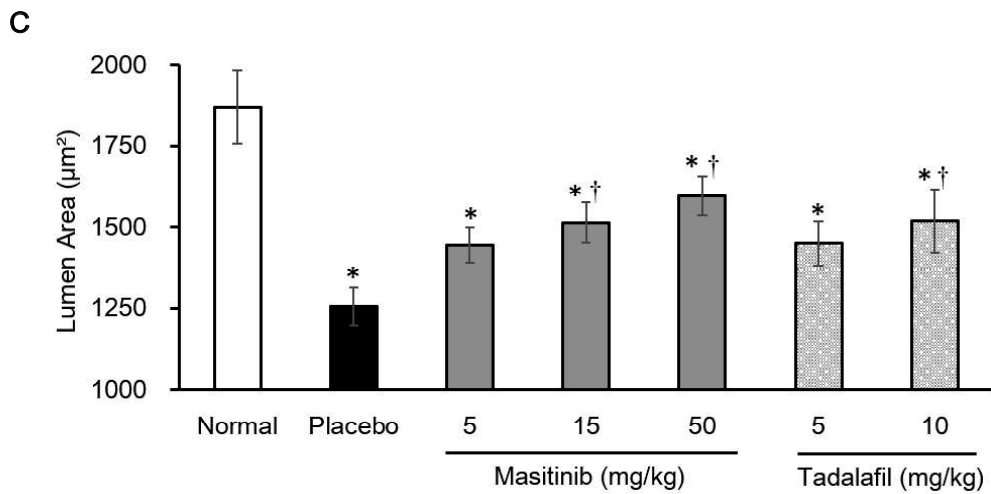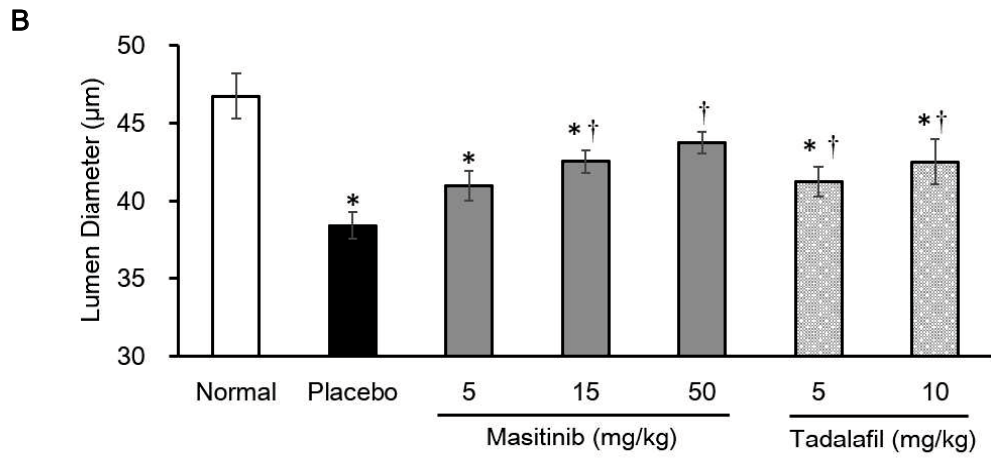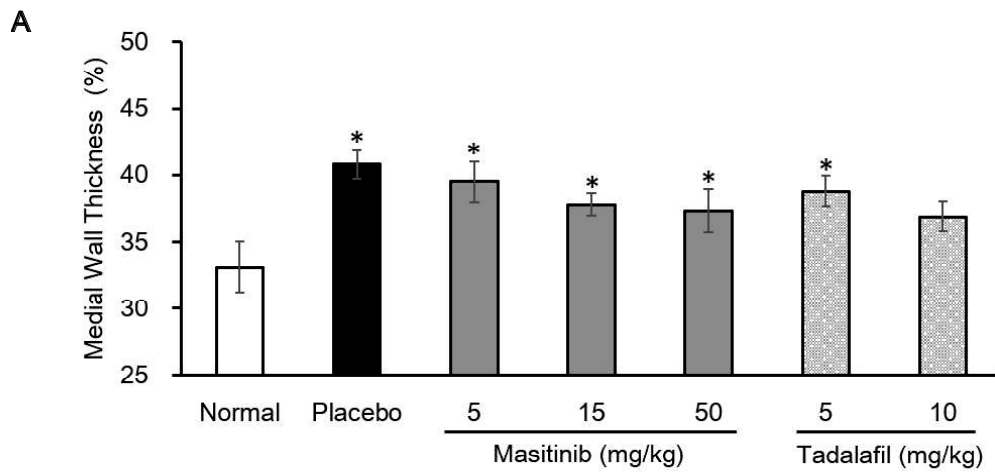
Fig. 18. Effects of masitinib and tadalafil on the 51–100 μm fully muscularized pulmonary arteries. (A) Medial wall thickness normalized to the external diameter, (B) lumen diameter, and (C) lumen area. Data are means ± SEM (n = 8 – 12). *$P < 0.05$ versus control, †$P < 0.05$ versus placebo.
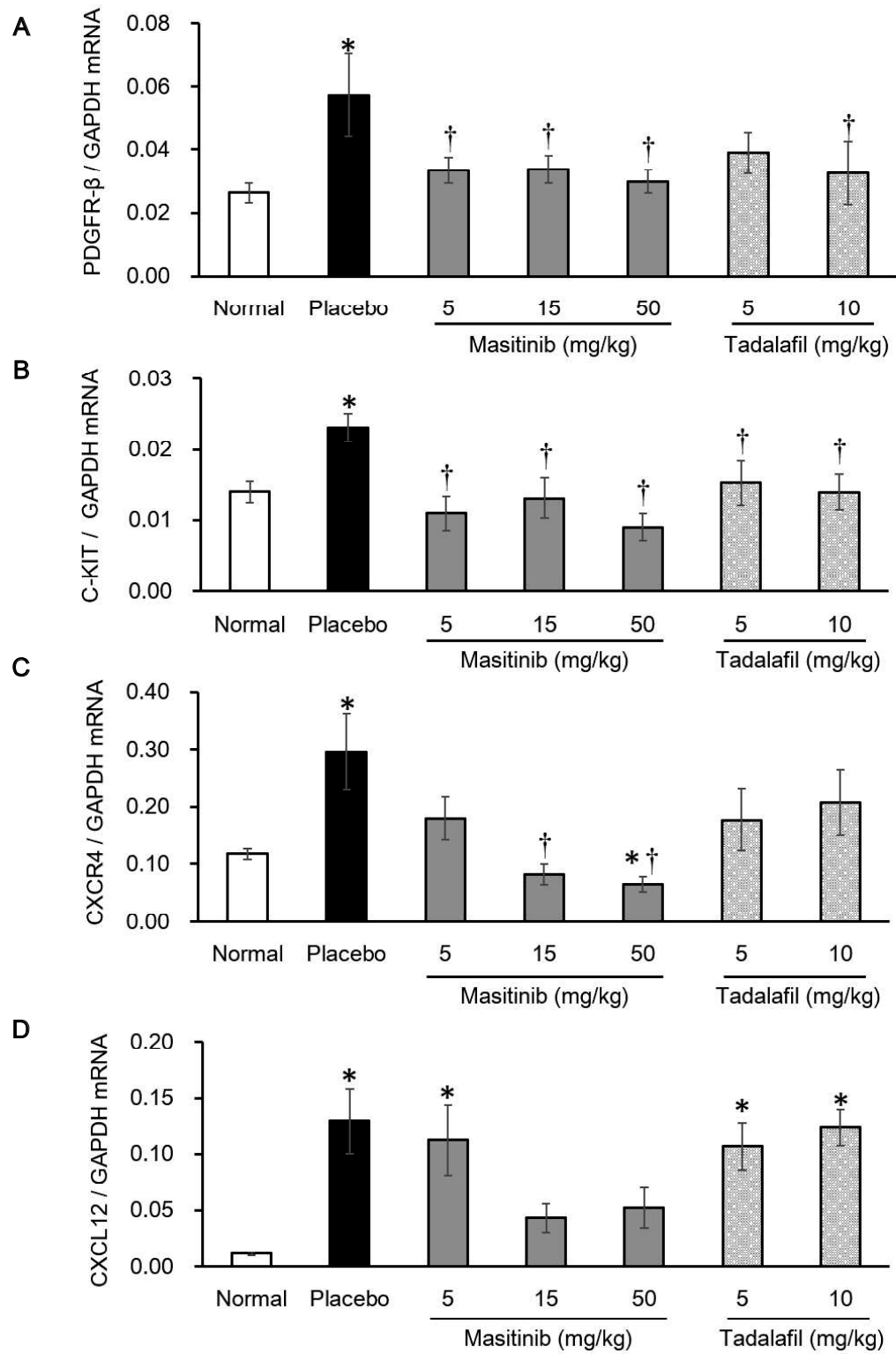
Fig. 19. Effects of masitinib and tadalafil on the expression of various target genes normalized to glyceraldehyde-3-phosphate dehydrogenase (GAPDH) mRNA in the lungs. (A) Platelet-derived growth factor receptor-β (PDGFR-β) (n = 7 − 11), (B) KIT proto-oncogene receptor tyrosine kinase (C-KIT) (n = 8 − 12), (C) C-X-C chemokine receptor type 4 (CXCR4) (n = 7 − 9), and (D) ligand 12 (CXCL12) (n = 8 − 10) in rat lungs. Data are means ± SEM. *P < 0.05 vs control, †P < 0.05 vs placebo.

A

B

C
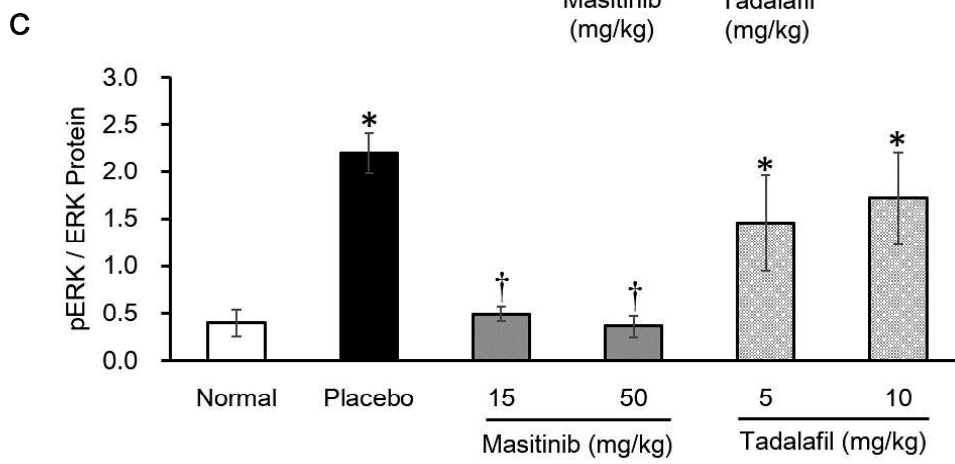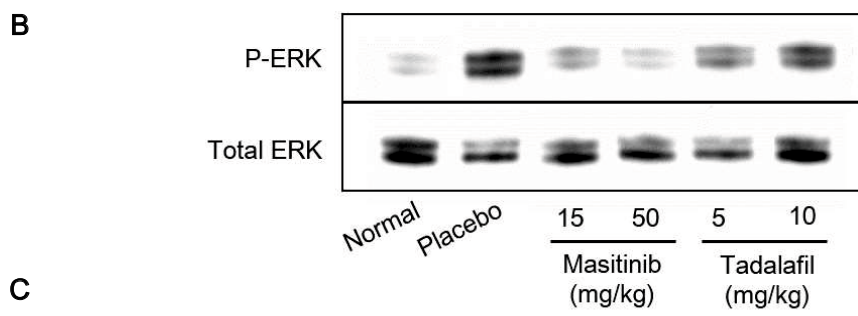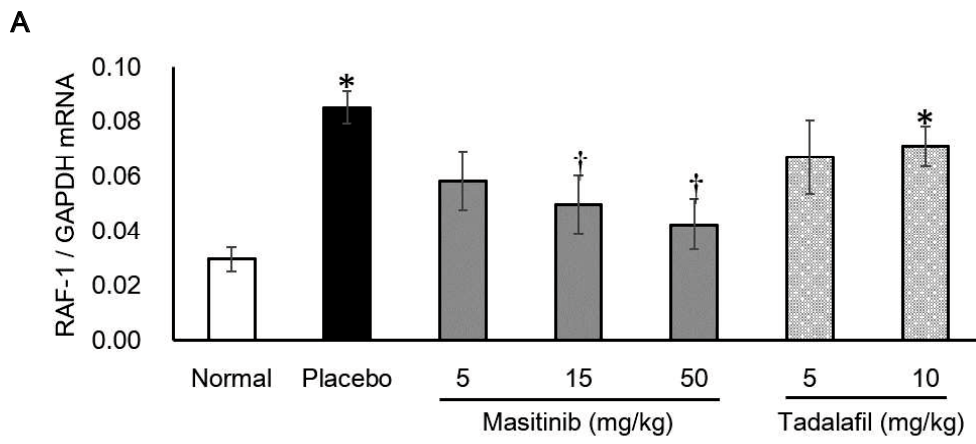
Fig. 20. Effects of masitinib and tadalafil on pulmonary (A) Raf-1 proto-oncogene serine/threonine kinase (Raf-1) mRNA expression (n = 8 – 9) and (B) extracellular-signal-related kinase (ERK)-1/2 protein phosphorylation, which constitute the mitogen-activated protein kinase signaling pathway. (C) Western blots represent phosphorylated versus total ERK protein of one individual from each treatment group (n = 4 – 6). Data are means ± SEM. *$P < 0.05$ versus control, $^{†}P < 0.05$ versus placebo.
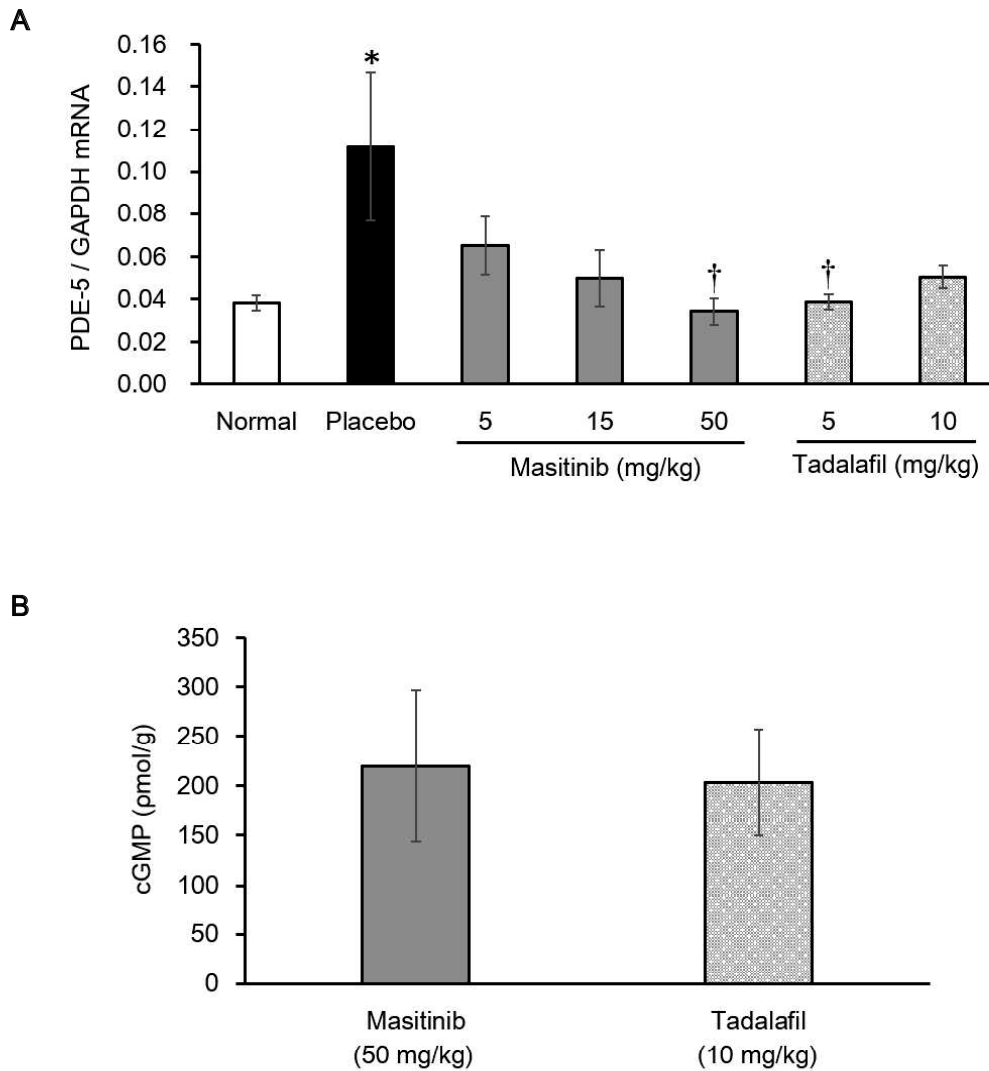
Fig. 21. Effects of masitinib and tadalafil on the nitrogen oxide/cyclic guanosine monophosphate (cGMP) pathway. (A) Expression of phosphodiesterase (PDE)-5 mRNA in all treatment groups (n = 8 – 9), (B) pulmonary cGMP level between the masi-50 and tada-10 groups (n = 3 – 4). Data are means ± SEM. *$P < 0.05$ versus control, [†]$P < 0.05$ versus placebo.
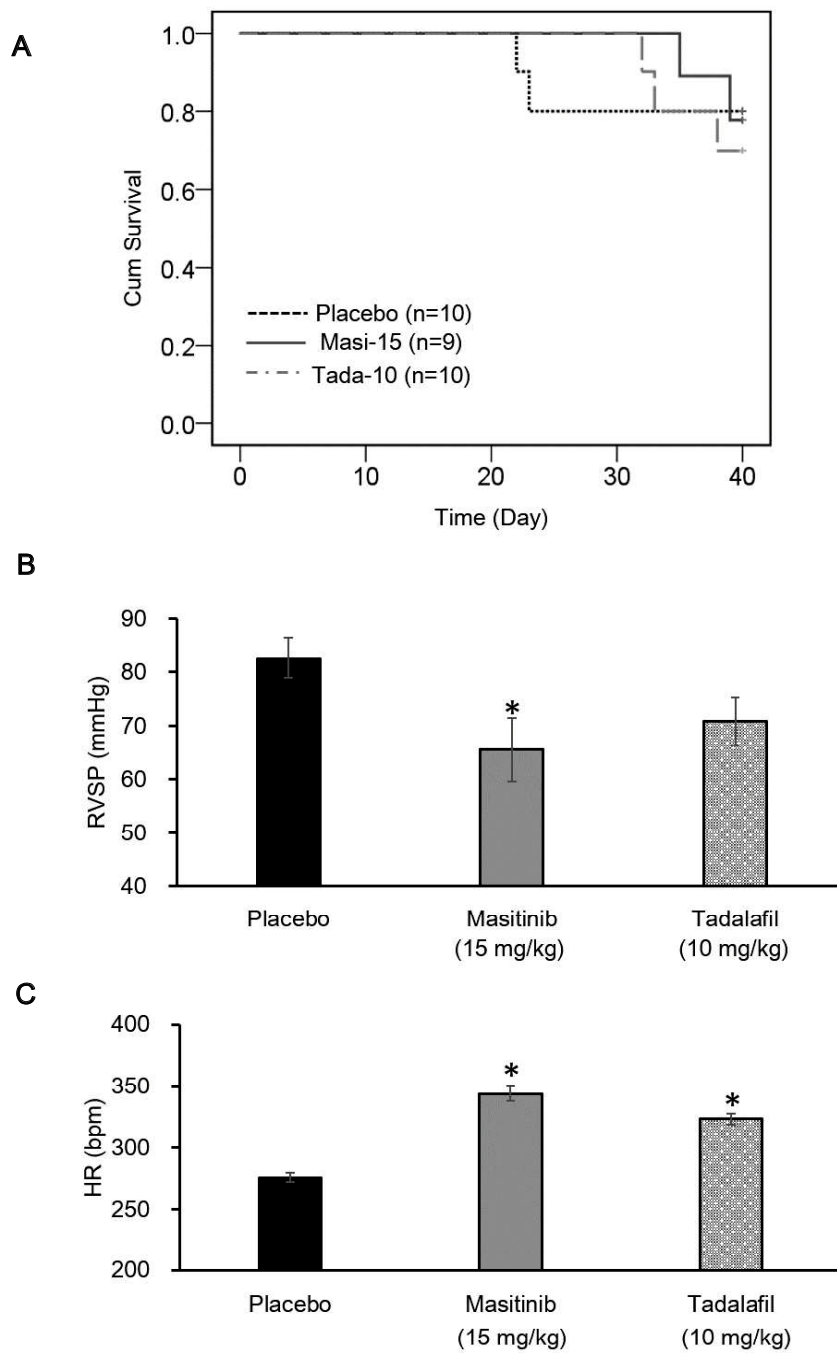
Fig. 22. Comparison of (A) long-term survival (n = 9–10), (B) right ventricular systolic pressure (RVSP) and (C) heart rate (HR) in rats after 28 days of treatment with masitinib (15 mg/kg) (n = 5) and tadalafil (10 mg/kg) (n = 6). Data are means ± SEM. *$P < 0.05$ versus placebo.

90

Discussion

This study provides new insight into the effects of masitinib, a tyrosine kinase inhibitor, versus tadalafil, a FDA-approved drug for the treatment of PAH. We demonstrated that masitinib exhibited more potent, dose-dependent reversal properties against pulmonary vascular remodeling and RV hypertrophy than tadalafil. Besides, masitinib also reduced RVSP in rats with monocrotaline-induced PAH, and both the 15 and 50 mg/kg rat dosages are statistically comparable in terms of the anti-remodeling and therapeutic efficacies. Further, the non-inferiority trial also showed that the low-dose masitinib exerts long-term beneficial effects as manifested by a more significant RV hemodynamic improvement and a greater survival outcome compared with those of the tadalafil therapy.

Masitinib targets on C-KIT and PDGFR-β with IC$_{50}$ values of 0.15 and 0.02, respectively [101]. Given its potent kinase activity, all masitinib doses suppressed pathogenic C-KIT and PDGFR-β mRNA expression in MCT-injected lungs. Masitinib also potently blocked the CXCR4 mRNA expression and insignificantly suppressed the CXCL12 mRNA upregulation, implying that it inhibited the CXCR4/CXCL12 axis, which drives PAH pathogenesis [85]. In the comparative tadalafil groups, we observed a significant C-KIT mRNA downregulation, thus confirming the role of the C-KIT blockade by the phosphodiesterase 5 inhibitor [100]. Although the 10 mg/kg tadalafil treatment inhibited PDGFR-β mRNA expression, it showed negligible inhibitory effects on the CXCR4/CXCL12 axis. Further, the PDGFR-β and C-KIT antagonism by tadalafil did not markedly inhibit the MAPK pathway, as evidenced by the insignificant proto-oncogene Raf-1 mRNA downregulation and ERK 1/2 dephosphorylation in the rat lungs.

91

In accordance with these findings, the reversal of PA muscularization was more significant in rats treated with masitinib than in those treated with tadalafil. The number of remodeled PAs, indicated by the FMPA percentage, was reduced by 10.5, 16.7, and 19.6% following treatments of 5, 15, and 50 mg/kg of masitinib, respectively. By contrast, the tadalafil therapy of 5 and 10 mg/kg decreased the FMPA percentage by 8.8 and 7.3%, respectively. Further, the anti-remodeling properties of masitinib were stronger than those of tadalafil, as reflected by the presence of a higher number of thin-walled PAs represented by the NMPA percentage in the masitinib-treated rats. With respect to the cardiac remodeling, tadalafil at 10 mg/kg significantly reduced the right ventricular hypertrophy (RVH) and the RV b-type natriuretic peptide mRNA expression, findings that were consistent with those of Sawamura et al [99]. Nonetheless, the tadalafil-treated rats showed higher RVH index and BNP mRNA expression than those treated with masitinib, suggesting that tadalafil possesses weaker cardiac reversal abilities.

Despite its weak cardiopulmonary reversal properties, tadalafil significantly reduced the RVSP in the MCT-injected rats, in agreement with the results by Sawamura et al. [99] and Egawa et al. [102]. The significant increases in lumen diameter and area of the 20–50 and 51–100 μm FMPAs in the tadalafil-treated rats strengthened our belief that these hemodynamic improvements were caused by PDE-5 inhibition-induced PA vasodilation. As expected, the tada-10 group demonstrated an average tissue cGMP level that was comparable to that reported by Sawamura et al. [99], despite the small sample size. Surprisingly, the highest dose of masitinib also yielded cGMP levels similar to those of tadalafil. Further gene analysis also revealed a significant PDE-5 mRNA downregulation in the masi-50 group, suggesting that masitinib might regulate the

nitrogen oxide/cGMP pathway when administered at high doses. This finding is in contrast with a previous study [103] which showed that imatinib dilated pulmonary venous beds in guinea pigs through cAMP, but not cGMP release. Indeed, the absence of PDE-5 mRNA downregulation in the rats medicated with a high-dose imatinib (50 mg/kg) (unpublished data) also led us to believe that this discrepancy might be due to pharmacological differences between masitinib and imatinib.

Tadalafil dosed at 10 mg/kg in the rats was equivalent to the dose recommended for the treatment of PAH in humans [99]. In comparing the survival benefit of a lower dose of masitinib (15 mg/kg) versus the therapeutic dose (10 mg/kg) of tadalafil for PAH, we showed that the 40-day survival of the masitinib-treated rats was 78%, versus 70% in the tadalafil group, indicating that the long-term treatment with a lower dose of masitinib was non-inferior than tadalafil pertaining to survival outcome, despite the small sample size. Hemodynamically, the 28-day treatment with masi-15 also significantly improved the RV functions in the rats as shown by an increased HR and a decreased RVSP. With respect to this, the greater reduction of RVSP observed in the masitinib-treated rats than the tadalafil-treated rats provided strong evidence that masitinib at a 15 mg/kg dose was more effective than tadalafil on the long-term control of severe PAH in the rats. These data may serve useful foundation for further clinical investigation on the use of a low-dose masitinib for treating PAH in humans.

In conclusion, the MAPK pathway-inhibiting masitinib elicited stronger cardiopulmonary reversal properties than tadalafil. The long-term therapy with a lower dose (15 mg/kg) attenuated the PAH severity and improved survival in the rats. Although tadalafil also improved the RVSP in the rats, its weak anti-remodeling abilities did not

confer greater long-term survival nor hemodynamic benefits than masitinib. Therefore, a

lower dose of masitinib may be applicable to the treatment of PAH in humans.

Chapter 4

Long-term effect of low-dose imatinib therapy for pulmonary hypertension due to chronic degenerative mitral valve disease in six dogs

Introduction

Chronic degenerative mitral valve disease (CDMVD) is the most common canine heart disease. It occurs in one-third of dog population aged more than 10 years old [104] and commonly results in post-capillary pulmonary hypertension [2]. The current therapy for canine PH depends mainly on vasodilating phosphodiesterase V inhibitor such as sildenafil [2]. Nevertheless, an effective treatment for PH is often hampered by the lack of a direct anti-remodeling property of the therapeutic agents.

In the past years, platelet-derived growth factor (PDGF) [10, 105] and C-KIT [33] receptors have been recognized to play a pathogenic role in the PH development. Imatinib, a tyrosine kinase inhibitor targeting PDGF and C-KIT receptors, reverses pulmonary and right ventricular (RV) remodeling [10, 67, 105] and exhibits systemic and pulmonary vasodilatory effects [103,105] in rats. However, studies using a high imatinib dose (200 to 400 mg) in human PH patients have yielded controversial outcomes [22,35,36].

Recently, we showed that imatinib at a dose of 15 mg/kg significantly reversed monocrotaline-induced RV hypertrophy and pulmonary arterial muscularization in rats [67]. Consistently, Hatano et al. [40] also reported significant improvements in diffusion capacity of the lung for carbon monoxide (DCLO) and varying hemodynamic responses in five PAH patients on a low-dose imatinib (100 mg/day) for 24 weeks. Similar results were also demonstrated in our previous study that the low-dose imatinib therapy (3 mg/kg) for 30 days improved clinical scores and echocardiographic outcomes in PH dogs [39]. This case report represents the study continuation to investigate long-term effects and safety of the low-dose imatinib treatment for CDMVD-associated PH in six dogs.

Case description

Patient signalment, history and clinical findings of the dogs are summarized in Table 1. In general, the dogs were presented with cough, respiratory distress and exercise intolerance despite being treated for CDMVD (ISACHC Class II–IIIa) with polypharmacy approaches. A series of work-ups which included hematology and serum biochemistry, plasma atrial natriuretic peptide (ANP) and serum N-terminal pro-brain natriuretic peptide (NT-proBNP) measurements, chest radiography, and echocardiography were carried out. The plasma ANP levels were measured by chemiluminescence enzyme immunoassay at Fukuyama Medical Laboratory, Hiroshima, whereas the serum NT-proBNP concentrations were measured by enzyme-linked immunosorbent assay (ELISA) at IDEXX Laboratories, Tokyo, Japan. We performed the echocardiography using methods as described in our previous study [39]. For simplicity, all data are shown as means ± standard deviation in the tables, and were analyzed for normality and statistical significance by one-way ANOVA and least significant difference post-hoc test for multiple comparisons.

The dogs had a VHS score of 11–11.5, indicating a cardiomegaly. On echocardiography, we documented a mean maximal systolic tricuspid regurgitation velocity (TRmax) of greater than 2.8 m/s (3.34 ± 0.58 m/s) (Table 2). Using the modified Bernoulli's equation ($4 \times TRmax^2$), a mean systolic pulmonary artery pressure (sPAP) of 45.68 ± 16.19 mmHg was obtained, confirming a diagnosis of PH in the dogs. Besides, there were an enlarged right atrium (right atrium to aorta ratio [RA/Ao]; reference range [RR] 1.23 ± 0.20) from the left parasternal apical 5-chamber view: 1.68 ± 0.12), a decreased right myocardial performance (right Tei index: 0.31 ± 0.09; RR < 0.17 ± 0.10),

and a reduced tricuspid annular plane systolic excursion (TAPSE) value (8.58 ± 2.07 mm) which collectively indicated compromised right heart functions. With owners' consent, imatinib (Glivec 100 mg, Novartis, United Kingdom), 3 mg/kg, every 24 hours, PO was initiated without changing the current therapy for CDMVD.

The dogs were reevaluated at 1, 3, 5, and 6 months after the imatinib therapy. According to the owners, the dog coughed less frequently. On follow-up echocardiography, we observed significant and substantial decreases in TRmax, sPAP and RA/Ao, implying a reduced PH severity. Further, there were decreases in the right Tei index and increases in the TAPSE index suggesting improved right heart functions.

In addition, the left heart echocardiography also showed substantial decreases in left ventricular internal diameter end systole (LVIDs), left ventricular internal diameter end diastole (LVIDd), ratio of peak velocity of early diastolic transmitral flow to early mitral annulus motion velocity (E/Em), indicating reduced preload and left atrial pressure. There were no noticeable changes in cardiac output, fractional shortening and ejection fraction to indicate compromised systolic functions.

The levels of serum n-terminal pro-brain natriuretic peptide (NT-pro BNP) and plasma atrial natriuretic peptide (ANP) decreased remarkably after one month of the treatment (Table 3). Although we were not able to sample blood for cardiac biomarker analyses from all the dogs at every time point of revisits, the biomarker levels at 4 months post-treatment did not exceed the pre-treatment levels. Besides, hematology and serum biochemistry did not show remarkable abnormalities.

We discontinued the imatinib therapy in one dogs (case 1) after it gained clinical stability. However, the owner claimed the dog became less active thereafter.

Echocardiography on day 68 of the withdrawal showed increases in TRmax and sPAP, from 2.22 m/s to 2.76 m/s and from 19.71 mmHg to 30.36 mmHg, respectively, as well as worsened left heart functions. There were also drastic increases in cardiac biomarkers levels (ANP: 106.2 ρg/mL, RR < 30 ρg/mL; NT-proBNP: 4419.0 ρmol/L, RR < 900 ρmol/L). Therefore, we decided to restart the dog on the imatinib treatment after which a clinical improvement was observed.

Out of the six dogs which received the imatinib treatment, two dogs (cases 5 and 6) survived 13 and 48 months after the therapy, respectively, while other dogs continue to receive the therapy till present without obvious side effects observed.

Table 1 Summary of patient signalment, medication history, physical examination and thoracic radiographic findings.

Case	1	2	3	4	5	6
Breed	Chihuahua	CKCS	Chihuahua	CKCS	Pomeranian	Shetland Sheepdog
Gender	Male castrated	Male castrated	Female intact	Male castrated	Male intact	Male castrated
Age	12	11	14	9	14	13
Clinical signs	Cough, exercise intolerance	Cough, exercise intolerance	Cough, lethargy, cyanosis when agitated	Cough, exercise intolerance	Syncope, frequent cough, cyanosis, tachypnea	Cough, exercise intolerance
Auscultation findings	Grade IV/VI LAM	Grade V/IV LAM	Grade IV/VI LAM, grade III/VI right apical murmur, harsh lung sounds	Grade IV/IV LAM	Grade IV/VI LAM, grade III/VI right apical murmur, harsh lung sounds	Grade IV/VI LAM, grade III/VI right apical murmur
Thoracic radiograph findings	VHS: 11, vascular lung pattern, perihilar pulmonary edema	VHS: 11.5 bronchial compression, perihilar pulmonary edema	VHS: 11, moderate perihilar and caudodorsal pulmonary edema, tortuous pulmonary vessels	VHS: 11, left atrial enlargement	VHS: 11.5, perihilar pulmonary edema, engorged pulmonary vessels	VHS: 11.5 and moderate pulmonary edema.
ISACHC	II	II	III a	II	III a	II
Treatment history prior to imatinib therapy	Alacepril (1.5 mg/kg, SID), pimobendan (0.15 mg/kg, BID)	Alacepril (1.5 mg/kg, SID), pimobendan (0.15 mg/kg, BID)	Enalapril (0.38 mg/kg, SID), isosorbide nitrate (2 mg/kg, SID)	Benazepril (0.5 mg/kg, SID)	Alacepril (1.5 mg/kg, BID), pimobendan (0.18 mg/kg, BID), furosemide (0.94 mg/kg, SID), vitamin B6 (10 mg/day), liver protectant Hepaact (1 tablet/day)	Benazepril (0.6 mg/kg, SID), pimobendan (0.15 mg/kg, BID), theophylline (6 mg/kg, BID), furosemide (1 mg/kg, BID)

CKCS, Cavalier King Charles Spaniel; LAM, left apical murmur; VHS, vertebral heart score; ISACHC, International Small Animal Cardiac Health Council; SID, every 12 hours; BID, every 24 hours.

Table 2 Hemodynamic data (means ± standard deviation).

Time (Month)	0 (n=6)	1 (n=6)	3 (n=5)	5 (n=4)	6 (n=5)
Heart rate (bpm)	112.47±18.51	111.16±17.07	118.68±15.21	113.93±12.37	113.40±4.49
Right atrium/aorta ratio	1.68±0.12	1.45±0.09*	1.59±0.27	1.67±0.22	1.35±0.07*
Right Tei index	0.31±0.09	0.30±0.08	0.29±0.10	0.33±0.19	0.25±0.10
Maximal systolic tricuspid regurgitation velocity (m/s)	3.34±0.58	2.26±0.80*	2.16±0.52*	2.94±0.64	2.47±0.55*
Systolic pulmonary artery pressure (mmHg)	45.68±16.19	22.50±15.64*	19.54±10.38*	35.81±16.48	25.37±9.92*
Tricuspid annular plane systolic excursion (mm)	8.58±2.07	8.95±2.60	8.71±0.60	9.17±1.20	8.48±0.84
Left atrium / aorta ratio	2.22±0.12	1.92±0.33	2.10±0.18	2.38±0.47	1.95±0.28
Maximum systolic mitral regurgitation velocity (m/s)	7.70±4.02	6.47±1.34	6.22±1.19	6.04±0.38	4.99±2.06
Left ventricular internal diameter end systole (mm)	16.88±4.99	12.35±4.32	14.91±4.14	12.90±5.68	14.82±5.63
Left ventricular internal diameter end diastole (mm)	30.18±6.60	25.25±7.20	29.10±6.70	26.13±7.86	28.00±7.39
Fractioning shortening (%)	44.63±7.76	51.59±7.85	49.06±4.75	51.55±10.43	48.65±9.29
Ejection fraction (%)	76.68±8.33	83.67±6.84	81.65±4.76	83.21±8.07	81.93±7.05
E/A	1.22±0.34	1.13±0.33	1.28±0.32	1.18±0.35	1.14±0.39
Deceleration time of early diastolic transmitral wave (ms)	82.36±17.91	105.69±14.40	99.40±33.59	108.08±6.70	97.75±25.39
E/Em	9.11±1.02	6.12±0.59*	8.35±1.33	6.01±2.03*	6.83±1.38*
Left Tei index	0.31±0.09	0.22±0.11	0.37±0.12	0.28±0.10	0.38±0.16

E/A, ratio of peak velocity of early diastolic transmitral flow to peak velocity of late diastolic transmitral flow; E/Em, ratio of early mitral annulus motion velocity to atrial systolic mitral annulus motion velocity.

*$P < 0.05$ versus 0-month treatment by one-way ANOVA and post-hoc least significant difference (LSD) test for multiple comparison

Table 3 Cardiac biomarker levels (means ± standard deviation).

Cardiac Biomarkers	Reference Range	Pre-Imatinib Therapy	1-Month Post Imatinib Therapy	4-Month Post Imatinib Therapy
Atrial natriuretic peptide (ANP) (ρg/mL)	< 30	74.64±6.40 (n = 5)	52.64±30.86 (n = 5)	58.1±28.57 (n = 2)
N-terminal pro-brain natriuretic peptide (NT-proBNP) (ρmol/L)	< 900	2442.83±2221.62 (n = 6)	1704.50±1412.54 (n = 6)	2094.67±1384.52 (n = 3)

Discussion

This case report describes six CDMVD dogs which developed PH and required a long-term, low-dose imatinib therapy despite polypharmacy approaches. A low-dose imatinib is defined as one-third of 10 mg/kg dosage indicated for treating canine neoplasms, and was given without any changes to the background therapy for CDMVD in the dogs to minimize influences from other drugs which may affect the study results. The imatinib therapy was chosen over the commonly used vasodilator such as sildenafil for treating the PH for its two properties: the direct, potent reversal effects on cardiopulmonary remodeling [10, 67, 105] and the vasodilative properties in the lungs [103, 105].

The advanced stage of CDMVD increased pulmonary capillary wedge pressure, leading to upregulation of PDGF [10, 105] and C-KIT [33] signaling pathways, which increased the downstream mitogen-activated protein kinase (MAPK) signaling pathway [49]. This subsequently triggered angioproliferation of pulmonary arteries in a process known as remodeling, and resulted in PH in the dogs. Regardless of the PH severity, the dogs showed improved PH and clinical signs after being treated with the low-dose imatinib. We believe that imatinib reversed pulmonary arterial muscularization via the PDGF inhibition [10], thus resulting in an improved PH (decreased TRmax, sPAP, right atrial size) and RV functions (increased right Tei index, an increase in the TAPSE). Further, the LVIDd, left atrium / aorta ratio (LA/Ao), and ratio of peak velocity of early diastolic transmitral flow to peak velocity of late diastolic transmitral flow (E/A) as indicators of CDMVD poor prognosis [106] also improved. In addition, we also speculate that imatinib relaxed systemic and pulmonary venous relaxation which subsequently

reduced preload and afterload [103, 105].

In a study by Hatano et al. [40], five human PAH patients who received a 100 mg/day imatinib dose (equivalent to canine dose of 3 mg/kg) for 12 weeks showed improved DLCO and hemodynamic parameters indicated by either a decreased mean pulmonary arterial pressure, a decreased pulmonary venous resistance, or an increased cardiac index. On an extension therapy to 24 weeks, only three patients with scleroderma-associated PAH showed sustained favorable results. However, the present study demonstrates sustained hemodynamic improvement in the dogs. Clinical and hemodynamic deterioration in the dog in case 1 after imatinib withdrawal also led us to believe that imatinib exhibits sustained, favorable effects on PH in dogs.

There were no remarkable changes in hematology and biochemistry profiles in the dogs to indicate an imatinib toxicity. In humans treated with a high-dose imatinib for PAH, adverse effects which included nausea, peripheral edema, and thrombocytopenia, right ventricular failure, anemia, and subdural hematoma were reported [14, 38]. In the dogs which were treated with a neoplastic dose (10–12 mg/kg), neutropenia, vomiting or elevation of serum liver enzymes, blood urea nitrogen (BUN) and serum creatinine were documented [107]. However, these side effects were not observed in the present study, indicating that the 3 mg/kg imatinib dose was well tolerated in the dogs. Furthermore, the potent anti-remodeling activity of the low-dose imatinib [67] was reflected by substantial clinical and hemodynamic improvements in the dogs. Taken together, we believe that this therapy is effective yet safe for the long-term treatment of canine PH.

In conclusion, this case report highlights encouraging, long-term clinical and hemodynamic outcomes of the low-dose imatinib treatment for CDMVD-associated PH

in dogs, without noticeable side effects. Because there were no changes in the background therapy, the beneficial effects were solely due to the administration of the low-dose imatinib therapy, which is believed to have inhibited pulmonary vascular remodeling and dilated systemic and pulmonary vasculatures simultaneously in the dogs. This therapy can be conveniently administered once daily, and may provide a promising treatment alternative for the treatment of PH in the dogs. However, a drug trial in a larger population of dogs may be deemed necessary.

General Conclusion

The lack of strong reversal properties against cardiopulmonary remodeling in many of the agents approved for the treatment of pulmonary arterial hypertension (PAH) had driven us to investigate the anti-remodeling effects of several tyrosine kinase inhibitors (TKIs), with an exclusive interest for the lower doses. These included the veterinary TKIs: imatinib, masitinib and toceranib, and the multi-kinase inhibitors: sunitinib and sorafenib.

In chapter 1, we showed that imatinib elicited dose-dependent anti-remodeling actions against right ventricular (RV) hypertrophy and pulmonary vascular remodeling in the MCT-induced rats. When dosed at 15 mg/kg, imatinib produced significant inhibition on the mitogen-associated protein kinase (MAPK) signaling pathway which drives the PAH pathogenesis. In comparing the tyrosine kinase activity between imatinib and multi-kinase inhibitor sunitinib, imatinib antagonized platelet-derived growth factor receptor (PDGFR)-β and Raf-1 proto-oncogene serine/threonine kinase (Raf-1), while sunitinib blocked PDGFR-β, fibroblast growth factor receptor (FGFR)-1, vascular endothelial growth factor (VEGF) receptor (VEGFR)-2, and VEGF-A. Ironically, sunitinib with a wider spectrum of kinase inhibition, when given at low doses, yielded weaker inhibition on the Raf-1 and extra-cellular-signal-related kinase (ERK) which constitute the MAPK pathway. Further, the higher number of remodeled pulmonary arteries in tandem with the upregulation of nestin mRNA, a marker of angiogenesis, collectively provided strong evidence that the potent suppression of the VEGFR-2/VEGF-A axis by sunitinib may be the cause of the equivocal cardiopulmonary reversal. Conversely, the low-dose imatinib therapy (15 mg/kg) may provide an option for treatment of PAH and concomitant RV

hypertrophy.

In chapter 2, we scrutinized the reversal effects of toceranib, a veterinary tyrosine kinase which resembles sunitinib, and compared it with sorafenib, which was reported to potently normalize PAH in human and animal studies. Gene analysis revealed significantly decreased pulmonary PDGFR-β and C-KIT mRNA levels in the rats treated with toceranib. However, a high-dose toceranib (10 mg/kg), equivalent to an anti-cancer dose in the dogs, only partially ameliorated cardiopulmonary remodeling (CPR) but showed no RV systolic pressure reversion. Unlike sunitinib, toceranib demonstrated weak inhibition on the VEGFR-2/VEGF-A axis and did not upregulate nestin nor C-X-C chemokine receptor type 4 (CXCR4) mRNAs, refuting escape angiogenesis as the cause of paradox. By contrast, sorafenib at the lowest dose (10 mg/kg) significantly blocked PDGFR-β, C-KIT and CXCR4 mRNAs, MAPK signaling, and upregulated p62 mRNA and microtubule-associated protein light chain 3 (LC3) protein. Hemodynamically, sorafenib also significantly normalized the RV systolic pressure and CPR in the MCT-injected rats. The reversal discrepancy between sorafenib and toceranib may be due to the concurrent potent antagonism on Raf-1 kinase and CXCR4, as well as the autophagy-inducing property of sorafenib. Therefore, toceranib was not recommended for the treatment of PAH but a low-dose sorafenib may be advocated for the PAH therapy.

In chapter 3, we continued to explore the cardiopulmonary reversal effects of another veterinary TKI, namely masitinib. Also, we examined the non-inferiority of masitinib with tadalafil, a FDA-approved medicine for treating PAH in humans. We demonstrated that the lower dose of masitinib (15 mg/kg) exhibited more potent MAPK inhibition via suppression of PDGFR-β, C-KIT, and CXCR4/C-X-C motif chemokine

(CXCL) 12 axis, compared with tadalafil. Besides, it also showed a stronger cardiopulmonary reversal ability than tadalafil at 10 mg/kg, an equivalent dose to that indicated for the human PAH. The blockade of PDGFR-β and C-KIT by tadalafil did not translate into a significant inhibition on the MAPK pathway nor the CPR, although it remarkably normalized the RV systolic pressures in the rats via PDE-5 inhibition. Pertaining to the long-term treatment with the lower masitinib dose (15 mg/kg) versus tadalafil (10 mg/kg), masitinib attenuated the RV hemodynamics more significantly than tadalafil. Moreover, masitinib also showed long-term survival that was non-inferior than that of tadalafil. Therefore, the potent anti-remodeling effects of a lower dose masitinib may be applicable to the long-term treatment of PAH in humans.

The chapter 4 represents a case report which evaluated the long-term effects of low-dose imatinib therapy (3 mg/kg) for treating pulmonary hypertension (PH) secondary to chronic degenerative mitral valve disease in 6 dogs. During the 6-month follow-up period, the maximal systolic tricuspid regurgitation velocity and estimated systolic pulmonary arterial pressure were consistently decreased, implying long-term favorable effects of the therapy. We speculated that imatinib conferred the hemodynamic improvements by inhibiting pulmonary vascular muscularization and dilating systemic and pulmonary vasculatures. Importantly, the complete blood count and serum biochemistry results did not reveal noticeable side effects that were often observed in the dogs on an anti-cancer dose. Therefore, the low-dose imatinib therapy (3 mg/kg) may provide a promising treatment alternative for the treatment of PH in the dogs.

In conclusion, a low-dose imatinib (15 mg/kg), sorafenib (10 mg/kg), and masitinib (15 mg/kg) in MCT-induced PAH rat model potently reversed the CPR and

improved the PAH severity via inhibition of the MAPK pathway. By contrast, sunitinib and toceranib showed disappointing results. Imatinib conferred long-term benefits without causing observable clinical and hemodynamic side effects in the dogs while masitinib improved long-term survival and RV hemodynamics in the rats. Therefore, the low-dose imatinib (15 mg/kg), sorafenib (10 mg/kg), and masitinib (15 mg/kg) may provide a novel reversal agent to target the CPR in the PAH. The results of our study may serve pivotal foundation for further clinical investigation on their use for the treatment of PAH in humans and dogs.

Abstracts

Chapter 1

High-dose imatinib reverses cardiopulmonary remodeling but adverse effects limit its clinical use. Efficacy of the multi-kinase inhibitor sunitinib remains questionable. We compared anti-remodeling effects of imatinib with sunitinib on monocrotaline-induced right ventricular (RV) hypertrophy and pulmonary arterial remodeling in rats, focusing on a lower dose. Fourteen days after monocrotaline injection, oral gavage of imatinib (5, 15, or 50 mg/kg), sunitinib (0.3, 1, 3, or 10 mg/kg), or water for 14 days was started. RV hypertrophy and brain natriuretic peptide mRNA levels were significantly and dose-dependently reduced, much greater in imatinib- than sunitinib-treated groups. Imatinib normalized muscularization of 20-50 μm intra-acinar pulmonary arteries more significantly than sunitinib. At transcript levels, sunitinib significantly upregulated pulmonary nestin, and downregulated platelet-derived growth factor receptor beta (PDGFR-β), fibroblast growth factor receptor 1, vascular endothelial growth factor receptor-2 and vascular endothelial growth factor (VEGF)-A, but not Raf-1 proto-oncogene serine/threonine kinase mRNAs. Sunitinib also suppressed VEGF-A, but not phosphorylated extra-cellular-signal-related kinase (ERK)-1/2 protein expression. The sole PDGFR-β antagonism of imatinib resulted in significant Raf-1 mRNA and phosphorylated ERK-1/2 protein downregulation, suggesting that the equivocal reversal effect of sunitinib may be due to its VEGF signaling inhibition in the lung. Imatinib's greater dose-dependent reversal on cardiopulmonary remodeling may make a low dose suitable for PAH treatment.

Graphical Abstract (Chapter 1)
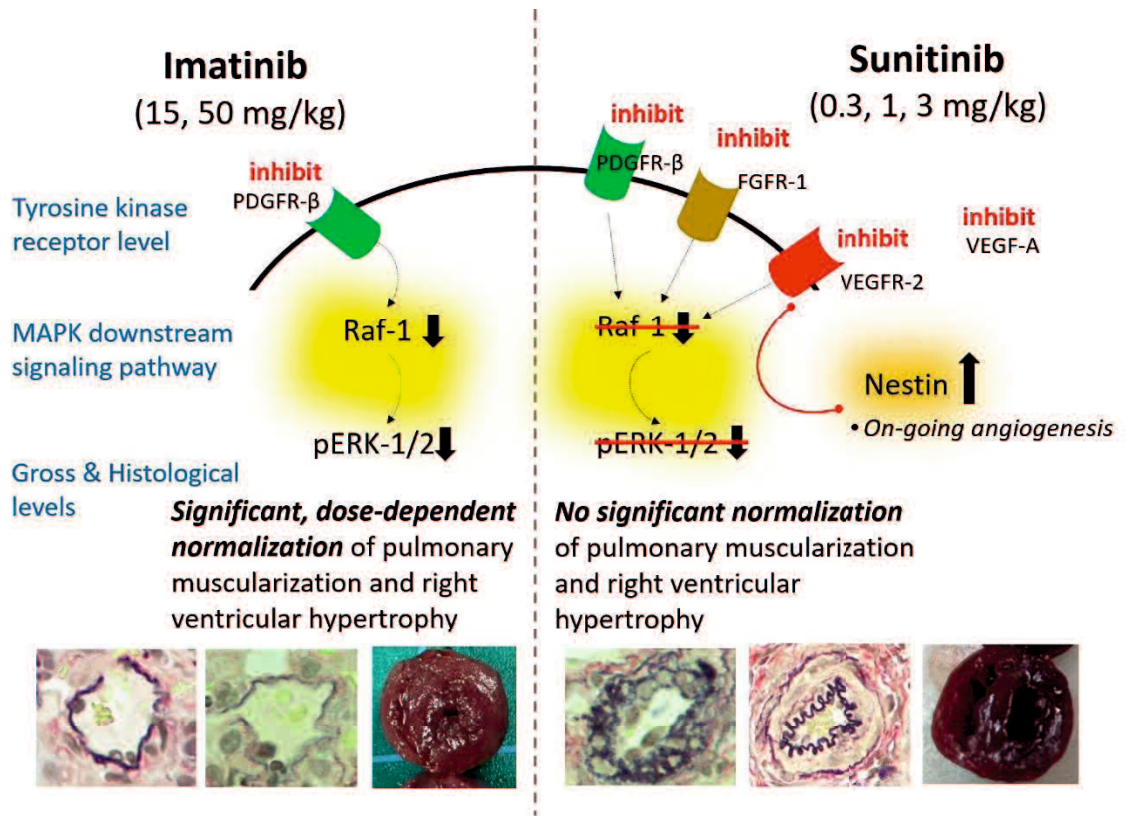
Chapter 2

Sorafenib reverses pulmonary arterial hypertension (PAH) and cardiopulmonary remodeling (CPR), but the effects of toceranib are unknown. This study investigated anti-remodeling effects and determined optimal doses of toceranib and sorafenib on monocrotaline (MCT)-induced PAH and CPR in rats. MCT-treated rats were orally treated with a 14-day course of sorafenib (10, 30, or 100 mg/kg), toceranib (1, 3, or 10 mg/kg), or water. Both sorafenib and toceranib significantly reversed the right ventricular (RV) hypertrophy at 10 mg/kg, but only sorafenib significantly improved the RV systolic and mean pressures. Sorafenib significantly normalized the B-type natriuretic peptide mRNA level of the RV and increased the non-muscularized pulmonary artery percentage. However, these effects were only observed at the highest toceranib dose, and neither toceranib dose reduced the fully muscularized pulmonary artery percentage. Further, the inhibition on vascular endothelial growth factor (VEGF) signaling was stronger in sorafenib than in toceranib. Besides the stronger inhibition on mitogen-activated protein kinase signaling, the greater reversal ability of sorafenib may be also due to the simultaneous blockade on the C-X-C chemokine receptor type 4 and autophagy induction. Toceranib insignificantly reversed CPR, and a high-dose therapy did not improve the RV hemodynamic outcomes. Sorafenib significantly reversed CPR, and a low-dose sorafenib therapy may be a suitable therapeutic agent for PAH.

Graphical Abstract (Chapter 2)
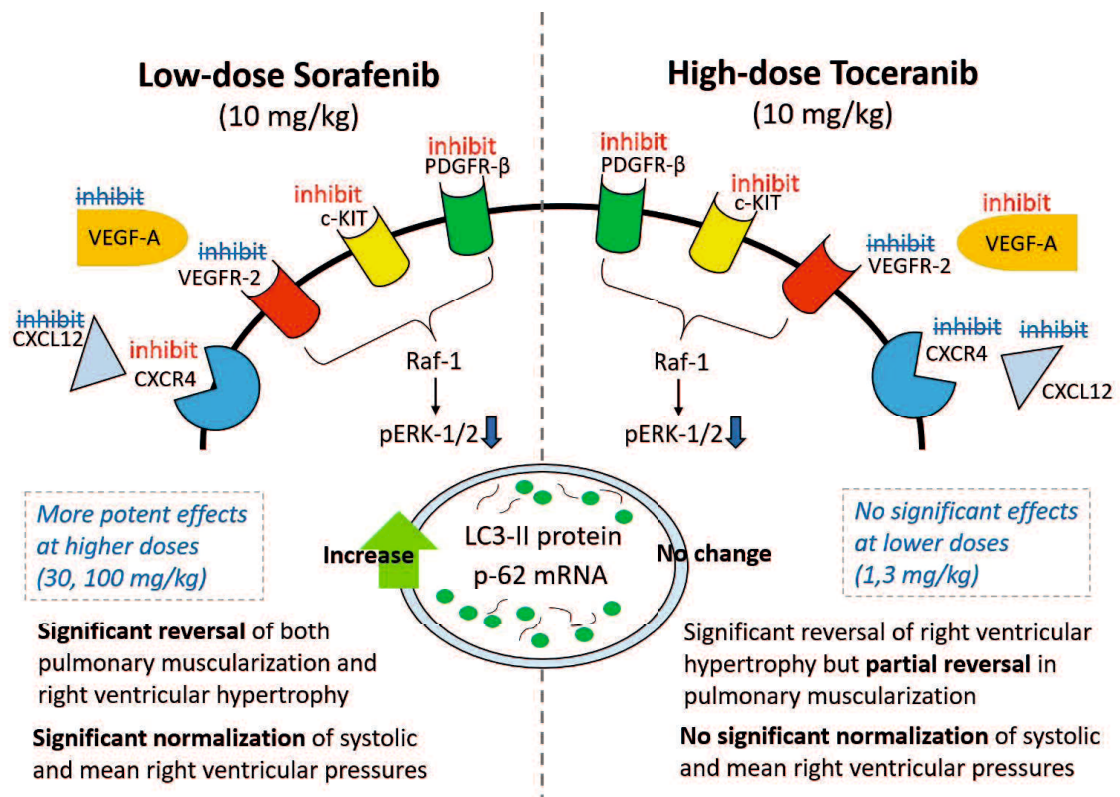
Chapter 3

Pulmonary arterial hypertension (PAH) is characterized by progressive pulmonary vascular remodeling, but current therapies are devoid of potent reversal properties. This study compared the cardiopulmonary reversal effects and survival benefits of masitinib (5, 15, 50 mg/kg) with tadalafil (5, 10 mg/kg) for the treatment of monocrotaline (MCT)-induced PAH in rats. In the masitinib (15, 50 mg/kg) groups, there was a significant reversal of the RV systolic pressure, right ventricular hypertrophy (RVH) and pulmonary vascular remodeling. Collectively, these indicate potent effects of masitinib against cardiopulmonary remodeling. By contrast, tadalafil at 10 mg/kg, equivalent to human dose for PAH treatment, significantly decreased the RVH and increased pulmonary arterial lumen diameter and area, but did not normalize vascular muscularization. Masitinib significantly suppressed mRNA expression of pulmonary platelet-derived growth factor receptor (PDGFR)-β, C-KIT, CXC chemokine receptor 4, proto-oncogene Raf-1, and protein phosphorylation of extracellular-signal-related kinase 1/2. However, tadalafil showed insignificant antagonism on the mitogen-activated protein kinase (MAPK) pathway, despite its significant PDGFR-β and C-KIT inhibition. Further, the high-dose masitinib (50 mg/kg) produced comparable pulmonary phosphodiesterase-5 mRNA and cyclic guanosine monophosphate (cGMP) levels to those of tadalafil, implying a role of masitinib in the nitrogen oxide/cGMP pathway. We also showed that the long-term masitinib therapy at a lower dose (15 mg/kg) improved the survival and RV hemodynamics in the rats. The potent reversal properties and the non-inferiority of a lower dose of masitinib compared with tadalafil may represent a novel approach to target the cardiopulmonary remodeling in PAH.

Chapter 4

Six dogs were diagnosed with pulmonary hypertension (PH) secondary to chronic degenerative mitral valve disease (CDMVD) on echocardiography. Imatinib (3 mg/kg, every 24 hours, PO) was initiated without any changes to the background therapy to treat the PH. Follow-up evaluations at 1, 3, 5 and 6 months revealed substantial clinical and hemodynamic improvements. One dog showed deterioration after the imatinib withdrawal to necessitate a restart therapy. No side effects were observed throughout the 6-month treatment course. A low-dose imatinib may provide a promising treatment alternative for the CDMVD-associated PH in dogs.

Acknowledgements

References

1. Ryan JJ, Thenappan T, Luo N, Ha T, Patel AR, Rich S, et al. The WHO classification of pulmonary hypertension: A case-based imaging compendium. *Pulm Circ* 2012; 2:107–121.

2. Kellihan HB and Stepien RL. Pulmonary hypertension in dogs: diagnosis and therapy. *Vet Clin North Am Small Anim Pract* 2010; 40: 623–641.

3. Farber HW, Miller DP, Poms AD, Badesch DB, Frost AE, Muros-Le Rouzic E, et al. Five-Year outcomes of patients enrolled in the REVEAL Registry. *Chest* 2015; 148: 1043–1054.

4. Kylhammar D, Persson L, Hesselstrand R and Rådegran G. Prognosis and response to first-line single and combination therapy in pulmonary arterial hypertension. *Scand Cardiovasc J* 2014; 48: 223–233.

5. Bach JF, Rozanski EA, MacGregor J, Betkowski JM and Rush JE. Retrospective evaluation of sildenafil citrate as a therapy for pulmonary hypertension in dogs. *J Vet Intern Med* 2006; 20: 1132–5.

6. Atkinson KJ, Fine DM, Thombs LA, Gorelick JJ and Durham HE. Evaluation of pimobendan and N-terminal probrain natriuretic peptide in the treatment of pulmonary hypertension secondary to degenerative mitral valve disease in dogs. *J Vet Intern Med* 2009; 23: 1190–1196.

7. Lajoie AC, Bonnet S and Provencher S. Combination therapy in pulmonary arterial hypertension: recent accomplishments and future challenges. *Pulm Circ* 2017; 7: 312–325.

8. Shimoda LA and Laurie SS. Vascular remodeling in pulmonary hypertension. *J*

Mol Med (Berl) 2013; 91: 297–309.

9. Boucherat O, Vitry G, Trinh I, Paulin R, Provencher S and Bonnet S. The cancer theory of pulmonary arterial hypertension. *Pulm Circ* 2017; 7: 285–299.

10. Schermuly RT, Dony E, Ghofrani HA, Pullamsetti S, Savai R, Roth M, et al. Reversal of experimental pulmonary hypertension by PDGF inhibition. *J Clin Invest* 2005; 115: 2811–2821.

11. Duggan N, Bonneau O, Hussey M, Quinn DA, Manley P, Walker C, et al. Comparison of effects of imatinib and nilotinib in a rodent model of pulmonary arterial hypertension. *Am J Respir Crit Care Med* 2010; 181: A6304.

12. Dahal BK, Cornitescu T, Tretyn A, Pullamsetti SS, Kosanovic D, Dumitrascu R, et al. Role of epidermal growth factor inhibition in experimental pulmonary hypertension. Am *J Respir Crit Care Med* 2010; 181: 158–167.

13. Kimura G, Kataoka M, Inami T, Fukuda K, Yoshino H and Satoh T. Sorafenib as a potential strategy for refractory pulmonary arterial hypertension. *Pulm Pharmacol Ther* 2017; 44: 46–49.

14. Frost AE, Barst RJ, Hoeper MM, Chang HJ, Frantz RP, Fukumoto Y, et al. Long-term safety and efficacy of imatinib in pulmonary arterial hypertension. *J Heart Lung Transplant* 2015; 34: 1366–1375.

15. Lee YS, Byun J, Kim JA, Lee JS, Kim KL, Suh YL, et al. Monocrotaline-induced pulmonary hypertension correlates with upregulation of connective tissue growth factor expression in the lung. *Exp Mol Med* 2005; 37: 27–35.

16. Galie N, Hoeper MM, Humbert M, Torbicki A, Vachiery JL, Barbera JA, et al. Guidelines for the diagnosis and treatment of pulmonary hypertension: the Task

Force for the Diagnosis and Treatment of Pulmonary Hypertension of the European Society of Cardiology (ESC) and the European Respiratory Society (ERS), endorsed by the International Society of Heart and Lung Transplantation (ISHLT). *Eur Heart J* 2009; 30: 2493–2537.

17. Humbert M. Update in pulmonary hypertension 2008. *Am J Respir Crit Care Med* 2009; 179: 650–656.

18. Hung VT, Emoto N, Vignon-Zellweger N, Nakayama K, Yagi K, Suzuki Y, et al. Inhibition of vascular endothelial growth factor under hypoxia causes severe, human-like pulmonary arterial hypertension in mice: Potential roles of interleukn-6 and endothelin. *Life Sci* 2014; 118: 313–328.

19. Kojonazarov B, Sydykov A, Pullamsetti SS, Luitel H, Dahal BK, Kosanovic D, et al. Effects of multikinase inhibitors on pressure overloaded-induced right ventricular remodeling. *Int J Cardiol* 2013; 167: 2630–2637.

20. Galie N, Corris PA, Frost A, Girgis RE, Granton J, Jing ZC, et al. Updated treatment algorithm of pulmonary arterial hypertension. *J Am Coll Cardiol* 2003; 62: D60–D72.

21. Galie N, Hoeper MM, Humbert M, Torbicki A, Vachiery J-L, Barbera JA, et al. Guidelines for the diagnosis and treatment of pulmonary hypertension. *Eur Respir J* 2009; 34: 1219–1263.

22. Ghofrani HA and Humbert M. The role of combination therapy in managing pulmonary arterial hypertension. *Eur Respir Rev* 2014; 23: 469–475.

23. Sitbon O, Jais X, Savale L, Cottin V, Bergot E, Macari EA, et al. Upfront triple combination therapy in pulmonary arterial hypertension: a pilot study. *Eur Respir J* 2014; 43: 1691–1697.

24. Sitbon O, Sattler C, Bertoletti L, Savale L, Cottin V, Jaïs X, et al. Initial dual oral combination therapy in pulmonary arterial hypertension. *Eur Respir J* 2016; 47: 1727–1736.

25. Montani D, Chaumais M-C, Guignabert C, Gunther S, Girerd B, Jais X, et al. Targeted therapies in pulmonary arterial hypertension. *Pharmacol Ther* 2014; 141: 172–191.

26. Klein M, Schermuly RT, Ellinghaus P, Milting H, Riedl B, Nikolova S, et al. Combined tyrosine and serine/threonine kinase inhibition by sorafenib prevents progression of experimental pulmonary hypertension and myocardial remodeling. *Circulation* 2008; 118: 2081–2090.

27. Balasubramaniam V, Le Cras TD, Ivy DD, Grover TR, Kinsella JP and Abman SH. Role of platelet-derived growth factor in vascular remodeling during pulmonary hypertension in the ovine fetus. *Am J Physiol Lung Cell Mol Physiol* 2003; 284: L826–L833.

28. Yu Y, Sweeney M, Zhang S, Platoshyn O, Landsberg J, Rothman A, et al. PDGF stimulates pulmonary vascular smooth muscle cell proliferation by upregulating TRPC6 expression. *Am J Physiol Lung Cell Mol Physiol* 2003; 284: C316–C330.

29. Benisty JI, McLaughlin VV, Landzberg MJ, Rich JD, Newburger JW, Rich S, et al. Elevated basic fibroblast growth factor levels in patients with pulmonary arterial hypertension. *Chest* 2004; 126: 1255–1261.

30.   Xin X, Johnson AD, Scott-Burden T, Engler D and Casscells W. The predominant form of fibroblast growth factor receptor expressed by proliferating human arterial smooth muscle cells in culture is type I. *Biochem Biophys Res Commun* 1994; 204: 557–564.

31.   Zheng Y, Ma H, Hu E, Huang Z, Cheng X and Xiong C. Inhibition of FGFR signaling with PD173074 ameliorates monocrotaline-induced pulmonary arterial hypertension and rescues BMPR-II expression. *J Cardiovasc Pharmacol* 2015; 66: 504–514.

32.   Farha S, Dweik R, Rahaghi F, Benza R, Hassoun P, Frantz R, et al. Imatinib in pulmonary arterial hypertension: C-Kit inhibition. *Pulm Circ* 2014; 4: 452–455.

33.   Montani D, Perros F, Gambaryan N, Girerd B, Dorfmuller P, Price LC, et al. C-kit-positive cells accumulate in remodeled vessels of idiopathic pulmonary arterial hypertension. *Am J Respir Crit Care Med* 2011; 184: 116–123.

34.   Chaumais MC, Perros F, Dorfmuller P, Traclet J, Cohen-Kaminsky S, Simonneau G, et al. Nilotinib and imatinib therapy in experimental pulmonary hypertension. *Am J Respir Crit Care Med* 2012; 185: A3419; doi: http://dx.doi.org/10.1164/ajrccm-conference.2012.185.1_MeetingAbstracts.A3419.

35.   Ghofrani HA, Morrell NW, Hoeper MM, Olschewski H, Peacock AJ, Barst RJ, et al. Imatinib in pulmonary arterial hypertension patients with inadequate response to established therapy. *Am J Respir Crit Care Med* 2010; 182: 1171–1177.

36.   Shah AM, Campbell P, Rocha GQ, Peacock A, Barst JB, Quinn D, et al. Effect of imatinib as add-on therapy on echocardiographic measures of right ventricular

function in patients with significant pulmonary arterial hypertension. *Eur Heart J* 2015; 36: 623–632.

37.   Souza R, Sitbon O, Parent F, Simonneau G and Humbert M. Long term imatinib treatment in pulmonary arterial hypertension. *Thorax* 2006; 61: 736.

38.   Hoeper MM, Barst RJ, Bourge RC, Feldman J, Frost AE, Galie N, et al. Imatinib mesylate as add-on therapy for pulmonary arterial hypertension: Results of the randomized IMPRES study. *Circulation* 2013; 127: 1128–1138.

39.   Arita S, Arita N and Hikasa Y. Therapeutic effect of low-dose imatinib on pulmonary arterial hypertension in dogs. *Can Vet J* 2013; 54: 255–261.

40.   Hatano M, Yao A, Shiga T, Kinugawa K, Hirata Y and Nagai R. Imatinib mesylate has the potential to exert its efficacy by down-regulating the plasma concentration of platelet-derived growth factor in patients with pulmonary arterial hypertension. *Int Heart J* 2010; 51: 272–276.

41.   Lalich JL, Johnson WD, Raczniak TJ and Shumaker RC. Fibrin thrombosis in monocrotaline pyrrole-induced cor pulmonale in rats. *Arch Pathol Lab Med* 1977; 101: 69–73.

42.   Zhang B, Niu W, Xu D, Li Y, Liu M, Wang Y, et al. Oxymatrine prevents hypoxia and monocrotaline-induced pulmonary hypertension in rats. *Free Radic Biol Med* 2014; 69: 198–207.

43.   Arcot SS, Lipke DW, Gillespie MN and Olson JW. Alterations of growth factor transcripts in rat lungs during development of monocrotaline-induced pulmonary hypertension. *Biochem Pharma* 1993; 46: 1086–1091.

44.   Farkas L, Farkas D, Ask K, Möller A, Gauldie J, Margetts P, et al. VEGF ameliorates pulmonary hypertension through inhibition of endothelial apoptosis in experimental lung fibrosis in rats. *J Clin Invest* 2009; 119: 1298–1311.

45.   Nadeau S, Baribeau J, Janvier A and Perreault T. Changes in expression of vascular endothelial growth factor and its receptors in neonatal hypoxia-induced pulmonary hypertension. *Pediatr Res* 2005; 58: 199–205.

46.   Partovian C, Adnot S, Eddahibi S, Teiger E, Levame M, Dreyfus P, et al. Heart and lung VEGF mRNA expression in rats with monocrotaline- or hypoxia-induced pulmonary hypertension. *Am J Physiol Cell Physiol* 1998; 44: H1948–H1956.

47.   Yamamoto A, Takahashi H, Kojima Y, Tsuda Y, Morio Y, Muramatsu M, et al. Downregulation of angiopoietin-1 and Tie in chronic hypoxic pulmonary hypertension. *Respiration* 2008; 75: 328–338.

48.   Kitagawa D, Yokota K, Gouda M, Narumi Y, Ohmoto H, Nishiwaki E, et al. Activity-based kinase profiling of approved tyrosine kinase inhibitors. *Genes Cells* 2013; 18: 110–122.

49.   Katz M, Amit I and Yarden Y. Regulation of MAPKs by growth factors and receptor tyrosine kinases. *Arch Biochem Biophys* 2007; 1773: 1161–1176.

50.   Dhillon AS and Kolch W. Untying the regulation of the Raf-1 kinase. *Arch Biochem Biophys* 2002; 404: 3–9.

51.   Vitalia SH, Hansmanna G, Rose C, Fernandez-Gonzalez A, Scheid A, Mitsialis SA, et al. The Sugen 5416/hypoxia mouse model of pulmonary hypertension revisited: Long-term follow-up. *Pulm Circ* 2014; 4: 619–629.

52.   Matsuda Y, Hagio M and Ishiwata T. Nestin: A novel angiogenesis marker and possible target for tumor angiogenesis. *World J Gastroenterol* 2013; 19: 42–48.

53.   Oikawa H, Hayashi K, Maesawa C, Masuda T and Sobue K. Expression profiles of nestin in vascular smooth muscle cells in vivo and in vitro. *Exp Cell Res* 2010; 316: 940–950.

54.   Aihara M, Sugawara K, Torii S, Hosaka M, Kurihara H, Saito N, et al. Angiogenic endothelium-specific nestin expression is enhanced by the first intron of the nestin gene. *Lab Invest* 2004; 84: 1581–1592.

55.   Ishiwata T, Teduka K, Yamamoto T, Kawahara K, Matsuda Y and Naito Z. Neuroepithelial stem cell marker nestin regulates the migration, invasion and growth of human gliomas. *Oncol Rep* 2011; 26: 91–99.

56.   Mokry J, Cízkova D, Filip S, Ehrmann J, Osterreicher J, Kolar Z, et al. Nestin expression by newly formed human blood vessels. *Stem Cells Dev* 2004; 13: 658–664.

57.   Chabot A, Meus MA, Naud P, Hertig V, Dupuis J, Villeneuve L, et al. Nestin is a marker of lung remodeling secondary to myocardial infarction and type I diabetes in the rat. *J Cell Physio* 2015; 230: 170–179.

58.   Saboor F, Reckmann AN, Tomczyk CU, Peters DM, Weissmann N, Kaschtanow A, et al. Nestin-expressing vascular wall cells drive development of pulmonary hypertension. *Eur Respir J* 2016; 47: 876–888.

59.   Carmeliete PK. Keystone Conference of Pulmonary Hypertension. September 10-15, 2012. Monterey, California USA. [Personal communication]

60. Nicolls M, Mizuno S, Taraseviciene-Stewart L, Farkas L, Drake JI, Husseini AA, et al. New models of pulmonary hypertension based on VEGF receptor blockade-induced endothelial cell apoptosis. *Pulm Circ* 2012; 2: 434–442.

61. Domigan CK, Ziyad S and Iruela-Arispe ML. Canonical and non-canonical VEGF pathways: New developments in biology and signal transduction. *Arterioscler Thromb Vasc Biol* 2015; 35: 30–39.

62. Voelkel NF, Vandivier RW and Tuder RM. Vascular endothelial growth factor in the lung. *Am J Physiol Lung Cell Mol Physiol* 2006; 290: L209–L221.

63. Mizuno S, Farkas L, Alhussaini A, Farkas D, Gomez-Arroyo L, Kraskauskas D, et al. Severe pulmonary arterial hypertension induced by SU5416 and ovalbumin immunization. *Am J Respir Cell Mol* 2012; 47: 679–687.

64. Guilhot F. Indications for imatinib mesylate therapy and clinical management. *Oncologist* 2004; 9: 271–281.

65. Isotani M, Ishida N, Tominaga M, Tamura K, Yagihara H, Ochi S, et al. Effect of tyrosine kinase inhibition by imatinib mesylate on mast cell tumors in dogs. *J Vet Intern Med* 2008; 22: 985–988.

66. Moreno-Vinasco L, Gomberg-Maitland M, Maitland ML, Desai AA, Singleton PA, Sammani S, et al. Genomic assessment of a multikinase inhibitor, sorafenib, in a rodent model of pulmonary hypertension. *Physiol Genomics* 2008; 33: 278–291.

67. Leong ZP, Okida A, Higuchi M, Yamano Y and Hikasa Y. Reversal effects of low-dose imatinib compared with sunitinib on monocrotaline-induced pulmonary and right ventricular remodeling in rats. *Vascul Pharmacol* 2018; 100: 41–50.

68.   Leblanc AK, Miller AN, Galyon GD, Moyers TD, Long MJ, Stuckey AC, et al. Preliminary evaluation of serial (18) FDG-PET/CT to assess response to toceranib phosphate therapy in canine cancer. *Vet Radiol Ultrasound* 2012; 53: 348–357.

69.   London CA, Hannah AL, Zadovoskaya R, Chien MB, Kollias-Baker C, Rosenberg M, et al. Phase I dose-escalating study of SU11654, a small molecule receptor tyrosine kinase inhibitor, in dogs with spontaneous malignancies. *Clin Cancer Res* 2003; 9: 2755–2768.

70.   London CA, Malpas PB, Wood-Follis SL, Boucher JF, Rusk AW, Rosenberg MP, et al. Multi-center, placebo-controlled, double-blind, randomized study of oral toceranib phosphate (SU11654), a receptor tyrosine kinase inhibitor, for the treatment of dogs with recurrent (either local or distant) mast cell tumor following surgical excision. *Clin Cancer Res* 2009; 15: 3856–3865.

71.   Lin JC, Huang WP, Liu CL, Lee JJ, Liu TP, Ko WC, et al. Sorafenib induces autophagy in human myeloid dendritic cells and prolongs survival of skin allografts. *Transplantation* 2013; 95: 791–800.

72.   Lin JC, Liu CL, Lee JJ, Liu TP, Ko WC, Huang WC, et al. Sorafenib induces autophagy and suppresses activation of human macrophage. *Int Immunopharmacol* 2013; 15: 333–339.

73.   Zhang CZ, Wang XD, Wang HW, Cai Y and Chao LQ. Sorafenib inhibits liver cancer growth by decreasing mTOR, AKT, and PI3K expression. *J BUON* 2015; 20: 218–222.

74. Kato F, Sakao S, Takeuchi T, Suzuki T, Nishimura R, Yasuda T, at al. Endothelial cell-related autophagic pathways in Sugen/hypoxia-exposed pulmonary arterial hypertensive rats. *Am J Physiol Lung Cell Mol Physiol* 2017; 313: L899–L915.

75. Lee SJ, Smith A, Guo L, Alastalo TP, Li M, Sawada H, et al. Autophagic protein LC3B confers resistance against hypoxia-induced pulmonary hypertension. *Am J Respir Crit Care Med* 2011; 183: 649–658.

76. Long L, Yang X, Southwood M, Lu J, Marciniak SJ, Dunmore BJ, et al. Chloroquine prevents progression of experimental pulmonary hypertension via inhibition of autophagy and lysosomal bone morphogenetic protein type II receptor degradation. *Circ Res* 2013; 112: 1159–1170.

77. Young KC, Torres E, Hatzistergos KE, Hehre D, Suguihara C and Hare JM. Inhibition of the SDF-1/CXCR4 axis attenuates neonatal hypoxia-induced pulmonary hypertension. *Circ Res* 2009; 104: 1293–1301.

78. Yoshii SR and Mizushima N. Monitoring and measuring autophagy. *Int J Mol Sci* 2017; 18: 1865.

79. London C, Mathie T, Stingle N, Clifford C, Haney S, Klein MK, et al. Preliminary evidence for biologic activity of toceranib phosphate (Palladia(®)) in solid tumours. *Vet Comp Oncol* 2012; 10: 194–205.

80. Yancey MF, Merritt DA, Lesman SP, Boucher JF and Michels GM. Pharmacokinetic properties of toceranib phosphate (Palladia, SU11654), a novel tyrosine kinase inhibitor, in laboratory dogs and dogs with mast cell tumors. *J Vet Pharmacol Ther*. 2010; 33:162–171.

81. Minami H, Kawada K, Ebi H, Kitagawa K, Kim YI, Araki K, et al. Phase I and pharmacokinetic study of sorafenib, an oral multikinase inhibitor, in Japanese patients with advanced refractory solid tumors. *Cancer Sci*. 2008; 99:1492–1498.

82. Strasser GA, Kaminker JS, Tessier-Lavigne M. Microarray analysis of retinal endothelial tip cells identifies CXCR4 as a mediator of tip cell morphology and branching. *Blood* 2010; 115: 5102–5110.

83. Xu J, Liang J, Meng YM, Yan J, Yu XJ, Liu CQ, et al. Vascular CXCR4 expression promotes vessel sprouting and sensitivity to sorafenib treatment in hepatocellular carcinoma. Clin Cancer Res 2017; 23: 4482–4492.

84. Aghi M, Cohen KS, Klein RJ, Scadden DT and Chiocca EA. Tumor stromal-derived factor-1 recruits vascular progenitors to mitotic neovasculature, where microenvironment influences their differentiated phenotypes. *Cancer Res* 2006; 66: 9054–9064.

85. Farkas D, Kraskauskas D, Drake JI, Alhussaini AA, Kraskauskiene V, Bogaard HJ, et al. CXCR4 inhibition ameliorates severe obliterative pulmonary hypertension and accumulation of C-kit^{+} cells in rats. *PLoS One* 2014; 9: e89810.

86. Gambaryan N, Perros F, Montani D, Cohen-Kaminsky S, Mazmanian M, Renaud JF, et al. Targeting of c-kit+ haematopoietic progenitor cells prevents hypoxic pulmonary hypertension. *Eur Respir J* 2011; 37: 1392–1399.

87. Zernecke A, Schober A, Bot I, von Hundelshausen P, Liehn EA, Möpps B, et al. SDF-1alpha/CXCR axis is instrumental in neointimal hyperplasia and recruitment of smooth muscle progenitor cells. *Circ Res* 2005; 96: 784–791.

88. Duong-Quy S, Bei Y and Liu Z. Role of Rho-kinase and its inhibitors in pulmonary hypertension. *Pharmacol Ther* 2013; 137: 352–364.

89. Church AC, Martin DH, Wadsworth R, Bryson G, Fisher AJ, Welsh DJ, et al. The reversal of pulmonary vascular remodeling through inhibition of p38 MAPK-alpha: a potential novel anti-inflammatory strategy in pulmonary hypertension. *Am J Physiol Lung Cell Mol Physiol* 2015; 309: L333–L347.

90. Leong ZP and Hikasa Y. Effects of toceranib compared with sorafenib on monocrotaline-induced pulmonary arterial hypertension and cardiopulmonary remodeling in rats. *Vascul Pharmacol* 2018; 110: 31–41.

91. Leong ZP, Arita S and Hikasa Y. Long-term effect of low-dose imatinib therapy for pulmonary hypertension due to chronic degenerative mitral valve disease in six dogs. *Thai J Vet Med* 2018; 48: 509–515.

92. Marech I, Patruno R, Zizzo N, Gadaleta C, Introna M, Zito AF, et al. Masitinib (AB1010), from canine tumor model to human clinical development: Where we are? *Crit Rev Oncol Hematol* 2014; 91: 98–111.

93. Kocic I, Sztormowska K and Jankowski Z. Protective effect of masitinib on cardiovascular function of rats with pulmonary hypertension: gender dependence. *Eur Heart J* 2017; 38: P1342.

94. Dubreuil P, Letard S, Ciufolini M, Gros L, Humbert M, Castéran N, et al. Masitinib (AB1010), a potent and selective tyrosine kinase inhibitor targeting KIT. *PLoS One* 2009; 30: e7258.

95. Falk JA, Philip KJ and Schwarz ER. The emergence of oral tadalafil as a once-daily treatment for pulmonary arterial hypertension. *Vasc Health Risk Manag* 2010; 6: 273–280.

96. Galiè N, Brundage BH, Ghofrani HA, Oudiz RJ, Simonneau G, Safdar Z, et al. Tadalafil therapy for pulmonary arterial hypertension. *Circulation* 2009; 119: 2894–2903.

97. Ghofrani HA, Voswinckel R, Reichenberger F, Olschewski H, Haredza P, Karadaş B, et al. Differences in hemodynamic and oxygenation responses to three different phosphodiesterase-5 inhibitors in patients with pulmonary arterial hypertension: a randomized prospective study. *J Am Coll Cardiol* 2004; 44: 1488–1496.

98. Aggarwal P, Patial RK, Negi PC and Marwaha R. Oral tadalafil in pulmonary artery hypertension: a prospective study. *Indian Heart J* 2007; 59: 329–335.

99. Sawamura F, Kato M, Fujita K, Nakazawa T and Beardsworth A. Tadalafil, a long-acting inhibitor of PDE5, improves pulmonary hemodynamics and survival rate of monocrotaline-induced pulmonary artery hypertension in rats. *J Pharmacol Sci* 2009; 111: 235–243.

100. Favre S, Gambini E, Nigro P, Scopece A, Bianciardi P, Caretti A, et al. Sildenafil attenuates hypoxic pulmonary remodelling by inhibiting bone marrow progenitor cells. *J Cell Mol Med* 2017; 21: 871–880.

101. Soria JC, Massard C, Magné N, Bader T, Mansfield CD, Blay JY, et al. Phase 1 dose-escalation study of oral tyrosine kinase inhibitor masitinib in advanced and/or metastatic solid cancers. *Eur J Cancer* 2009; 45: 2333–2341.

102. Egawa M, Ishikura F, Nishikawa R, Ihara M, Takano Y, Kawaguchi N, et al. Effects of tadalafil to prevent thickening of pulmonary artery in monocrotaline-induced pulmonary hypertension rats: compared with echocardiographic findings: pp.13.485. *J. Hypertens* 2010; 28: e196–e197.

103. Maihöfer NA, Suleiman S, Dreymüller D, Manley PW, Rossaint R, Uhlig S, et al. Imatinib relaxes the pulmonary venous bed of guinea pigs. *Respir Res* 2017; 18: 32.

104. Reynolds CA, Brown DC, Rush JE, Fox PR, Nguyenba TP, Lehmkuhl LB, et al. Prediction of first onset of congestive heart failure in dogs with degenerative mitral valve disease: the PREDICT cohort study. *J Vet Cardiol* 2012; 14: 193–202.

105. Pankey EA, Thammasiboon S, Lasker GF, Baber S, Lasky JA and Kadowitz PJ. Imatinib attenuates monocrotaline pulmonary hypertension and has potent vasodilator activity in pulmonary and systemic vascular beds in the rat. *Am J Physiol Heart Circ Physiol* 2013; 305: H1288–H1296.

106. Hezzell MJ, Boswood A, Moonarmart W and Elliott J. Selected echocardiographic variables change more rapidly in dogs that die from myxomatous mitral valve disease. *J Vet Cardiol* 2012; 14: 269–279.

107. Bonkobara M. Dysregulation of tyrosine kinases and use of imatinib in small animal practice. *Vet J* 2015; 205: 180–188.